Meshing or not meshing?

Iso/sub/super-geometric analysis

(adaptive unfitted methods for real-time simulations)

Immersed collocation methods

Stéphane P.A. Bordas, University of Luxembourg and Cardiff University

University College London, UCL, 20180103-04

Computational Mechanics of Interfaces

with Engineering and Medical Applications

Stéphane P.A. Bordas
stephane.bordas@alum.northwestern.edu

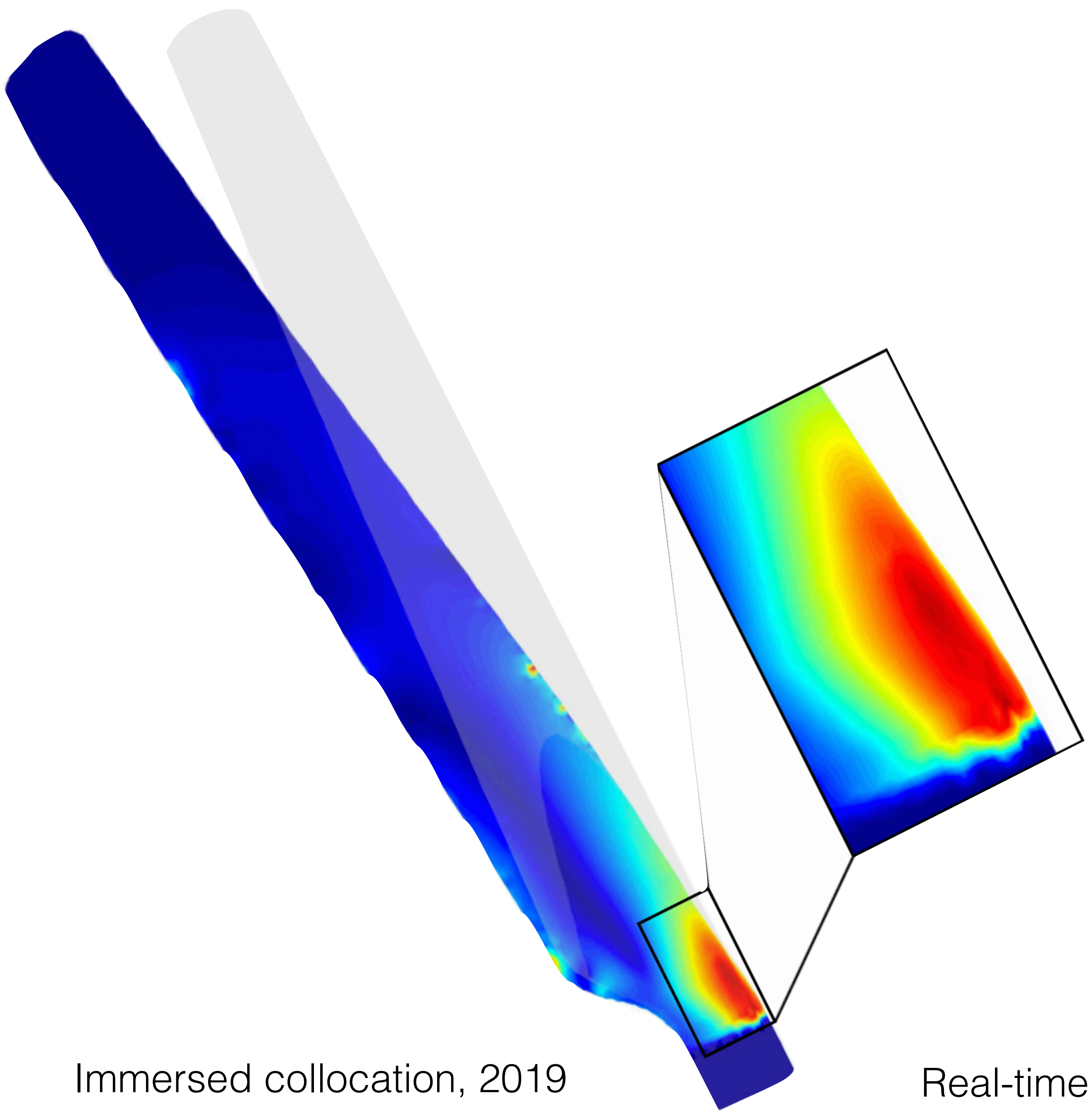

Immersed collocation, 2019

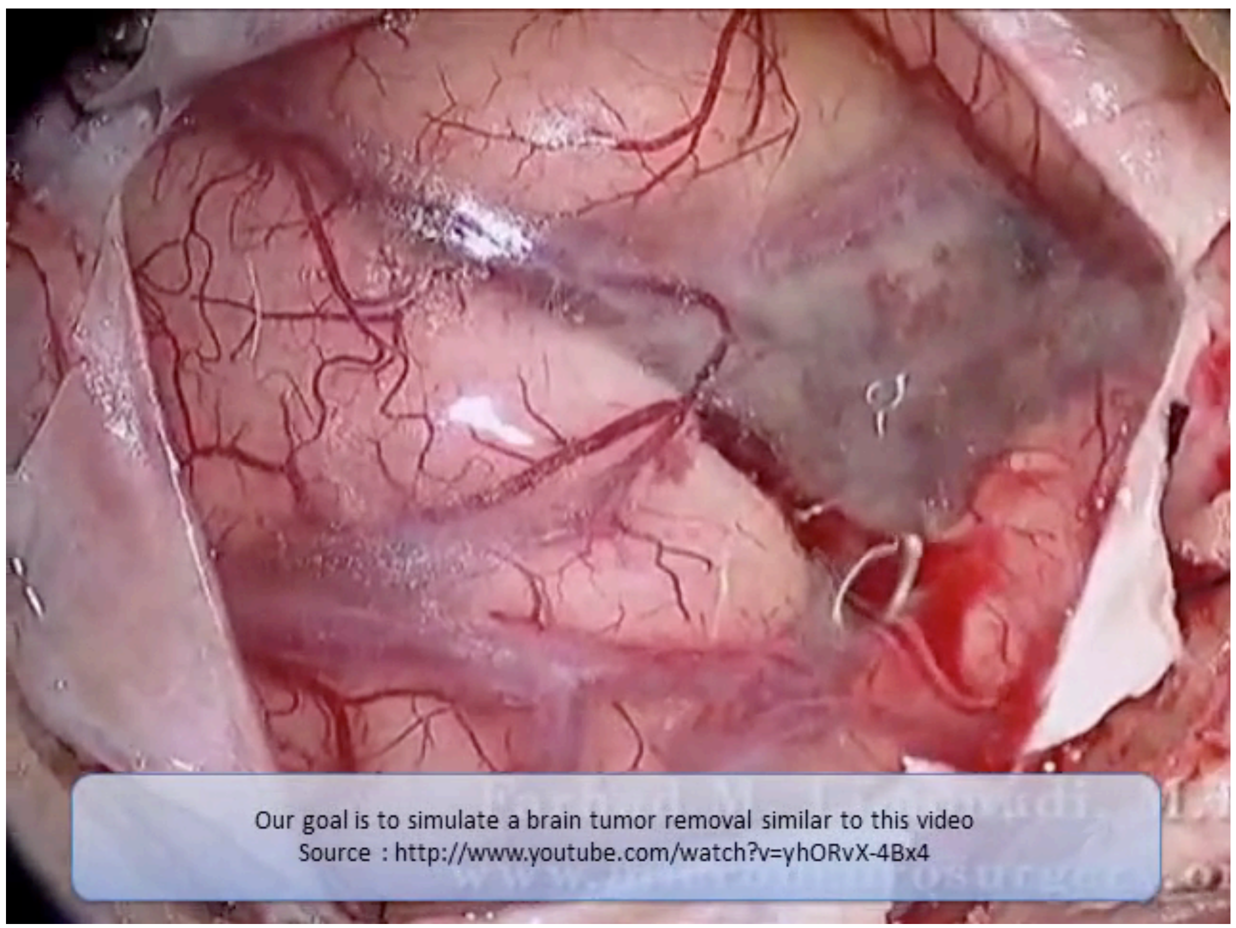

Real-time cutting, MEDIA2014, IEEE2017, IJNMBE2018, CMAME2018

One machine, one minute, three billion tetrahedra

Célestin Marot* | Jeanne Pellerin | Jean-François Remacle

[1]Université catholique de Louvain, iMMC,
Avenue Georges Lemaitre 4, bte L4.05.02,
1348 Louvain-la-Neuve, Belgium

Correspondence
*Corresponding author: Email:
celestin.marot@uclouvain.be

Summary

This paper presents a new scalable parallelization scheme to generate the 3D Delaunay triangulation of a given set of points. Our first contribution is an efficient serial implementation of the incremental Delaunay insertion algorithm. A simple dedicated data structure, an efficient sorting of the points and the optimization of the insertion algorithm have permitted to accelerate reference implementations by a factor three. Our second contribution is a multi-threaded version of the Delaunay kernel that is able to concurrently insert vertices. Moore curve coordinates are used to partition the point set, avoiding heavy synchronization overheads. Conflicts are managed by modifying the partitions with a simple rescaling of the space-filling curve. The performances of our implementation have been measured on three different processors, an Intel core-i7, an Intel Xeon Phi and an AMD EPYC, on which we have been able to compute 3 billion tetrahedra in 53 seconds. This corresponds to a generation rate of over 55 million tetrahedra per second. We finally show how this very efficient parallel Delaunay triangulation can be integrated in a Delaunay refinement mesh generator which takes as input the triangulated surface boundary of the volume to mesh.

One machine, one minute, three billion tetrahedra

Célestin Marot* | Jeanne Pellerin | Jean-François Remacle

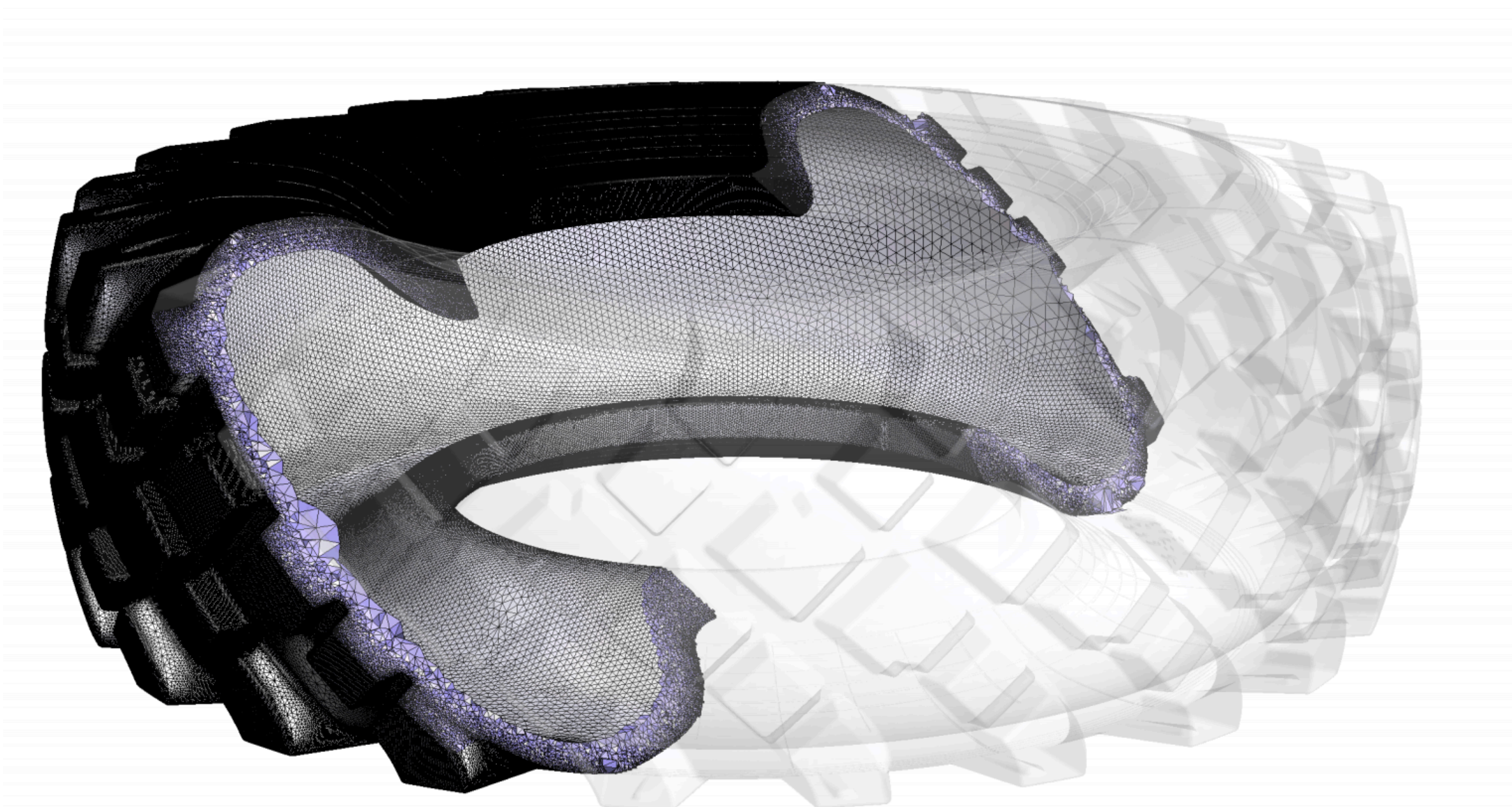

Truck tire

# threads	# tetrahedra	Timings (s)		
		BR	Refine	Total
1	123 640 429	75.9	259.7	364.7
2	123 593 913	74.5	166.8	267.1
4	123 625 696	74.2	107.4	203.6
8	123 452 318	74.2	95.5	190.0

One machine, one minute, three billion tetrahedra

Célestin Marot* | Jeanne Pellerin | Jean-François Remacle

Truck tire

# threads	# tetrahedra	Timings (s) BR	Refine	Total
1	123 640 429	75.9	259.7	364.7
2	123 593 913	74.5	166.8	267.1
4	123 625 696	74.2	107.4	203.6
8	123 452 318	74.2	95.5	190.0

One machine, one minute, three billion tetrahedra

Célestin Marot* | Jeanne Pellerin | Jean-François Remacle

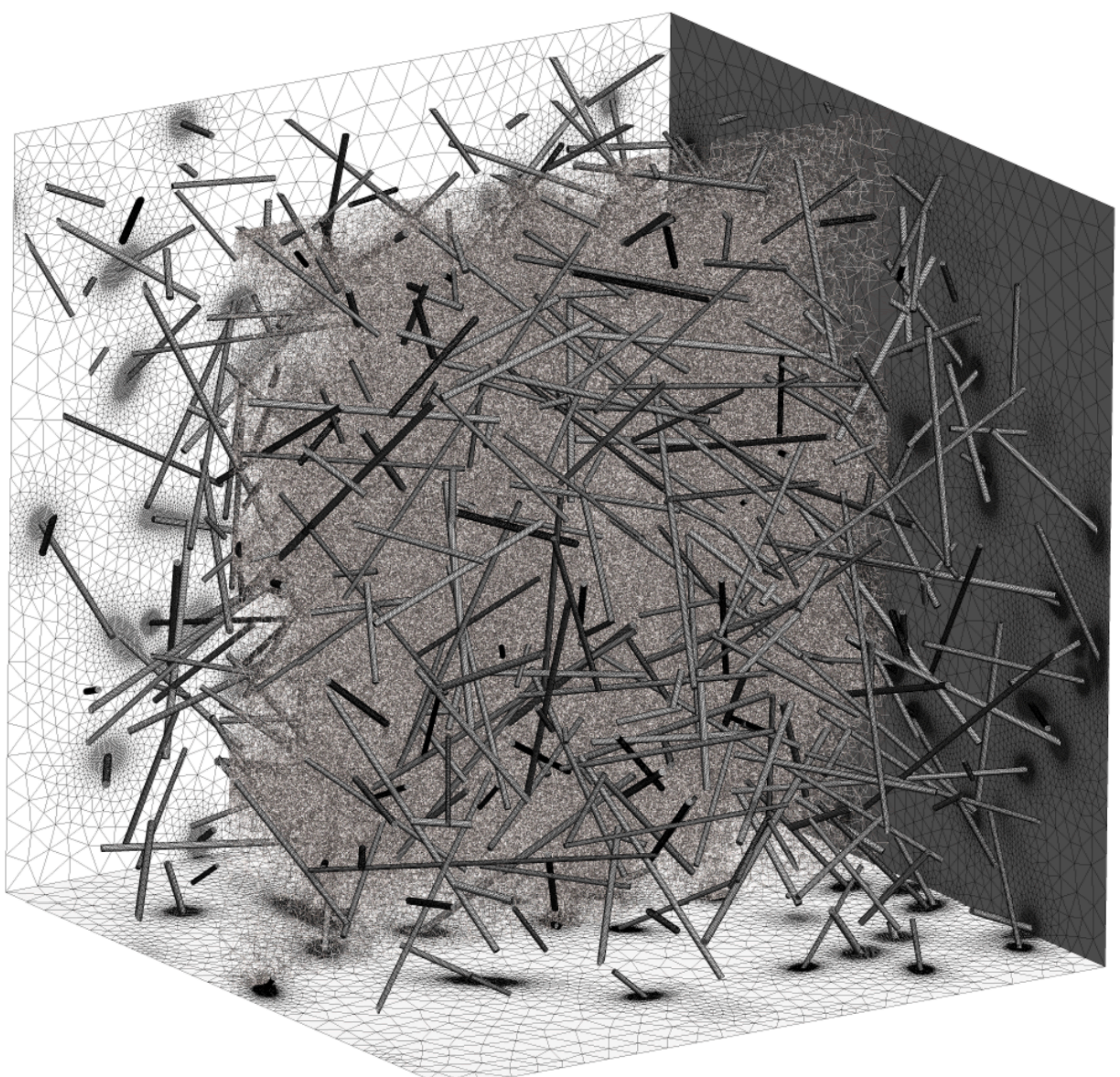

100 thin fibers

# threads	# tetrahedra	Timings (s) BR	Refine	Total
1	325 611 841	3.1	492.1	497.2
2	325 786 170	2.9	329.7	334.3
4	325 691 796	2.8	229.5	233.9
8	325 211 989	2.7	154.6	158.7
16	324 897 471	2.8	96.8	100.9
32	325 221 244	2.7	71.7	75.8
64	324 701 883	2.8	55.8	60.1
127	324 190 447	2.9	47.6	52.0

500 thin fibers

# threads	# tetrahedra	Timings (s) BR	Refine	Total
1	723 208 595	18.9	1205.8	1234.4
2	723 098 577	16.0	780.3	804.8
4	722 664 991	86.6	567.1	659.8
8	722 329 174	15.8	349.1	370.1
16	723 093 143	15.6	216.2	236.5
32	722 013 476	15.6	149.7	169.8
64	721 572 235	15.9	119.7	140.4
127	721 591 846	15.9	114.2	135.2

One machine, one minute, three billion tetrahedra

Célestin Marot* | Jeanne Pellerin | Jean-François Remacle

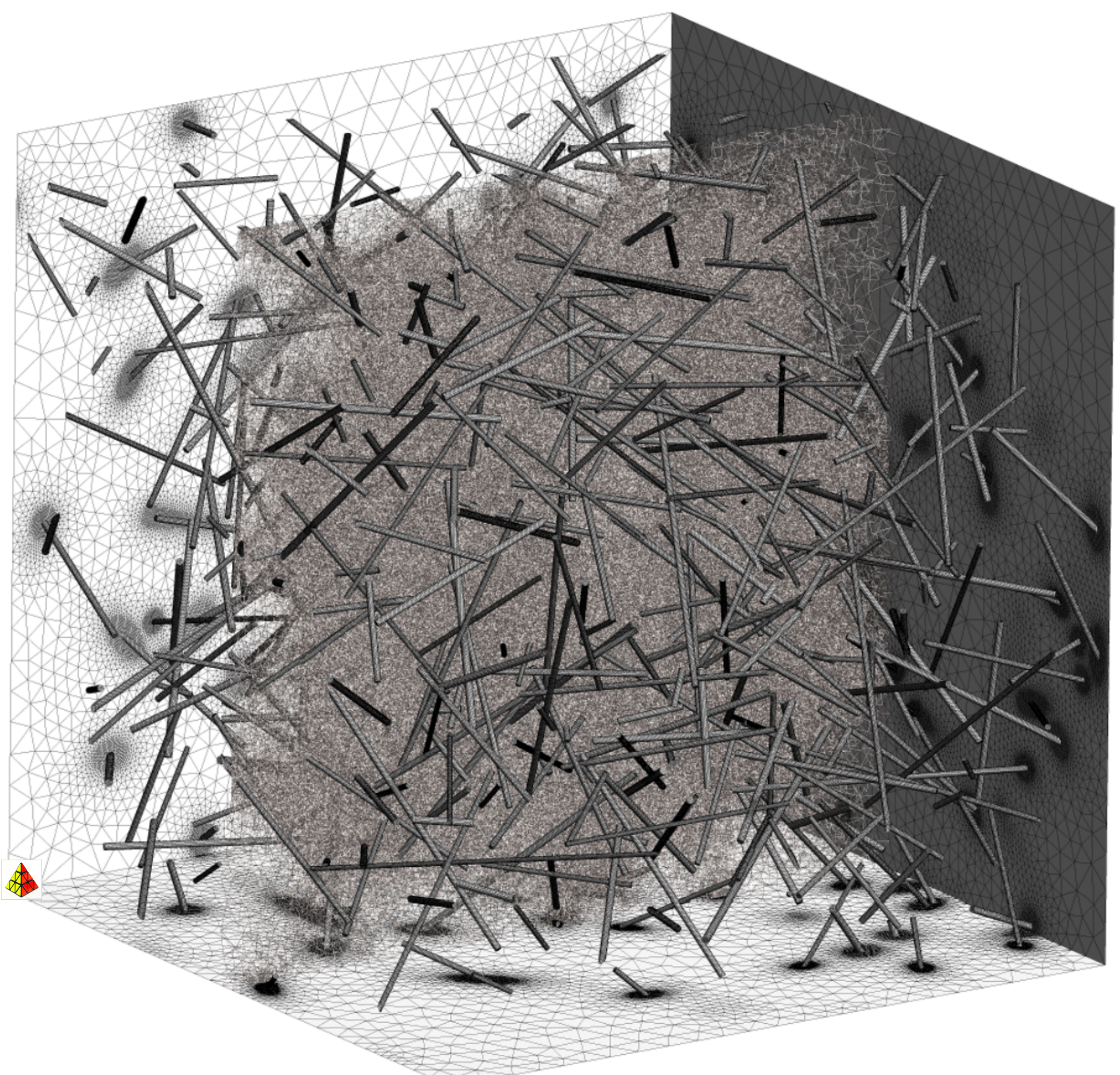

100 thin fibers

# threads	# tetrahedra	Timings (s)		
		BR	Refine	Total
1	325 611 841	3.1	492.1	497.2
2	325 786 170	2.9	329.7	334.3
4	325 691 796	2.8	229.5	233.9
8	325 211 989	2.7	154.6	158.7
16	324 897 471	2.8	96.8	100.9
32	325 221 244	2.7	71.7	75.8
64	324 701 883	2.8	55.8	60.1
127	324 190 447	2.9	47.6	52.0

500 thin fibers

# threads	# tetrahedra	Timings (s)		
		BR	Refine	Total
1	723 208 595	18.9	1205.8	1234.4
2	723 098 577	16.0	780.3	804.8
4	722 664 991	86.6	567.1	659.8
8	722 329 174	15.8	349.1	370.1
16	723 093 143	15.6	216.2	236.5
32	722 013 476	15.6	149.7	169.8
64	721 572 235	15.9	119.7	140.4
127	721 591 846	15.9	114.2	135.2

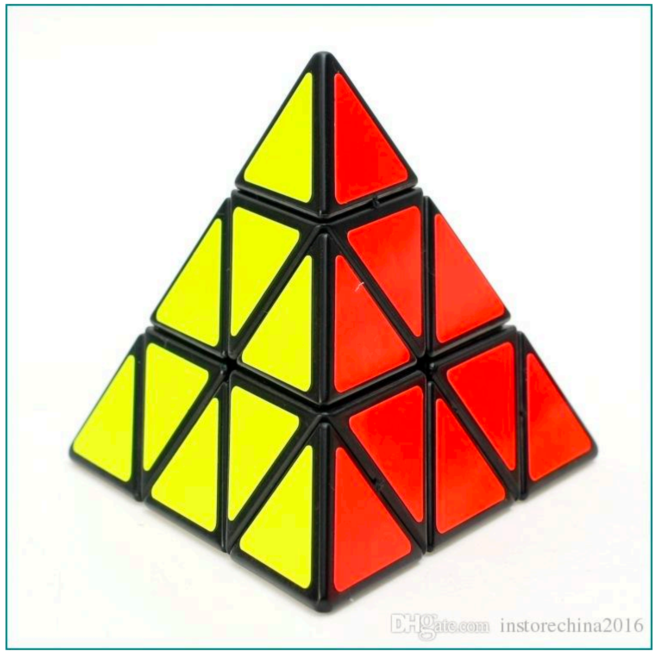

Linear tetrahedral elements are limited

- Stiff
- Locking
- …

Alternative elements - polyhedral - virtual elements, HHO, SBFEM, smoothed FEM…

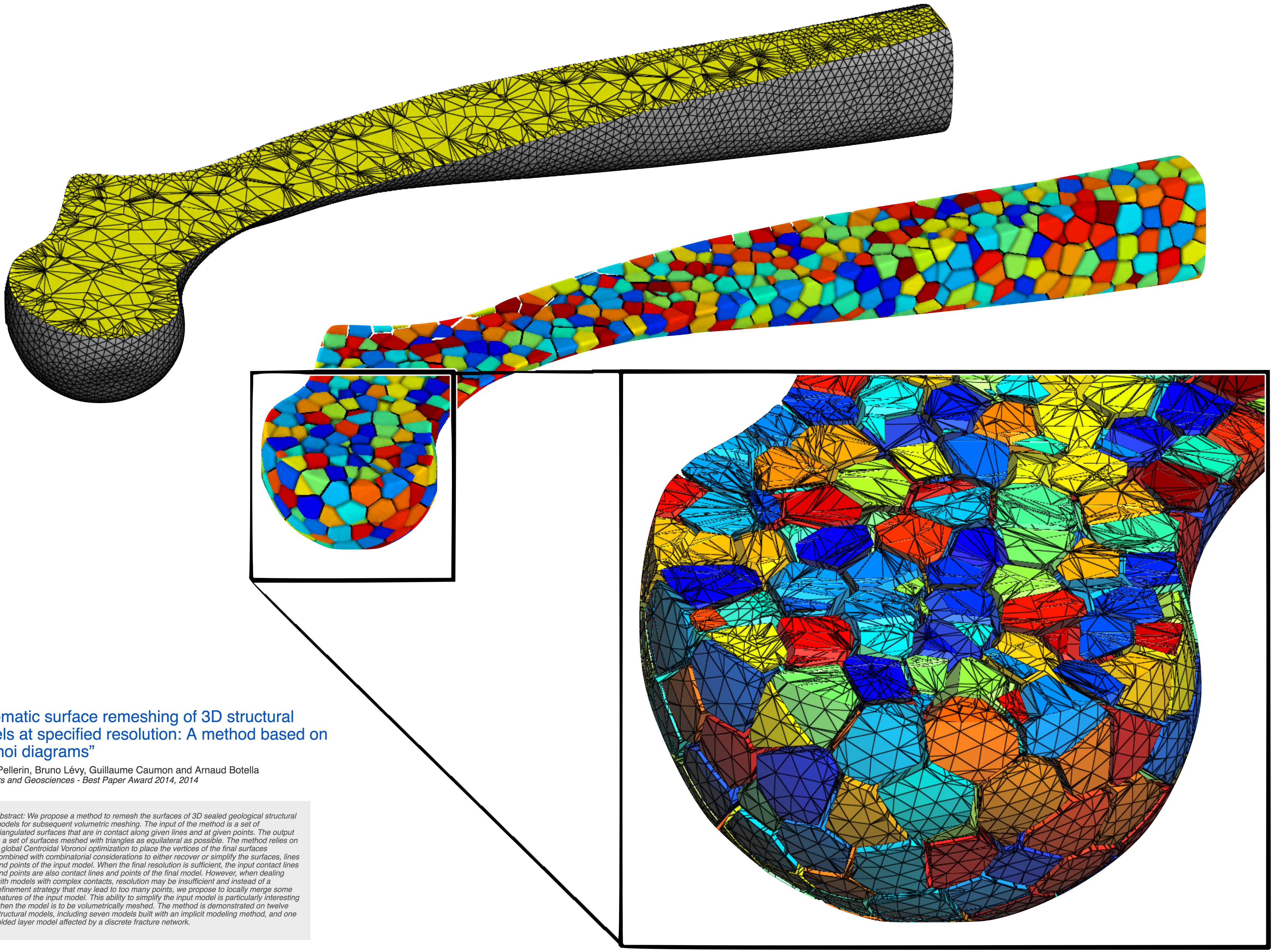

“Automatic surface remeshing of 3D structural models at specified resolution: A method based on Voronoi diagrams”

Jeanne Pellerin, Bruno Lévy, Guillaume Caumon and Arnaud Botella

Computers and Geosciences - Best Paper Award 2014, 2014

Abstract: We propose a method to remesh the surfaces of 3D sealed geological structural models for subsequent volumetric meshing. The input of the method is a set of triangulated surfaces that are in contact along given lines and at given points. The output is a set of surfaces meshed with triangles as equilateral as possible. The method relies on a global Centroidal Voronoi optimization to place the vertices of the final surfaces combined with combinatorial considerations to either recover or simplify the surfaces, lines and points of the input model. When the final resolution is sufficient, the input contact lines and points are also contact lines and points of the final model. However, when dealing with models with complex contacts, resolution may be insufficient and instead of a refinement strategy that may lead to too many points, we propose to locally merge some features of the input model. This ability to simplify the input model is particularly interesting when the model is to be volumetrically meshed. The method is demonstrated on twelve structural models, including seven models built with an implicit modeling method, and one folded layer model affected by a discrete fracture network.

Use polyhedra

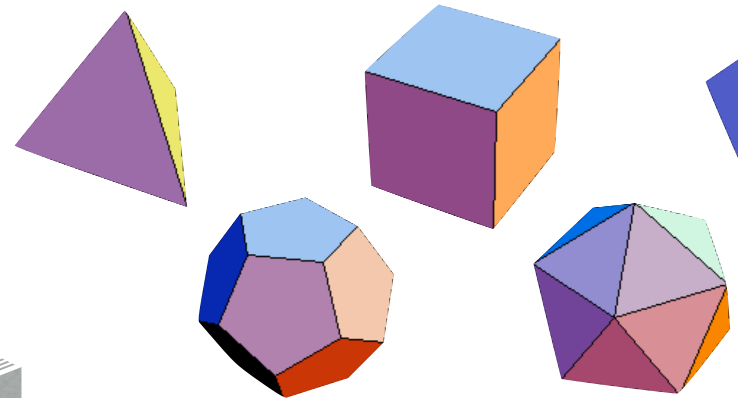

Mesh generators…

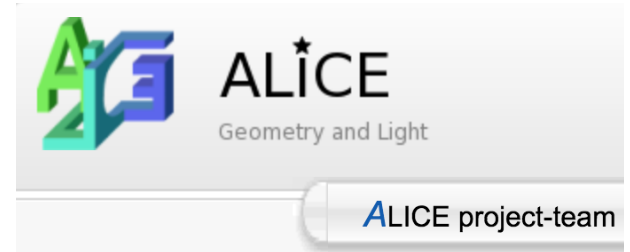

Bruno Lévy

3D NOffset mixed-element mesh generator approach

Claudio Lobos and Nancy Hitschfeld-Kahler
Depto Ciencias de la Computación,
FCFM, Universidad de Chile,
Blanco Encalada 2120,
Santiago - Chile, Zip code: 837-0459
clobos@dcc.uchile.cl, nancy@dcc.uchile.cl

Claudio Lobos

Virtual elements (cf. Silvia Bertoluzza)

The hitchhiker's guide to the **virtual element method**

Virtual and smoothed finite elements: A connection and its application to polygonal/polyhedral finite element methods (Natarajan, Ooi, Bordas)

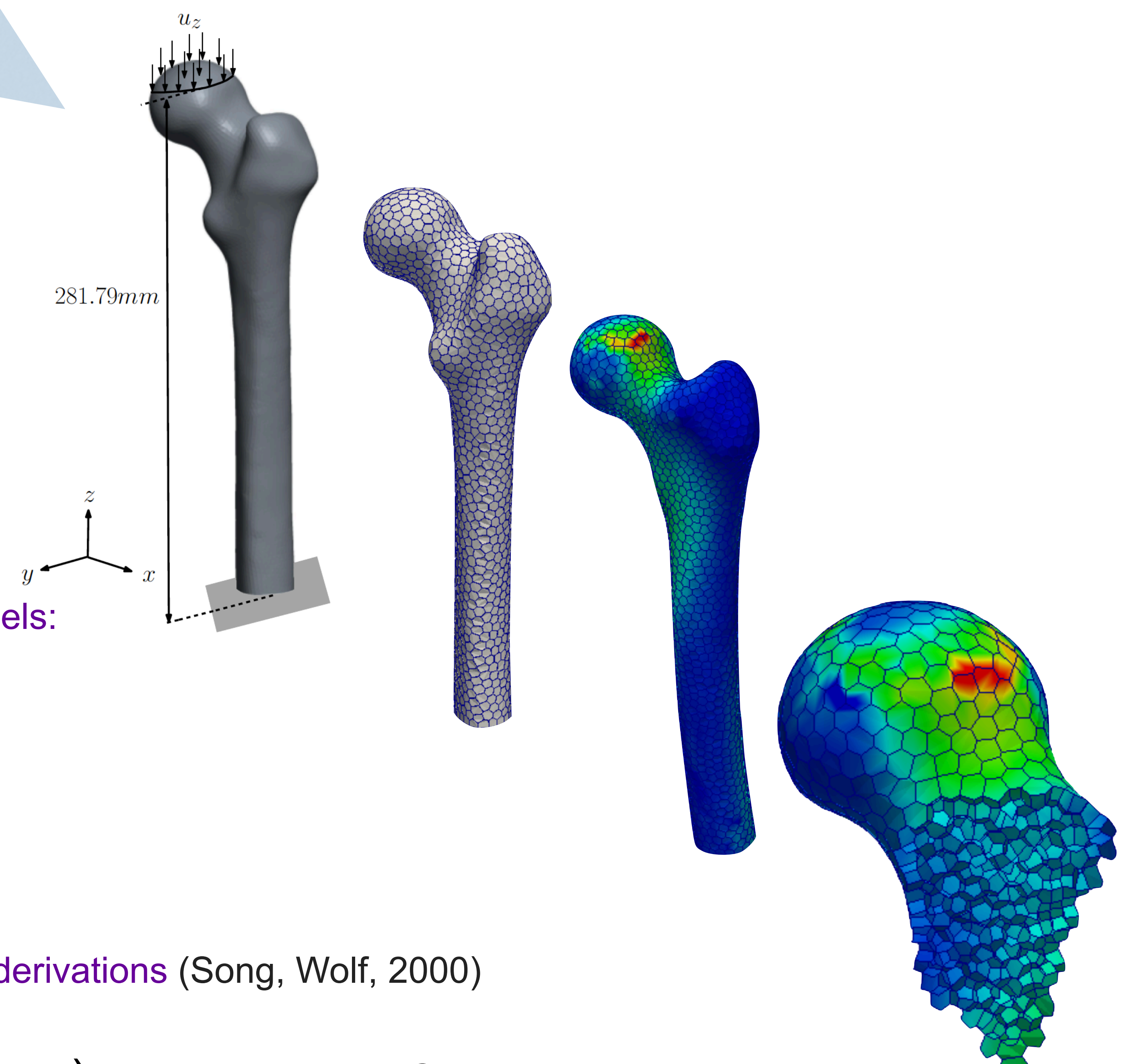

Smoothed FEM

A theoretical study on the **smoothed FEM** (S−**FEM**) models: Properties, accuracy and convergence rates (G.R. Liu, Nguyen et al)

On the approximation in the **smoothed** finite element method (SFEM) (Natarajan, Bordas)

Scaled boundary FEM

The **scaled boundary finite-element** method–a primer: derivations (Song, Wolf, 2000)

HHO (cf. F. Chouly and G. Delay)

Smoothed polyhedral FEMs
Francis, Natarajan, Lévy, Bordas, 2019

Avoid meshing complex/evolving interfaces through unfitted methods

Implicit boundaries and error control for real time simulations

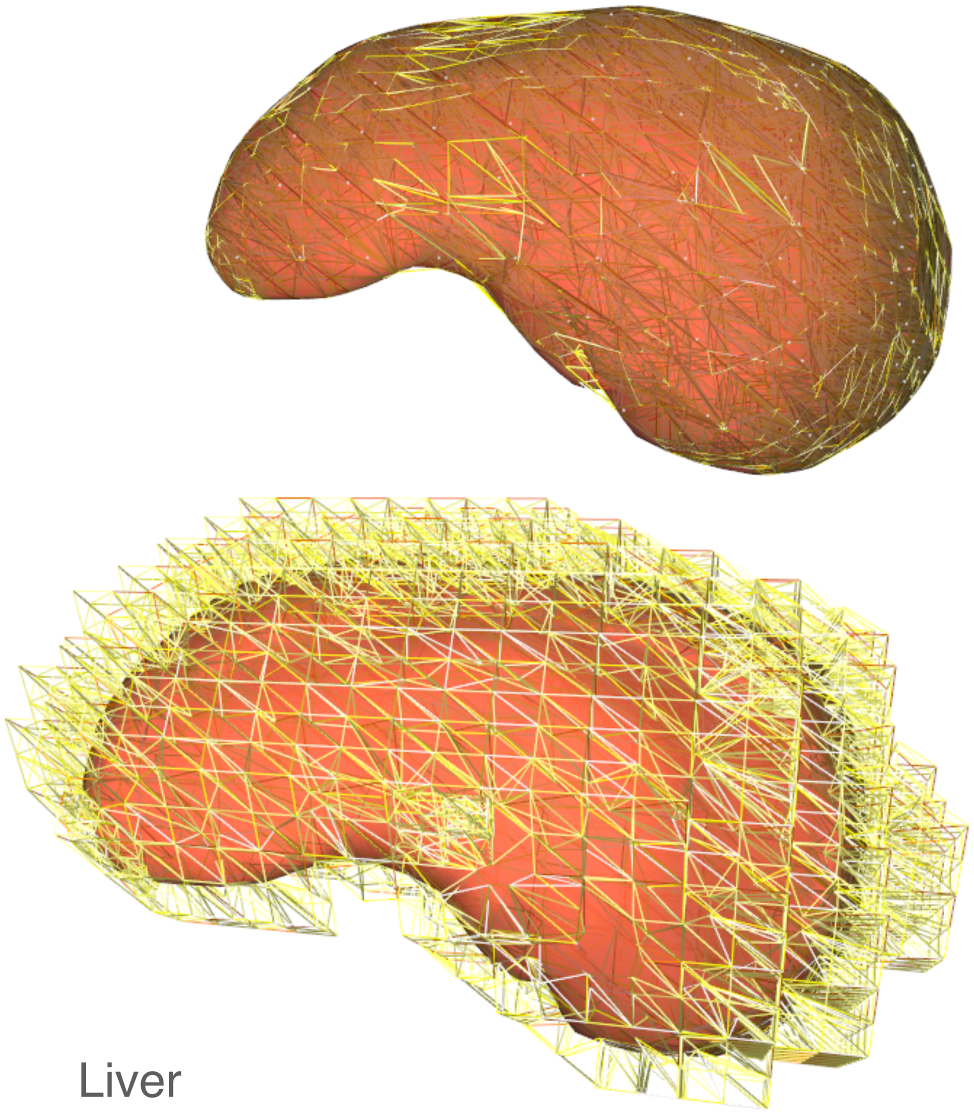

Liver

Deep brain stimulation simulation

Real-time Error Control for Surgical Simulation, HP **Bui** et al, **IEEE Trans. Biomed. Eng., 2016.**

Controlling the Error on Target Motion through Real-time Mesh Adaptation: Applications to Deep Brain Stimulation, HP **Bui** et al, **Int J Numer Meth Bio, 2017.**

Corotational Cut Finite Element Method for real-time surgical simulation: application to needle insertion simulation, HP **Bui** et al, **arXiv**:1712.03052[cs.CE] **2018**.

RealTCut

Handling interfaces numerically

Couple geometry & analysis

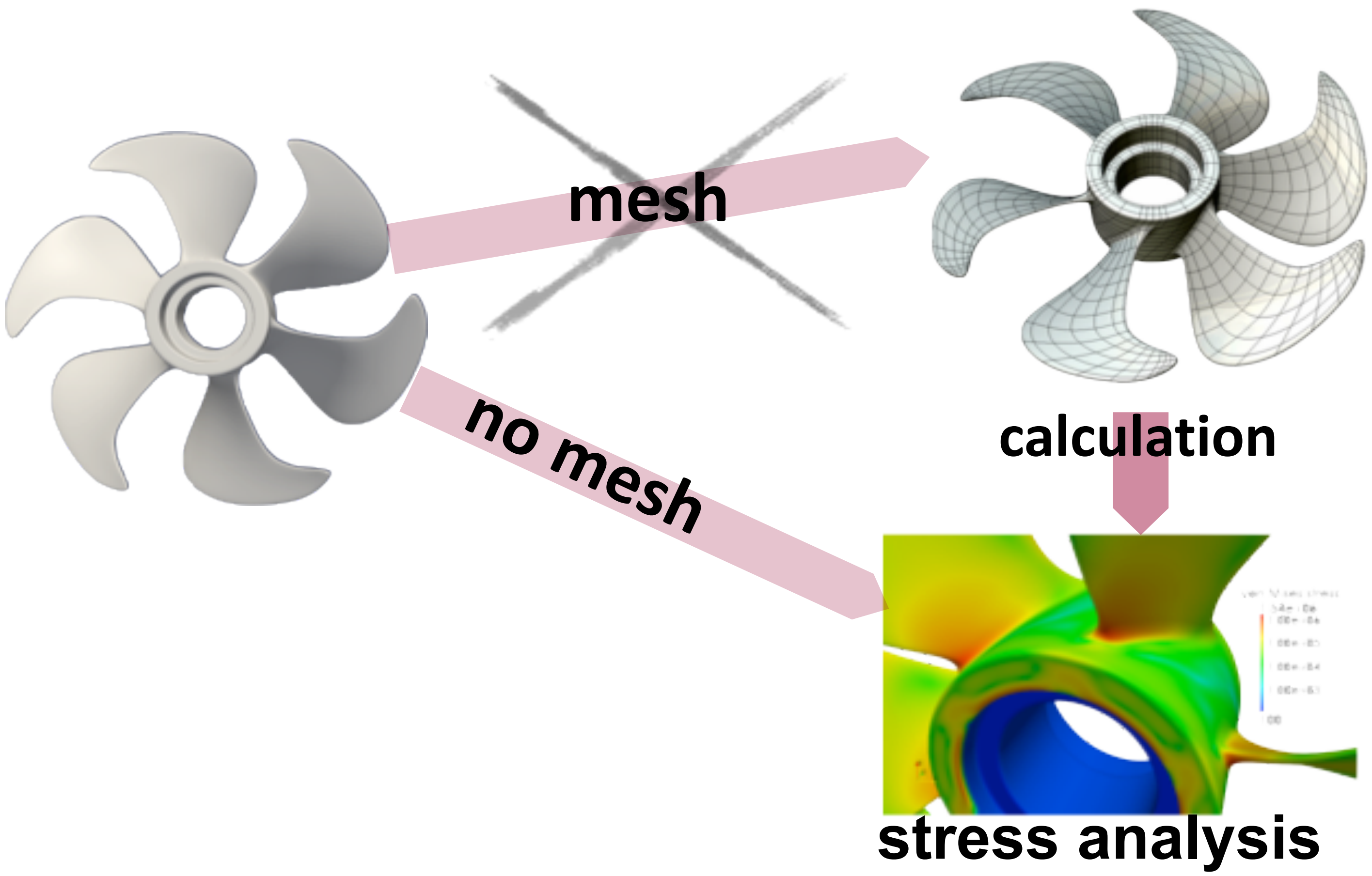

Isogeometric analysis

Decouple geometry from analysis

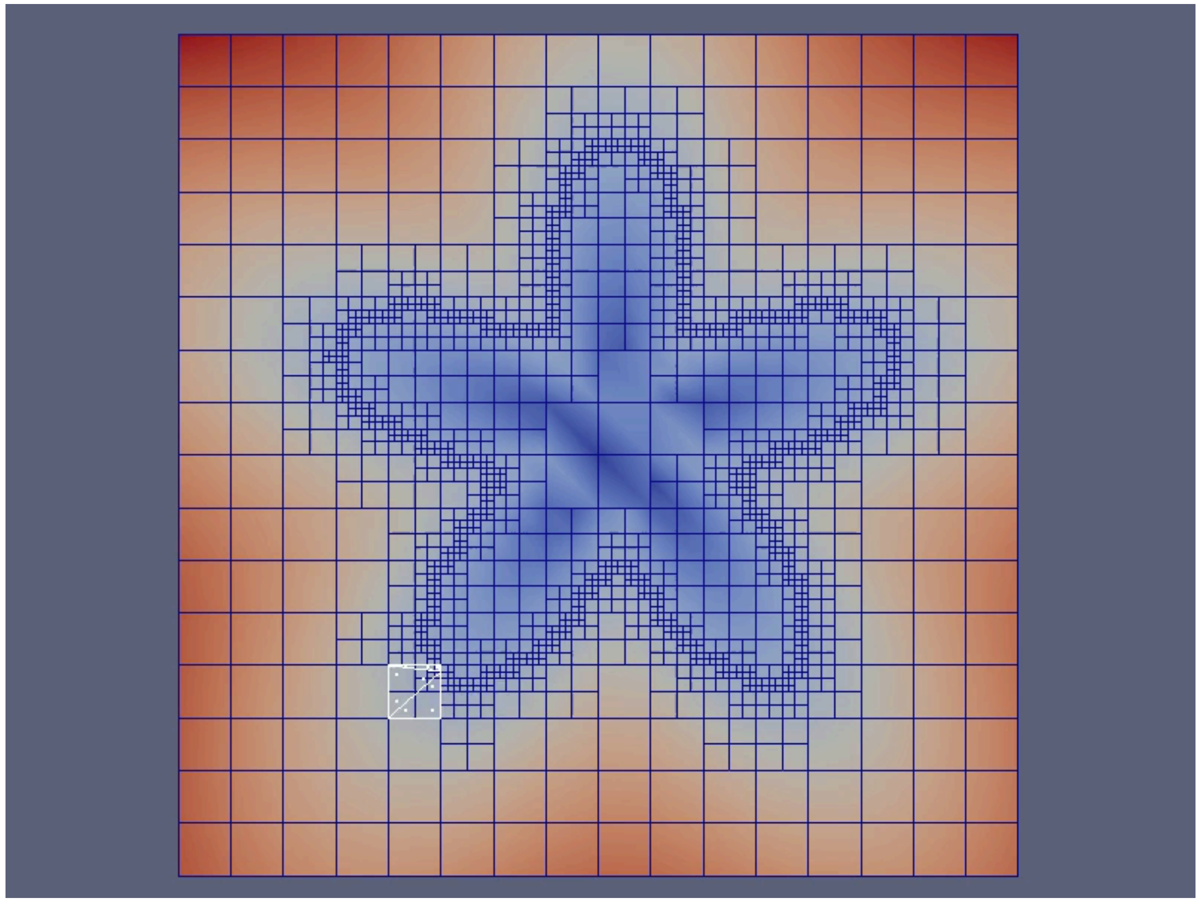

Implicit interfaces/unfitted

Stéphane Pierre Alain BORDAS, Department of Computational Engineering & Sciences University of Luxembourg and Cardiff University

Immersed collocation generalized FD

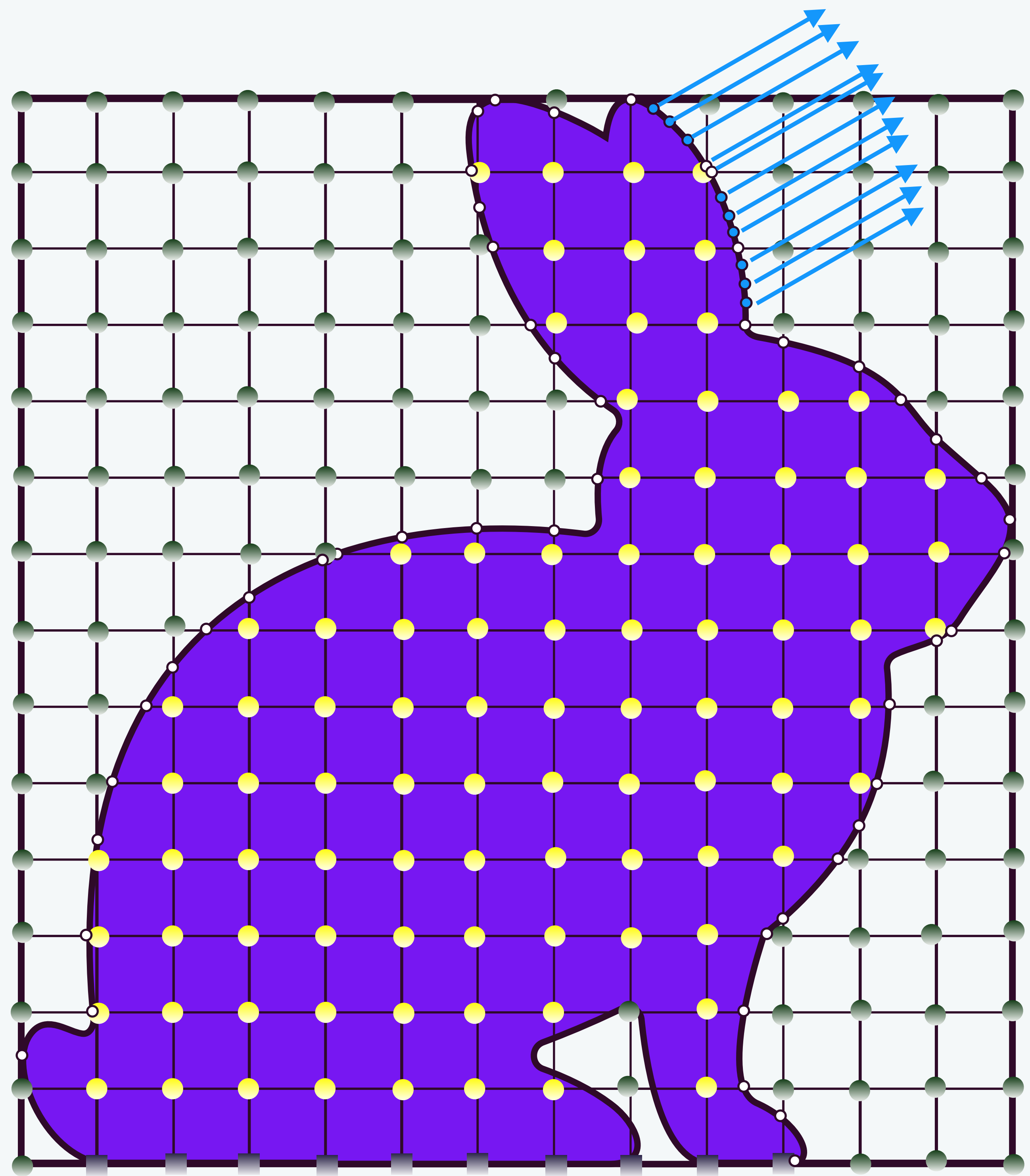

Computed in Luxembourg

Main collaborators

Kostas	Agathos
Cosmin	Anitescu
Elena	Atroshchenko
Davide	Baroli
Lars	Beex
Phuoc	Bui
Eleni	Chatzi
Leilei	Chen
Franz	Chouly
Susanne	Claus
Sofia	Farina
Jack	Hale
Paul	Hauseux
Qingyuan	Hu
Pierre	Kerfriden
Tahsin	Khajah
Alexei	Lozinski
Thibault	Jacquemin
Haojie	Lian
Mohammed	Moumnassi
Xuan	Peng
Timon	Rabczuk
Hussein	Rappel
Sundar	Natarajan
Danas	Sutula
Satyendra	Tomar
Javier	Videla
Gang	Xu
Peng	Yu
Andreas	Zilian

UNIVERSITÉ DU LUXEMBOURG

Simplify CAD-Analysis
Isogeometric analysis

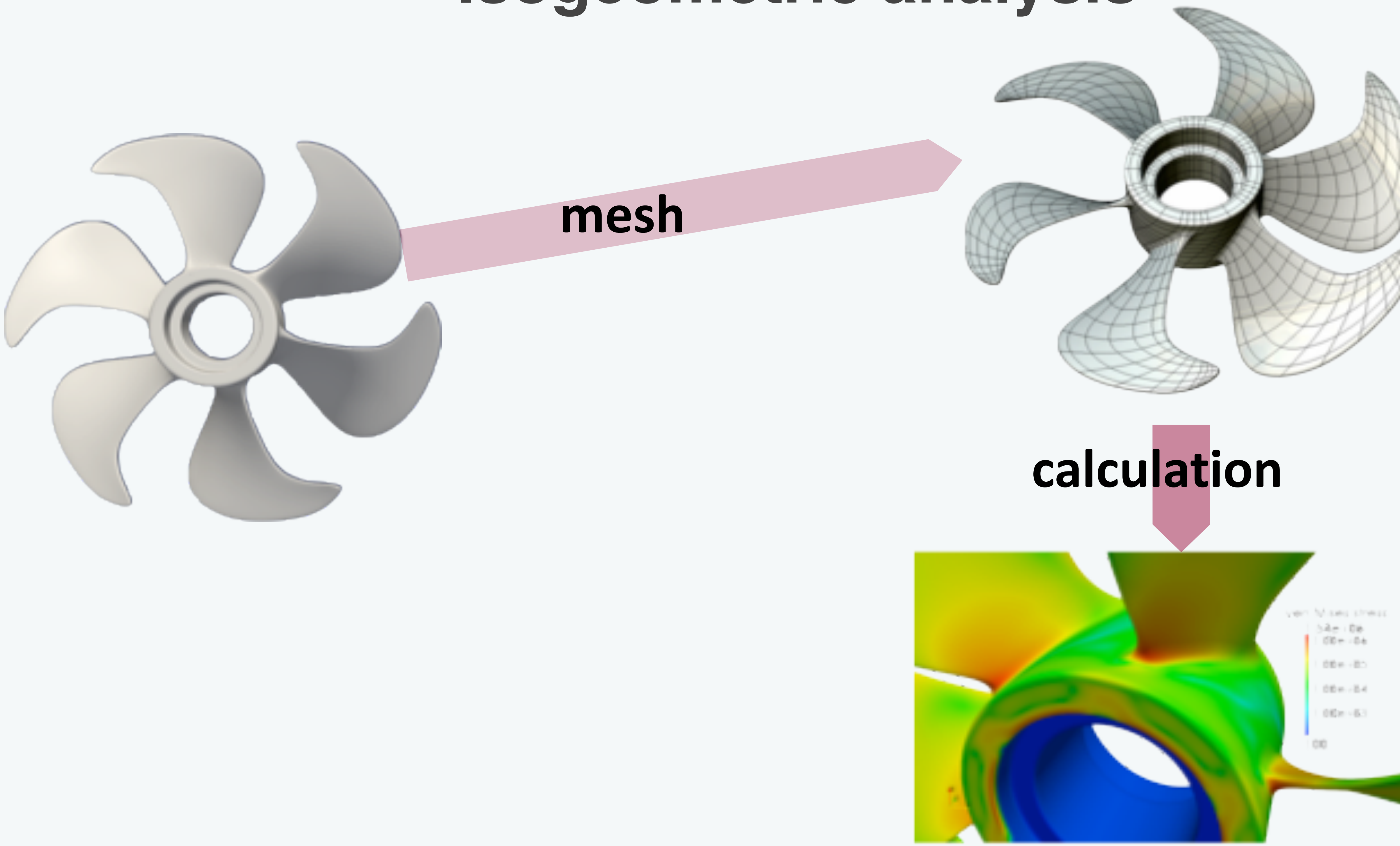

stress analysis

Isogeometric analysis

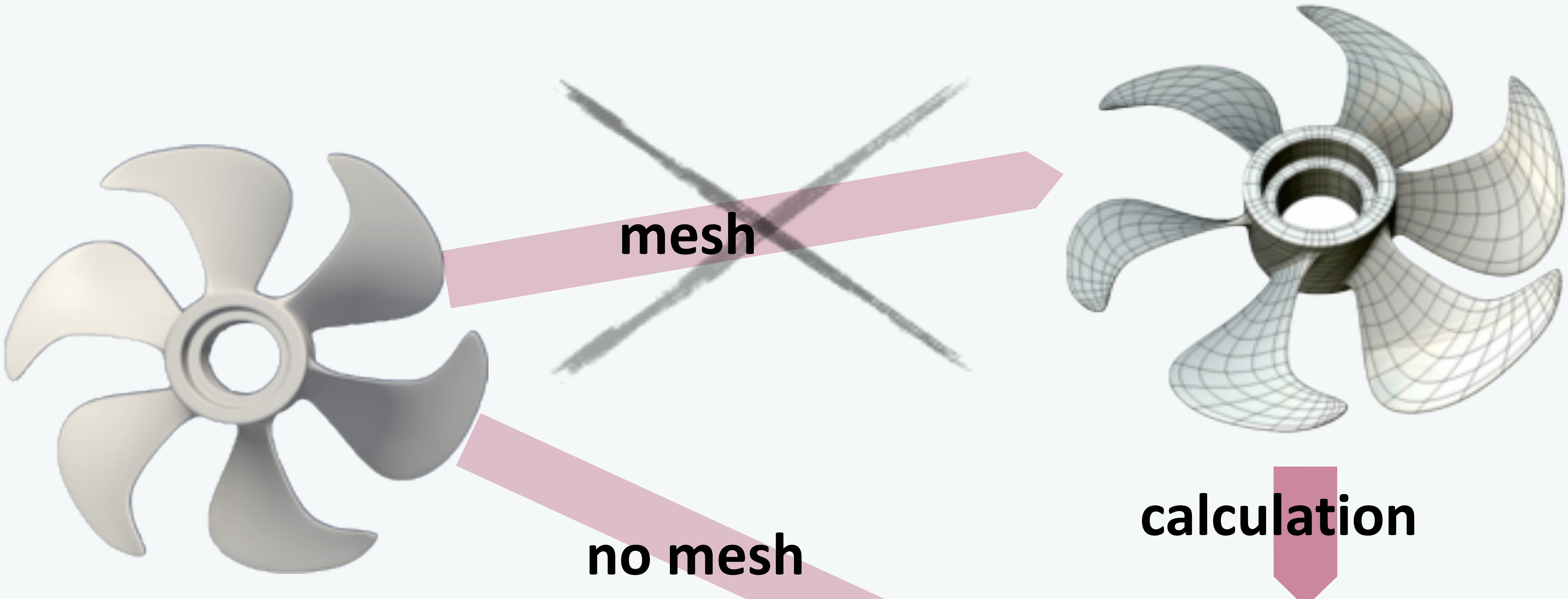

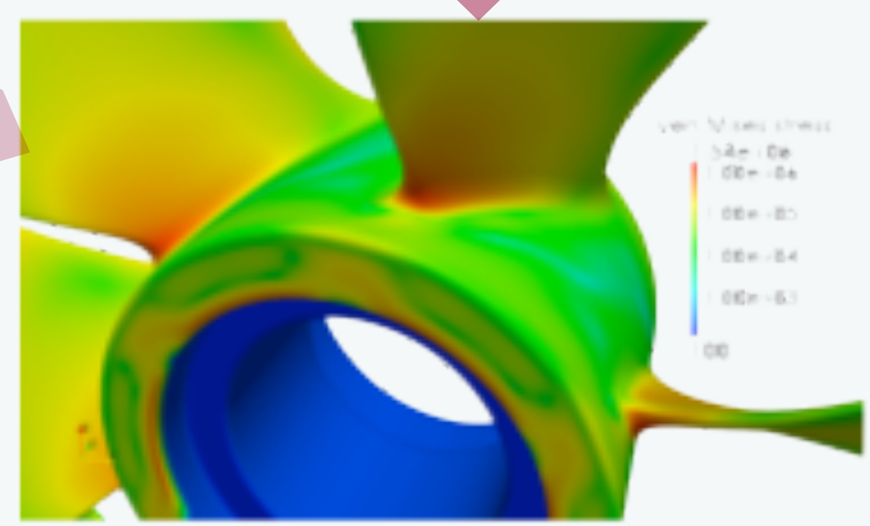

Idea: Hughes et al. 2005. Do not discard geometric information by creating a mesh. Use the CAD information to solve the finite element problem.

Isogeometric analysis

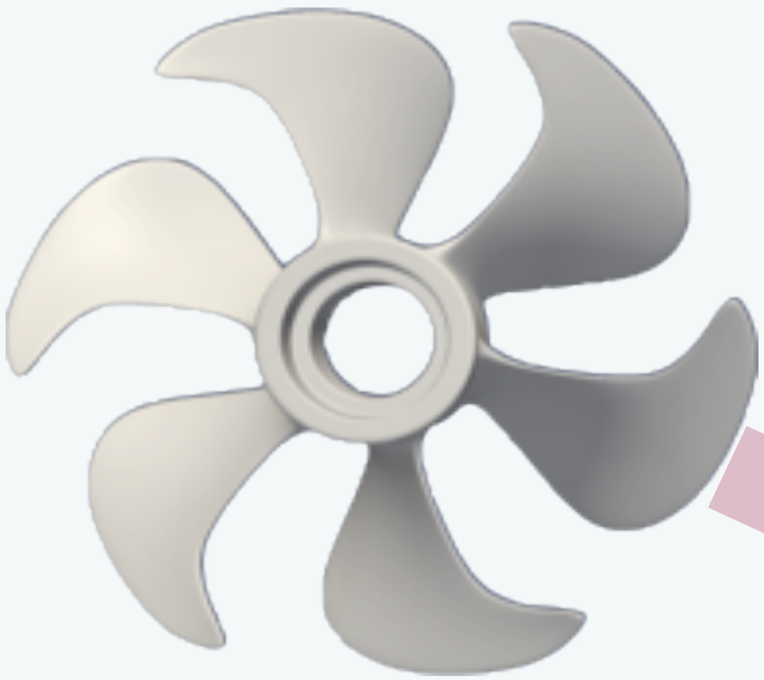

direct calculation

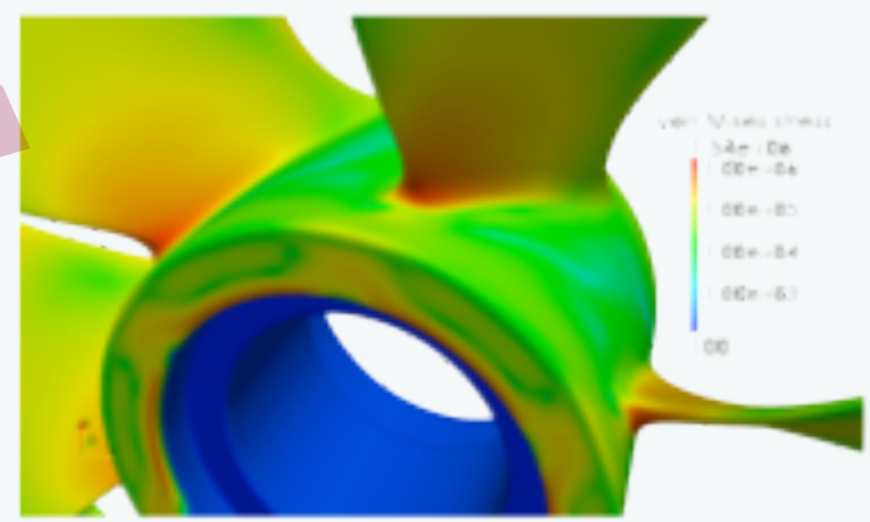

stress analysis

- Isogeometric analysis: CAD, finite elements, NURBS, exact geometry and mesh refinement (CMAME05, T.J.R Hughes et al)
- Isogeometric boundary element analysis using unstructured T-splines (CMAME13, M.A. Scott et al)

Isogeometric analysis

CAD: described by NURBS

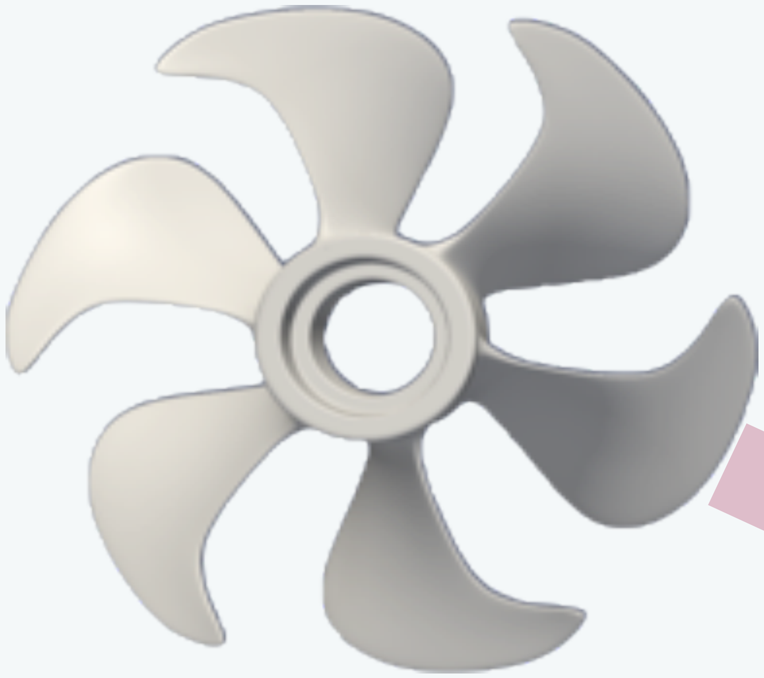

Use NURBS as basis functions

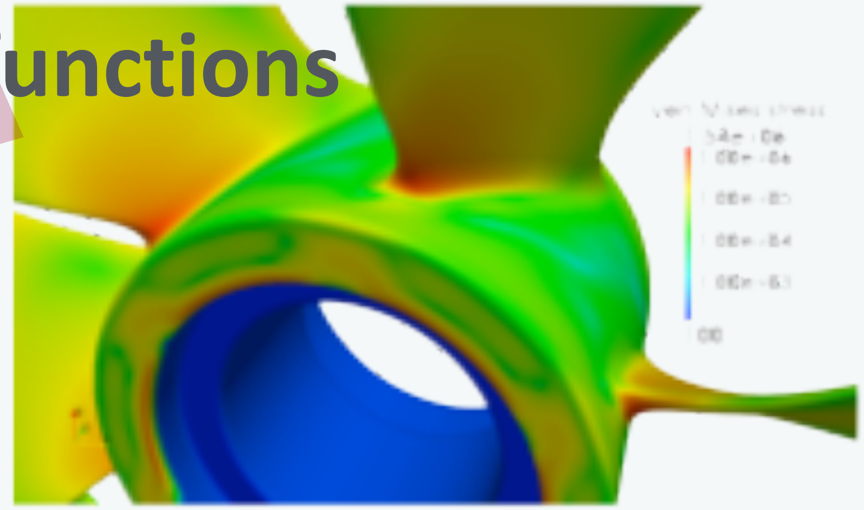

stress analysis

- Isogeometric analysis: CAD, finite elements, NURBS, exact geometry and mesh refinement (CMAME05, T.J.R Hughes et al)
- Isogeometric boundary element analysis using unstructured T-splines (CMAME13, M.A. Scott et al)

CAD techniques

NURBS

Universality.
Industrial standard.
Not watertight.
No local refinement

Fig. 1: NURBS
(source: Rhino3D website)

T-splines

Water tight.
Local refinement.
No trimming operations.
No linear independence.

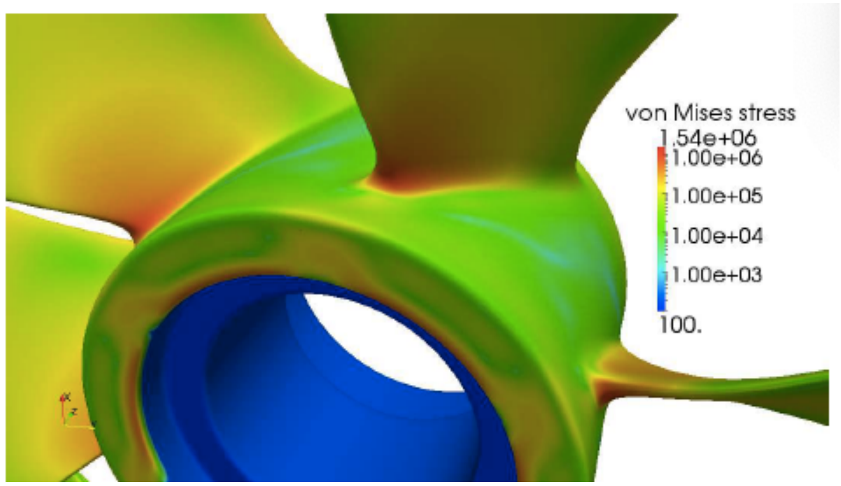

Fig. 2: T-splines

Subdivision Surfaces

Watertight.
Flexibility.
3D printing.
Low order smoothness.

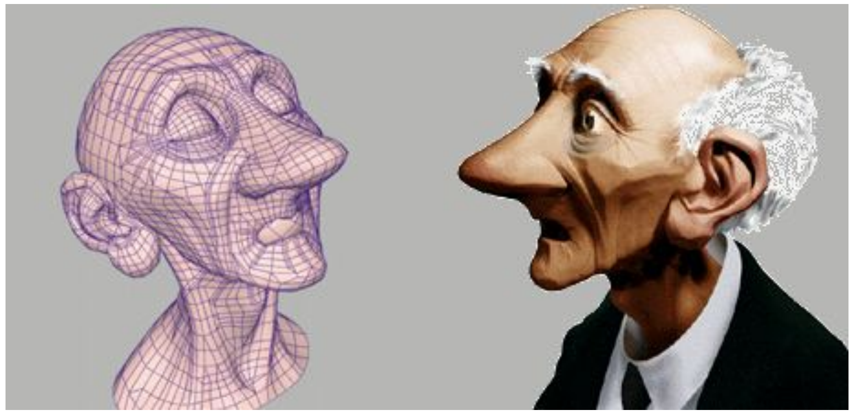

Fig. 3: Subdivision surfaces
(source: Geri's game)

All are boundary representations

[Isogeometric analysis: an overview and computer implementation aspects](#)
VP Nguyen, C Anitescu, SPA Bordas, T Rabczuk
Mathematics and Computers in Simulation 117, 89-116

NURBS

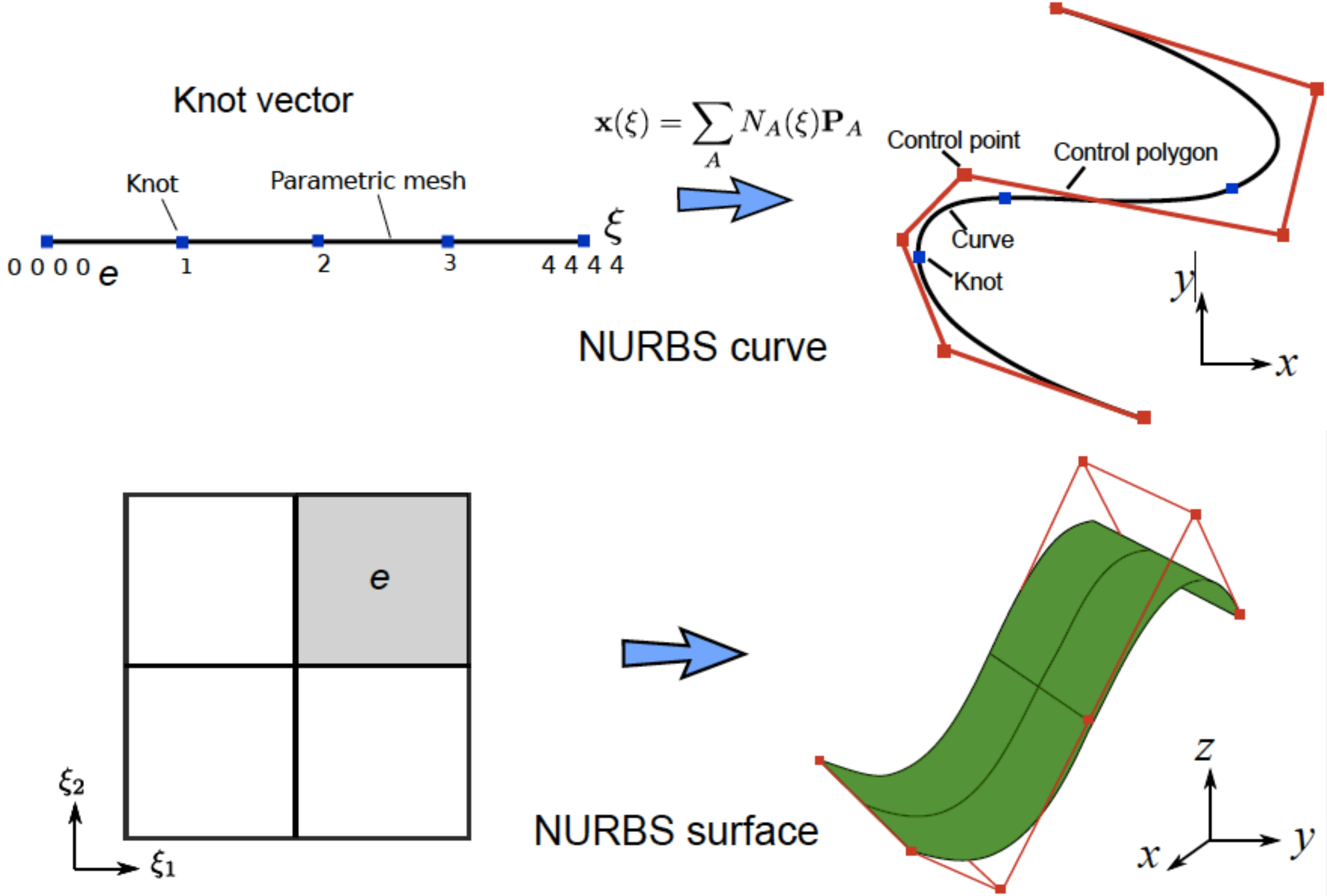
Knot vector
Knot
Parametric mesh
ξ
0 0 0 0 e 1 2 3 4 4 4 4
$\mathbf{x}(\xi) = \sum_A N_A(\xi)\mathbf{P}_A$
Control point
Control polygon
Curve
Knot
y
x
NURBS curve
e
ξ_2
ξ_1
NURBS surface
z
x
y

NURBS

T-splines

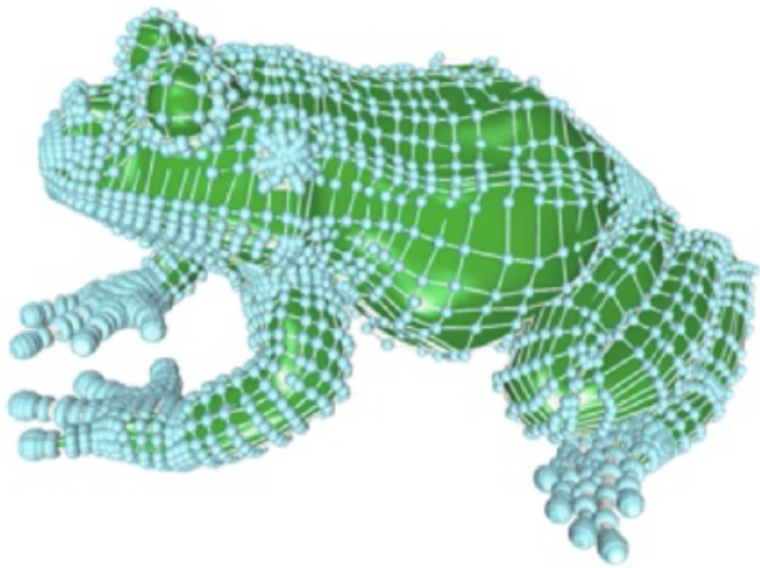

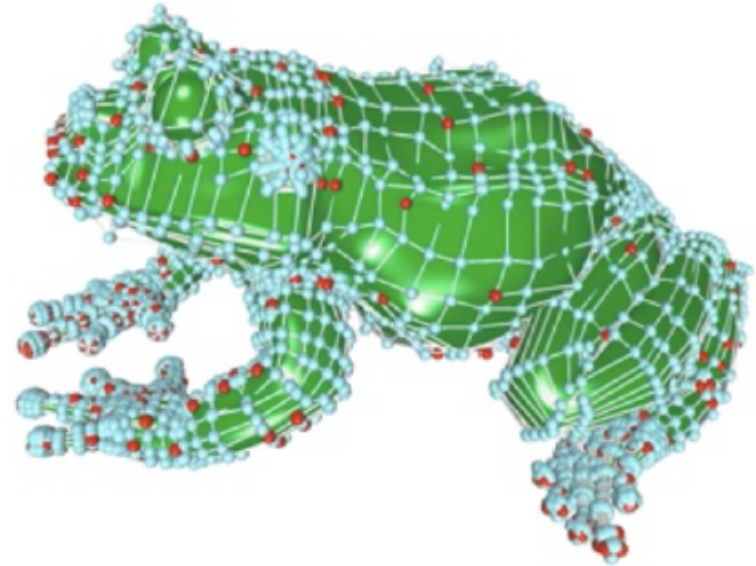

Fewer control points for the same geometry

Fig. 1: NURBS(source: Rhino3D website)

Fig. 2: T-splines(source: Rhino3D website)

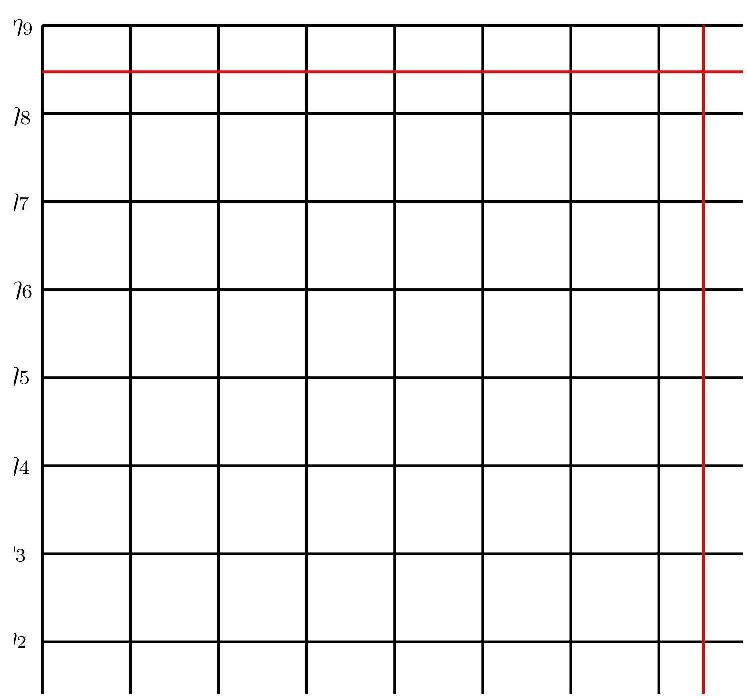

Fig. 3: NURBS mesh topology

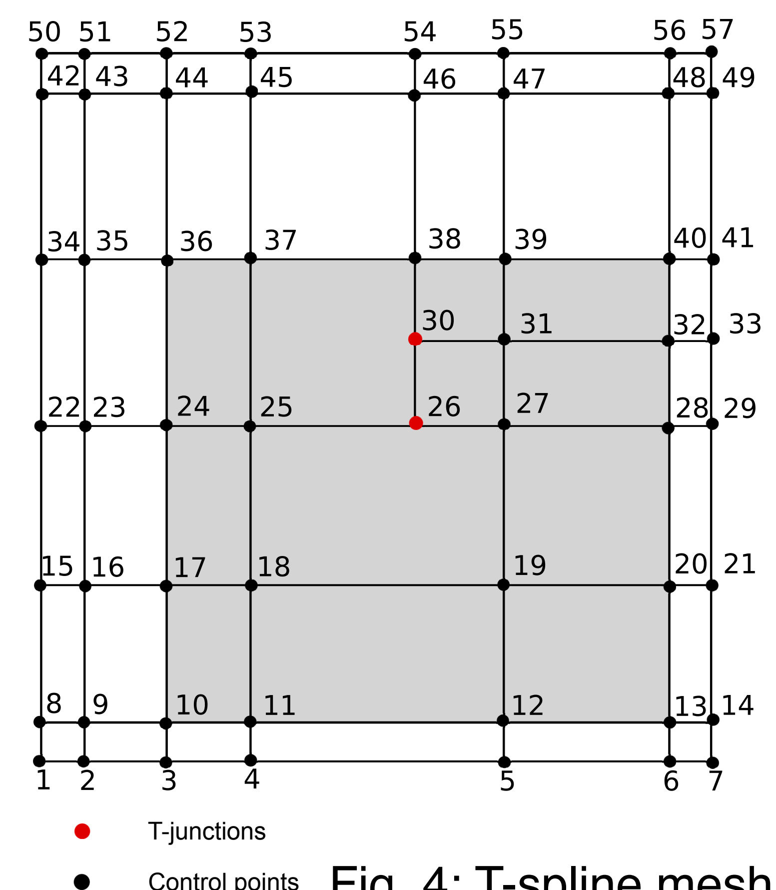

Fig. 4: T-spline mesh

Difficulties

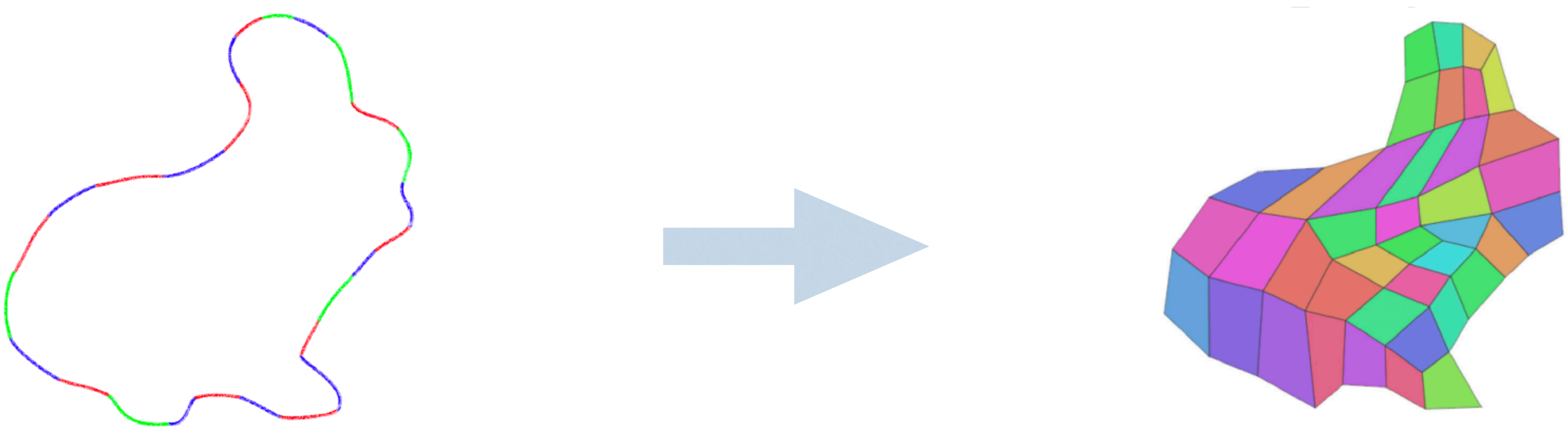

Given by CAD **Needed by IGAFEM**

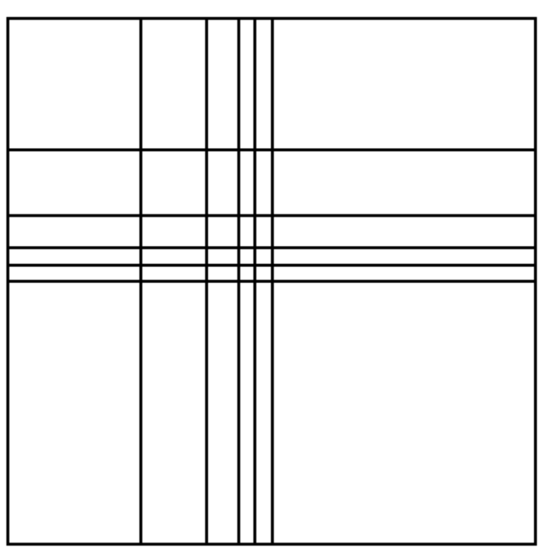

Local refinement

Patch coupling

IGABEM vs. IGAFEM

Question: How can we fully benefit from the "IGA" concept?

☑ Suppress the mesh generation and regeneration completely

Isogeometric FEM

☑ For shell-like domains

☐ For volumes (needs volume parameterisation, aka meshing)

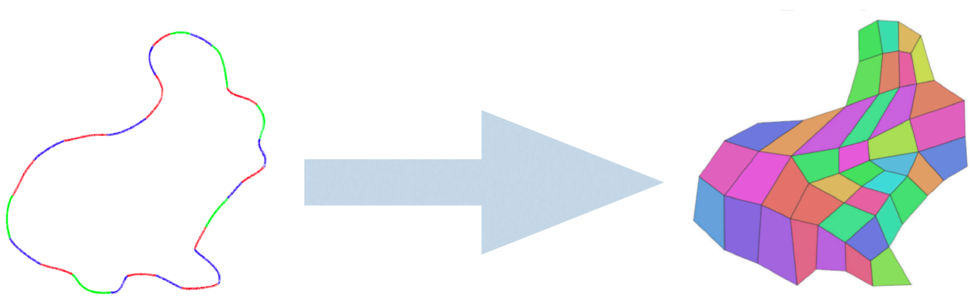

Stress analysis and shape optimisation directly from CAD

H. Lian et al. (2017). CMAME*:* 317: 1-41.

H. Lian et al. (2015). IJNME

H. Lian et al. (2013). EACM:166(2):88-99.

M. Scott et al. (2013) CMAME 254: 197-221.

R. N. Simpson et al. (2013) CAS 118: 2-12.

R. N. Simpson et al. (2012) CMAME Feb 1;209:87-100.

Isogeometric BEM

☑ For shell-like domains

☑ For volumes

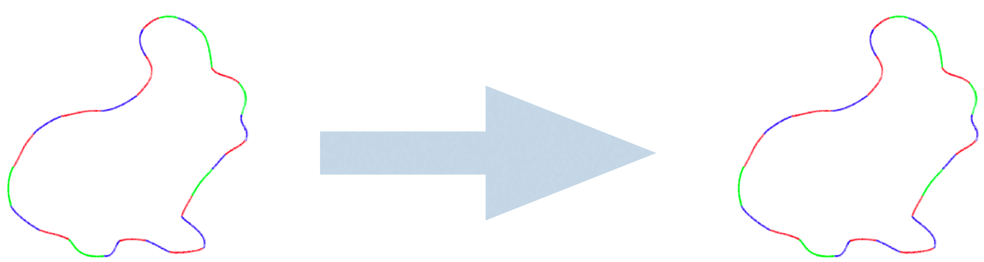

Fracture mechanics directly from CAD

X. Peng, et al. (2017). *IJF*, 204(1), 55–78.

X. Peng, et al. (2017). *CMAME*, 316, 151–185.

Nitsche's method for two and three dimensional NURBS **patch coupling** (CMECH2014, Nguyen)

Skew-symmetric Nitsche's formulation in isogeometric analysis: Dirichlet and symmetry conditions, **patch coupling** and frictionless **contact** (Qu, Chouly, Bordas…)

Stéphane Pierre Alain BORDAS, Department of Computational Engineering & Sciences University of Luxembourg and Cardiff University

Mesh refinement in NURBS-IGA

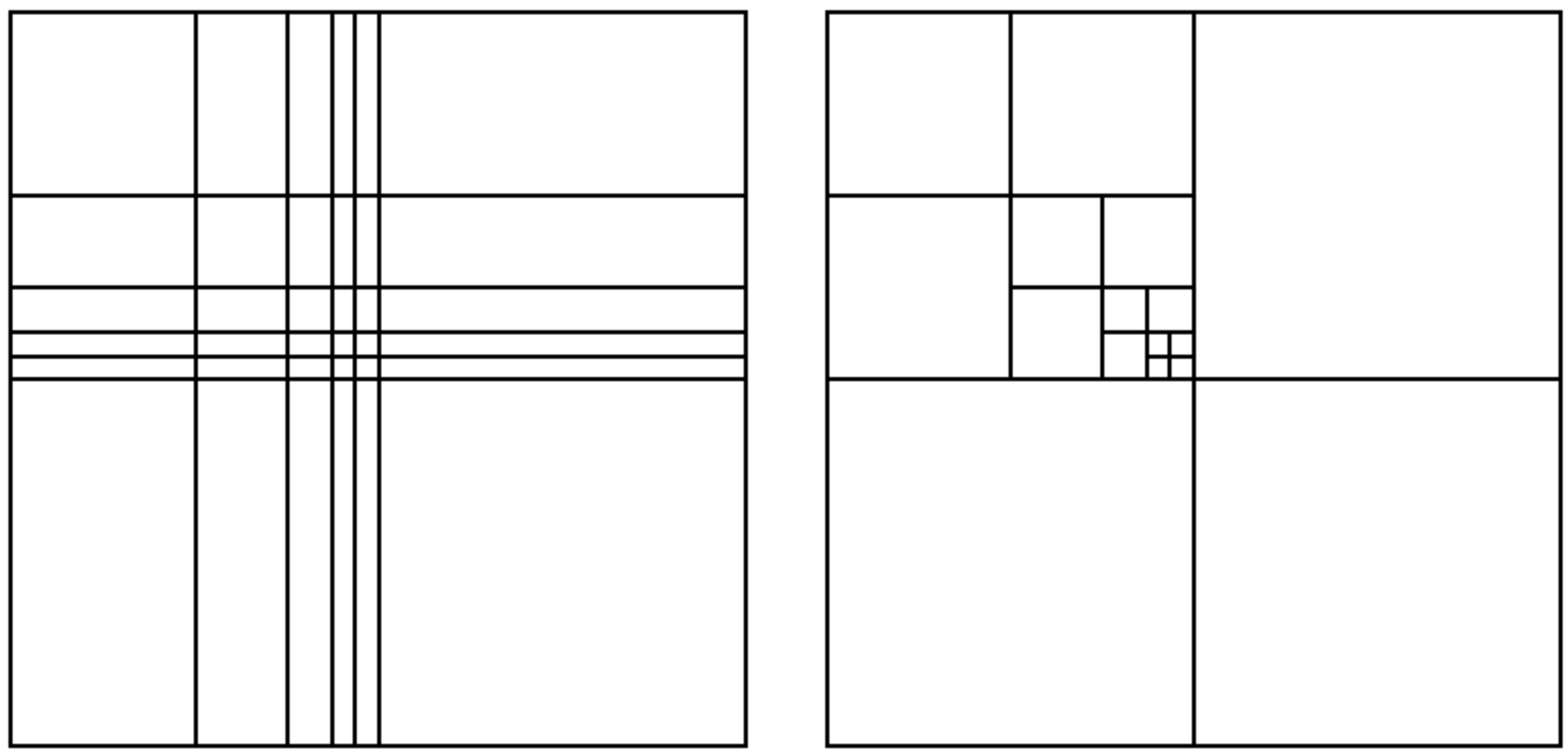

Global refinement (tensor-product mesh) vs local refinement (T-mesh)

Stéphane Pierre Alain BORDAS, Department of Computational Engineering & Sciences University of Luxembourg and Cardiff University

GIFT/sub/super-geometric approach

Question: How can we fully benefit from the “IGA” concept?

☑ Refine the field approximation independently from the geometry

Geometry Independent Field approximaTion (GIFT)

☑ Super/Sub-geometric

Boundary Element Analysis with trimmed NURBS and a generalized IGA approach
G Beer, B Marussig, J Zechner, C Dünser, TP Fries (2014)
arXiv preprint arXiv:1406.3499

Fast isogeometric boundary element method based on independent field approximation
B Marussig, J Zechner, G Beer, TP Fries
Computer Methods in Applied Mechanics and Engineering 284, 458-488 (2015)

Atroshchenko, E, et al. "Weakening the tight coupling between geometry and simulation in isogeometric analysis: From sub-and super-geometric analysis to Geometry-Independent Field approximaTion (GIFT)." International Journal for Numerical Methods in Engineering 114.10 (2018): 1131-1159.

Permalink: http://hdl.handle.net/10993/31469

Isogeometric analysis

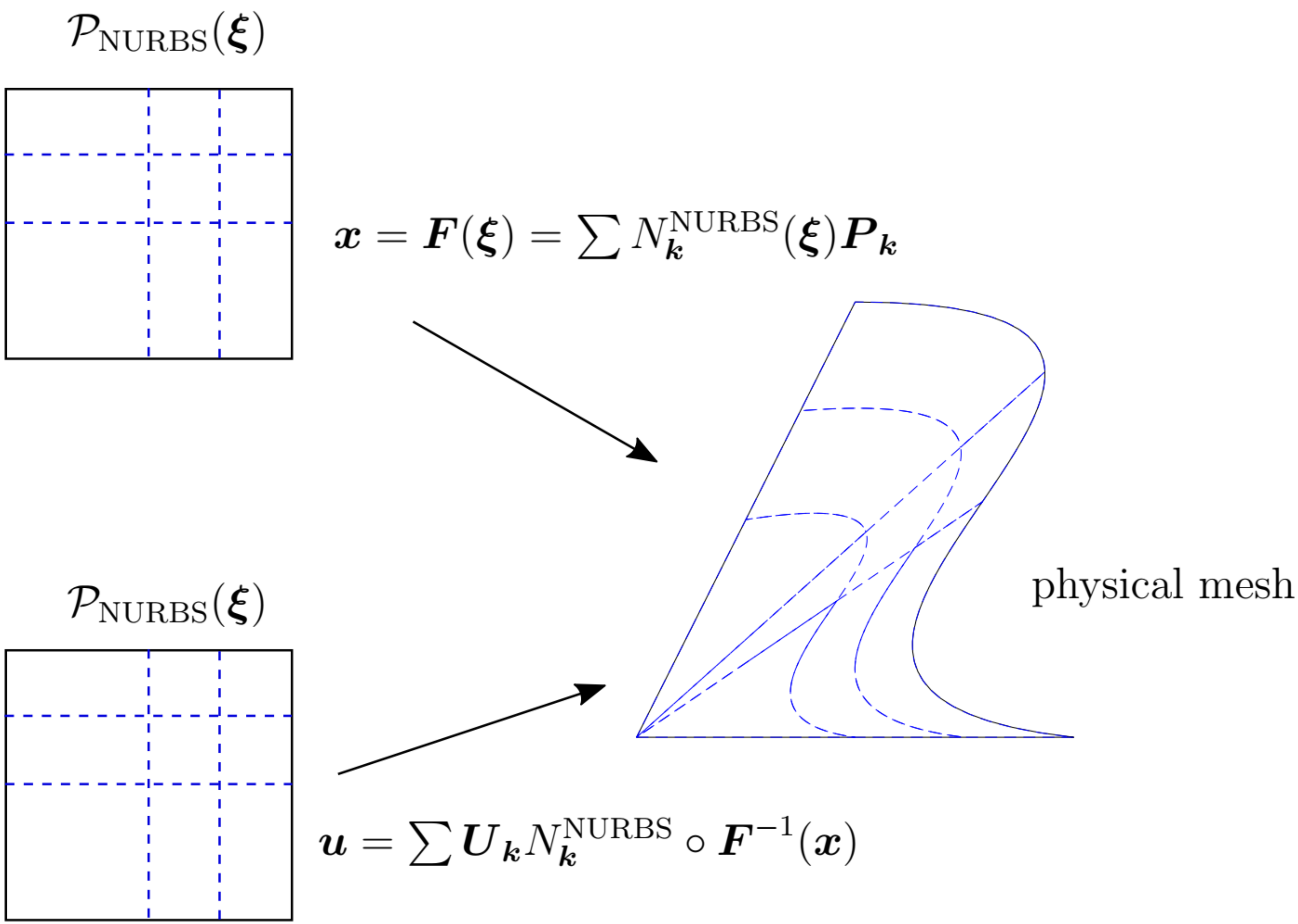

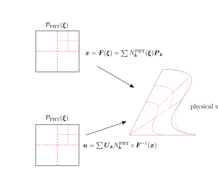

Atroshchenko, E, et al. International Journal for Numerical Methods in Engineering 114.10 (2018): 1131-1159.

Isogeometric analysis - PHT

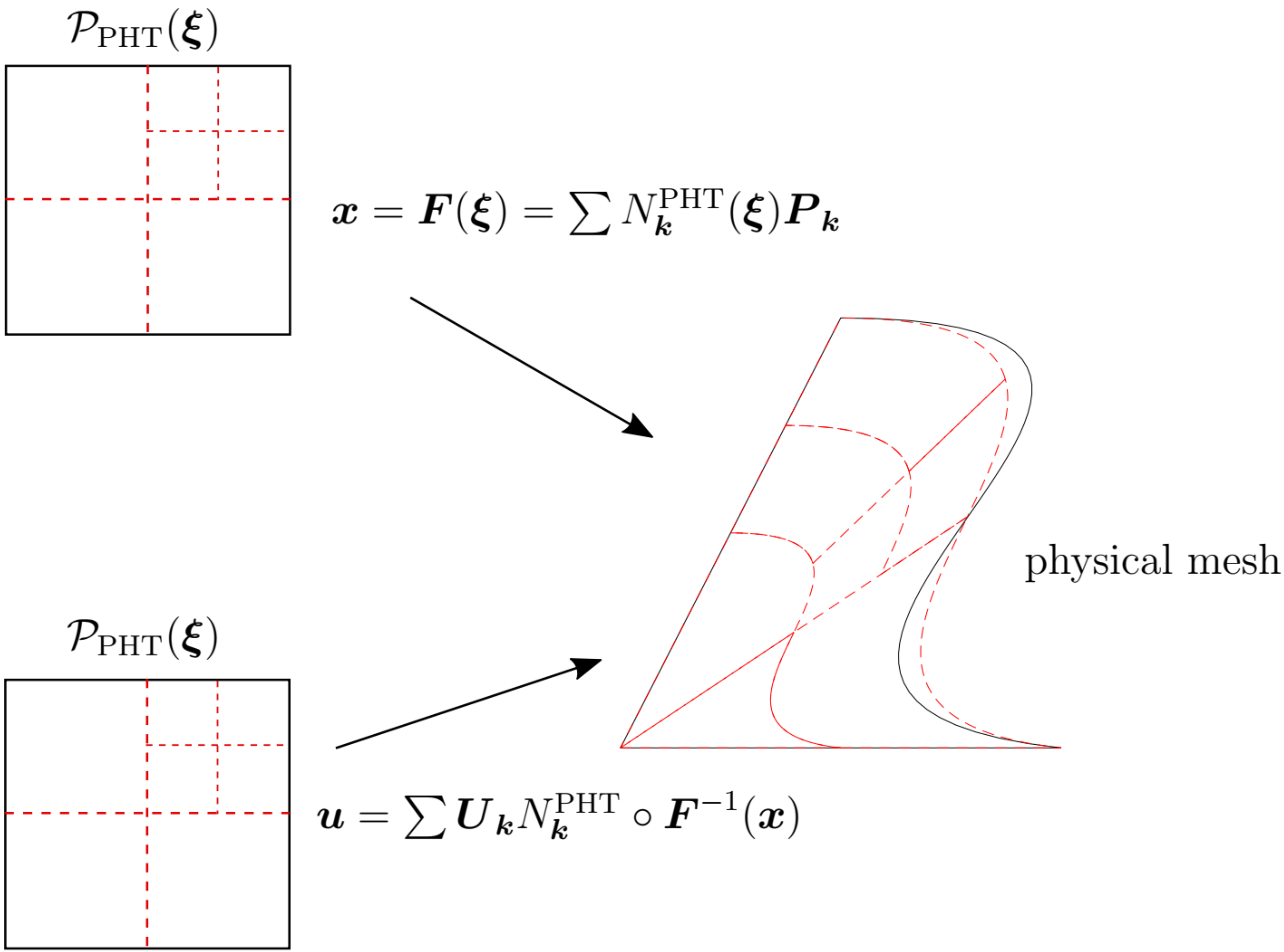

$$\boldsymbol{x} = \boldsymbol{F}(\boldsymbol{\xi}) = \sum N_{\boldsymbol{k}}^{\mathrm{PHT}}(\boldsymbol{\xi})\boldsymbol{P}_{\boldsymbol{k}}$$

$$\boldsymbol{u} = \sum \boldsymbol{U}_{\boldsymbol{k}} N_{\boldsymbol{k}}^{\mathrm{PHT}} \circ \boldsymbol{F}^{-1}(\boldsymbol{x})$$

Atroshchenko, E, et al. International Journal for Numerical Methods in Engineering 114.10 (2018): 1131-1159.

Geo-independent field approximaTion

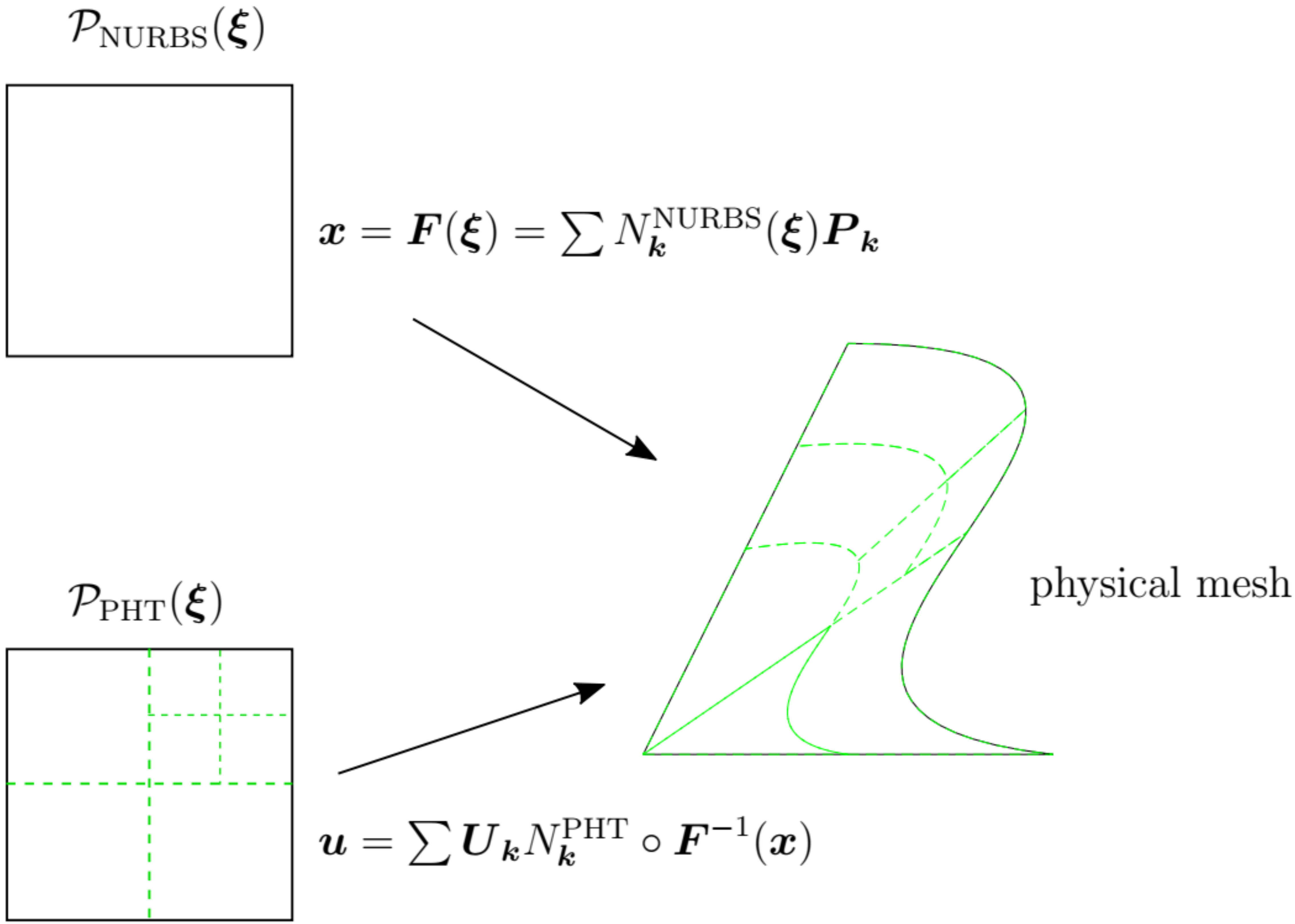

Atroshchenko, E, et al. International Journal for Numerical Methods in Engineering 114.10 (2018): 1131-1159.

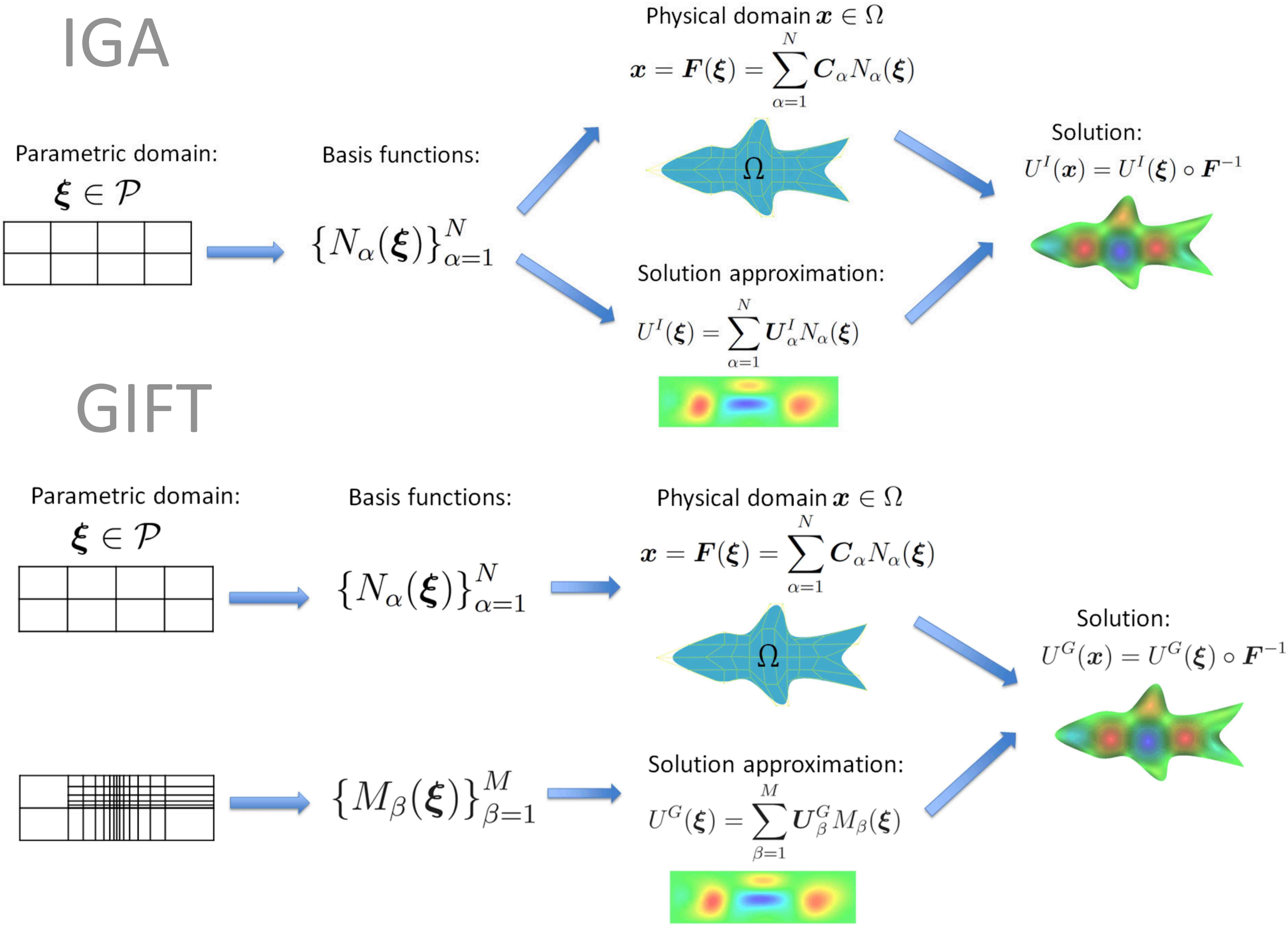

Atroshchenko, E, et al. International Journal for Numerical Methods in Engineering 114.10 (2018): 1131-1159.

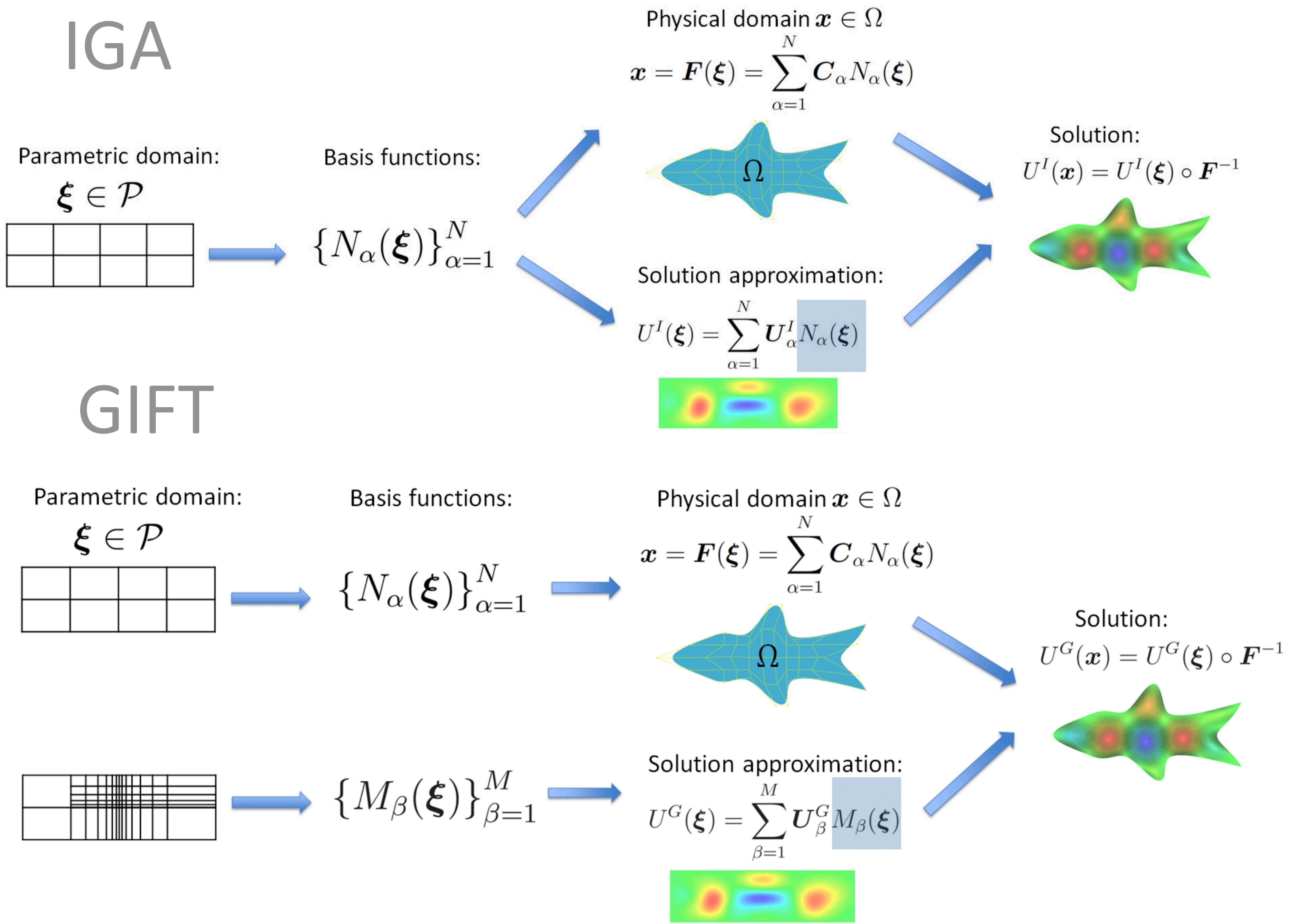

Atroshchenko, E, et al. International Journal for Numerical Methods in Engineering 114.10 (2018): 1131-1159.

Geometry parameterization	Solution basis	Degree parity	Patch test	Optimal convergence
Q_0	A_1	Iso-geometric	✓	✓
Q_0	A_2	Super-geometric	✓	✓
Q_0	C_1	Iso-geometric	×	✓
Q_0	C_2	Super-geometric	×	✓
A_1	A_1	Iso-geometric	✓	✓
A_1	A_2	Super-geometric	✓	✓
A_2	A_1	Sub-geometric	✓	✓
B_1	A_1	Iso-geometric	✓	✓
B_1	A_2	Super-geometric	✓	✓
B_2	A_1	Sub-geometric	✓	✓
C_1	C_1	Iso-geometric	✓	✓
C_1	C_2	Super-geometric	✓	✓
C_2	C_1	Sub-geometric	✓	✓
C_1	A_1	Iso-geometric	×	✓
C_1	A_2	Super-geometric	×	✓
C_2	A_1	Sub-geometric	×	✓
A_1	D_1	Iso-geometric	×	✓
A_1	D_2	Super-geometric	×	✓
A_1	D_0	Sub-geometric	×	✓

GIFT - key features

- ☑ The same basis functions, which are used in CAD to represent the geometry, are used in the IGA as shape functions to approximation the unknown solution
- ☑ Geometry is exact at any stage of the solution refinement process
- ☑ Better accuracy per DOF in comparison with Lagrange Iso-parametric FEM but higher computational cost (bandwidth…)

Numerical observations - no proof…

Together with the given (exact) geometry parametrization at the coarsest level, the convergence rate is entirely defined by the solution basis, and does not depend on the further refinement of the geometry parametrization:

- For a given geometry parameterization, the degree of the solution basis can be increased or decreased without changing the degree of the geometry (from iso-geometric to super-geometric and sub-geometric elements)
- For solution approximation, using same degree B-Splines or NURBS yields almost identical results

Adaptive/enriched GIFT - FEM/BEM

Adaptive GIFT for Helmholtz

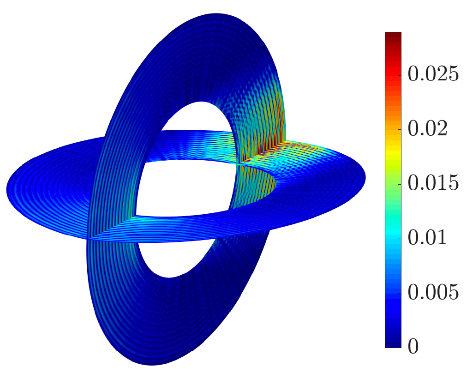

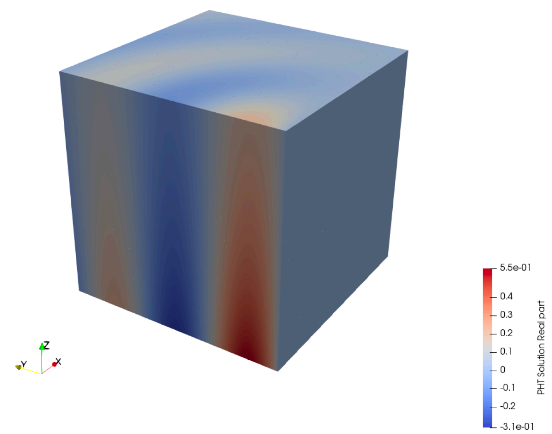

Figure 21: The unit cube problem: numerical solution for $k = 10$ and $n = 1$.

Crack growth

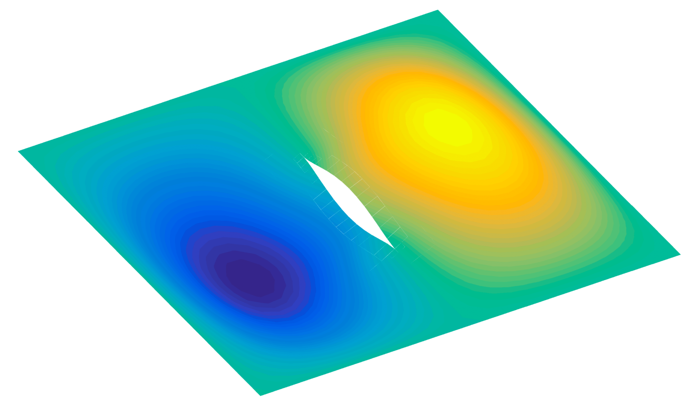

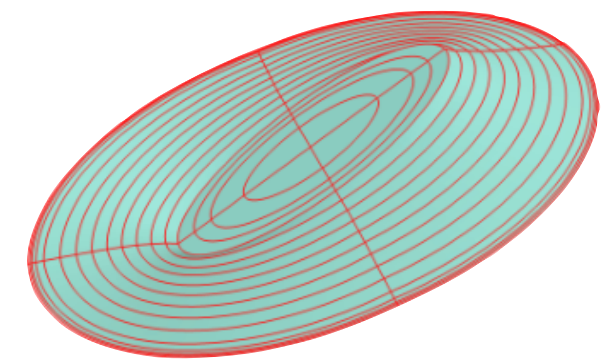

No meshing/remeshing

Space-time adaptivity

$$Q(u) = \int_0^T \int_{\partial\Omega_Q} u e_x w(t) d\Gamma dt$$

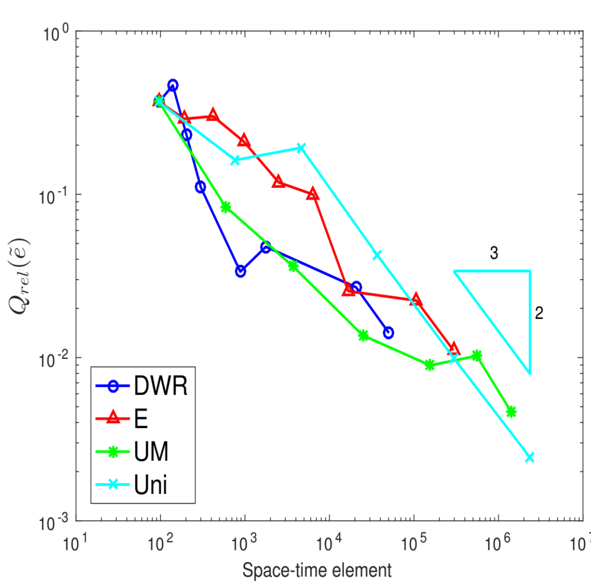

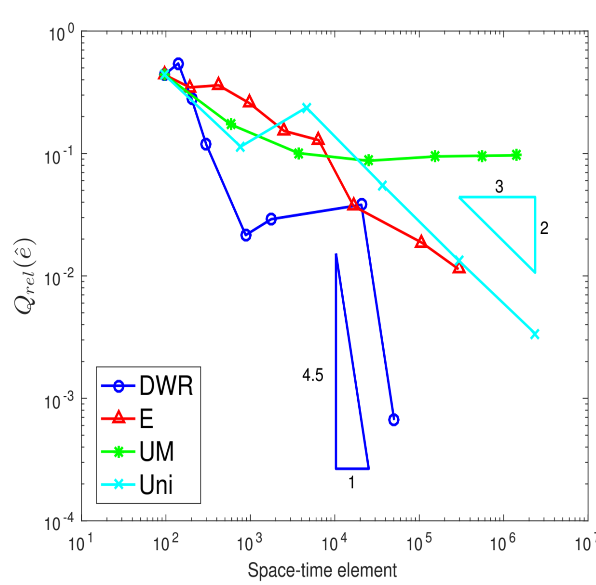

Shape optimisation elasticity & acoustics

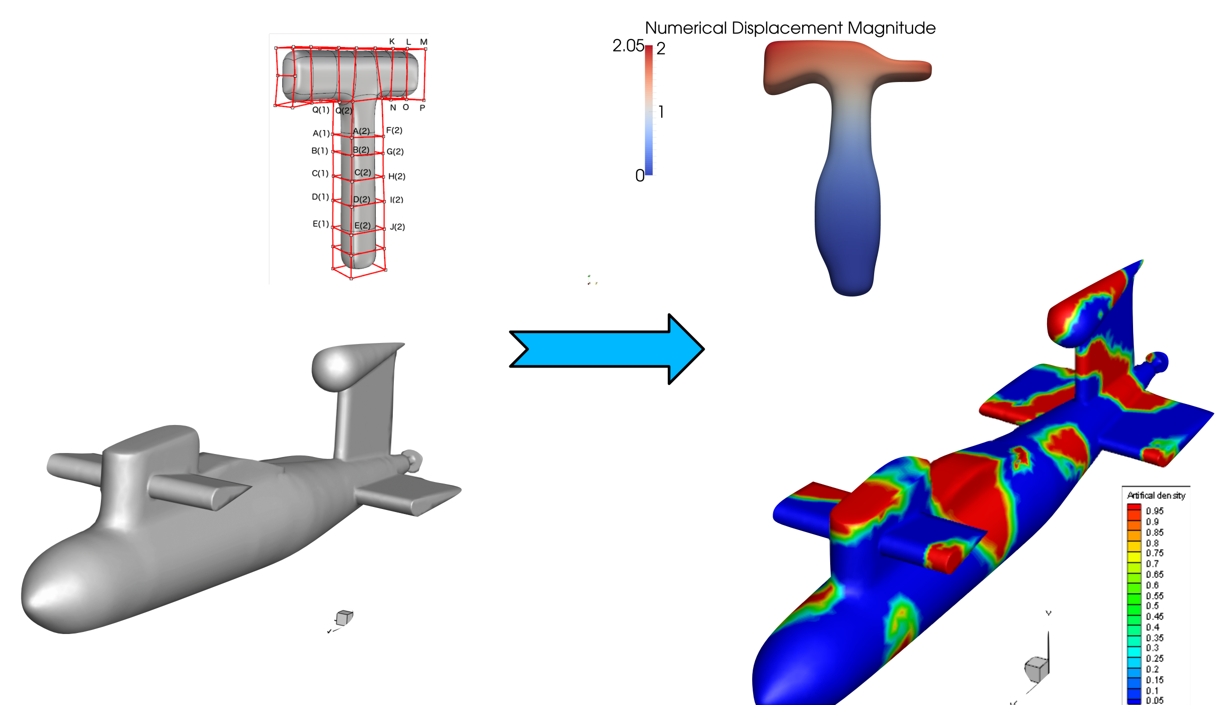

Control variables = control points

Stéphane Pierre Alain BORDAS, Department of Computational Engineering & Sciences University of Luxembourg and Cardiff University

Adaptive GIFT-Helmholtz

- Residual-based and recovery based error indicators perform similarly
- Optimal convergence rates
- Adaptivity is effective only for “fine meshes”
- Failure in the “pre-asymptotic range” where effectivity per dof deteriorates

$$\frac{kh}{p} < 1$$

h– and p– adaptivity driven by recovery and residual-based error estimators for PHT-splines applied to time-harmonic acoustics Videla, Anitescu, Khajah, Bordas, Atroshchenko, 2019

Plane-wave enriched Partition of Unity GIFT for Helmholtz equation with PHT-Splines Videla, Tomar, Bordas, Atroshchenko, 2019

Structural optimisation with IGABEM

Employ the same basis functions in CAD to discretize Boundary Integral Equations (BIE) :

$$C_{ij}(\mathbf{s})u_j(\mathbf{s}) + \int_S T_{ij}(\mathbf{s},\mathbf{x})u_j(\mathbf{x})\mathrm{d}S(\mathbf{x}) = \int_S U_{ij}(\mathbf{s},\mathbf{x})t_j(\mathbf{x})\mathrm{d}S(\mathbf{x})$$

1. Seamlessly compatible with CAD due to boundary representation.
2. CAD in and CAD out. (Fig. 2)
3. Infinite domain: acoustics, electro-magnetics.

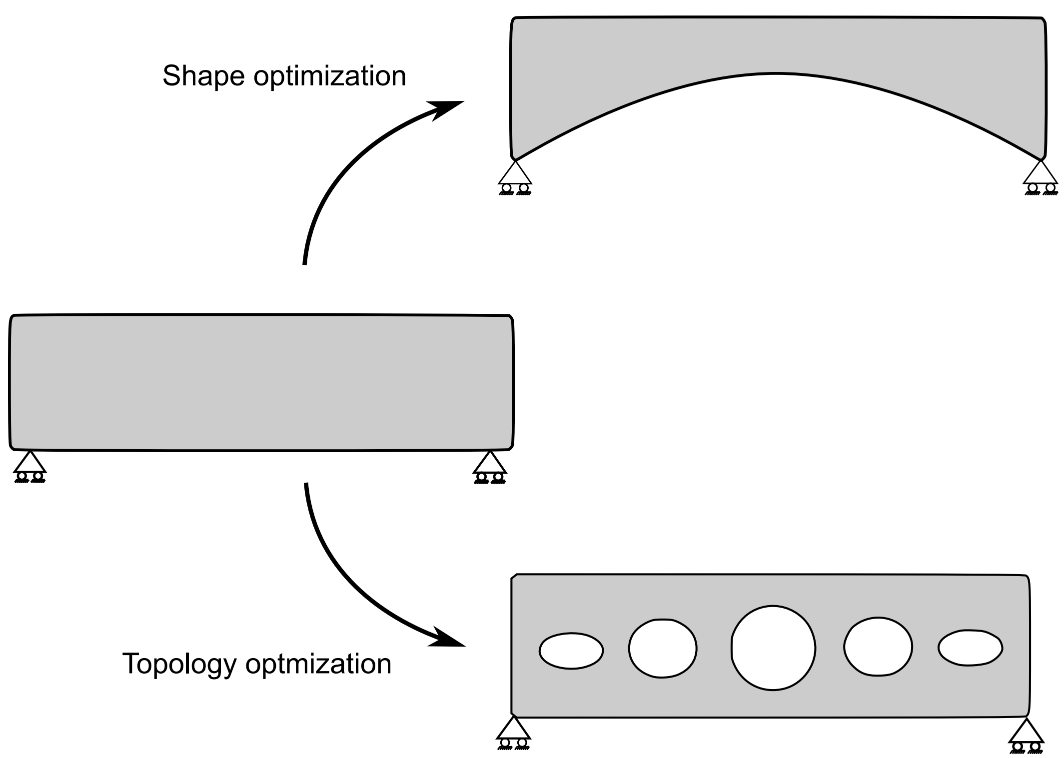

Fig. 1: Structural optimisation

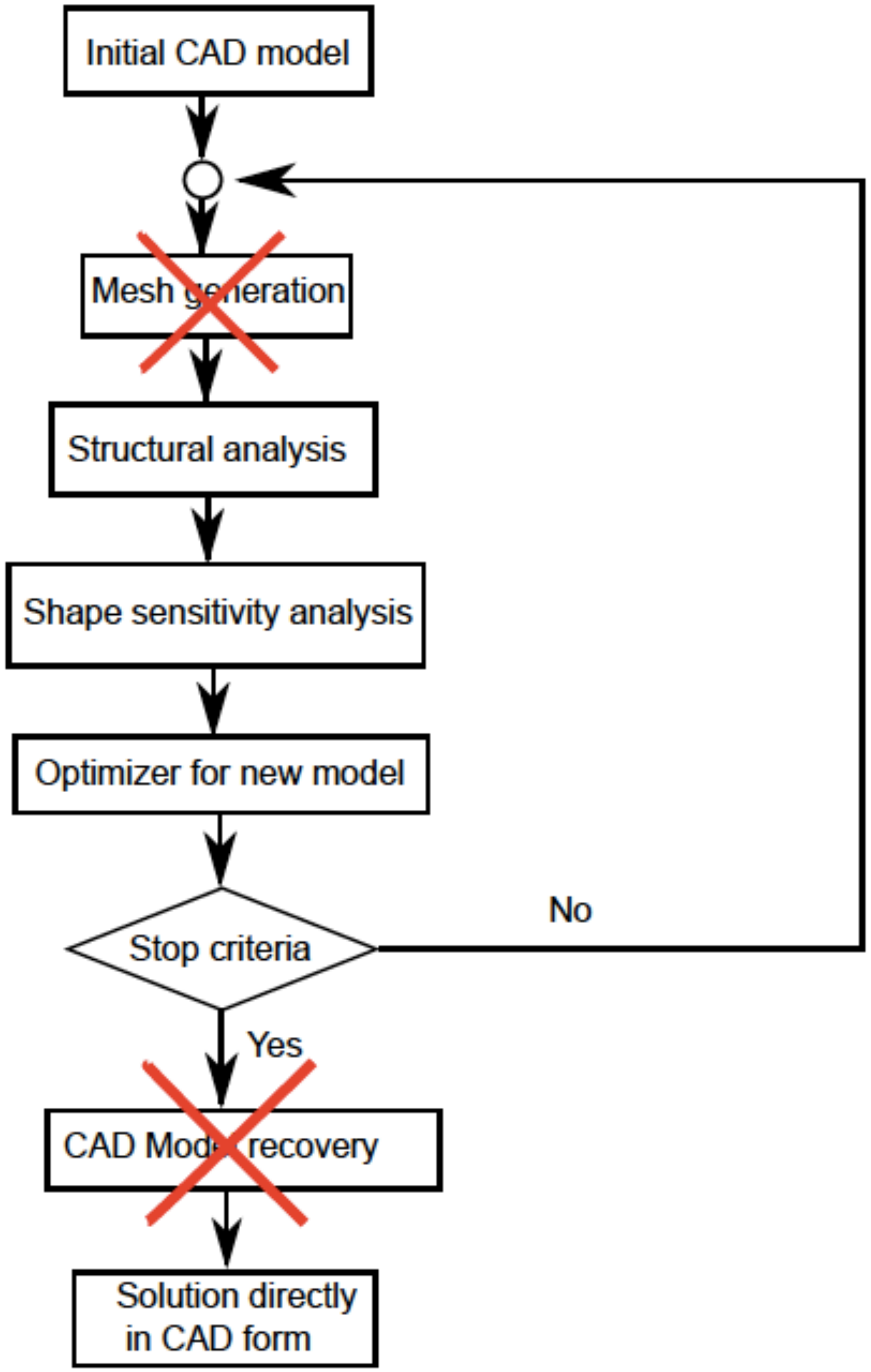

Fig. 2: IGABEM structural optimisation

H. Lian et al. (2017). CMAME: 317: 1-41. — H. Lian et al. (2015). IJNME — H. Lian et al. (2013). EACM:166(2):88-99.

Elastic shape optimisation using IGABEM with T-splines

CAD in & CAD out!

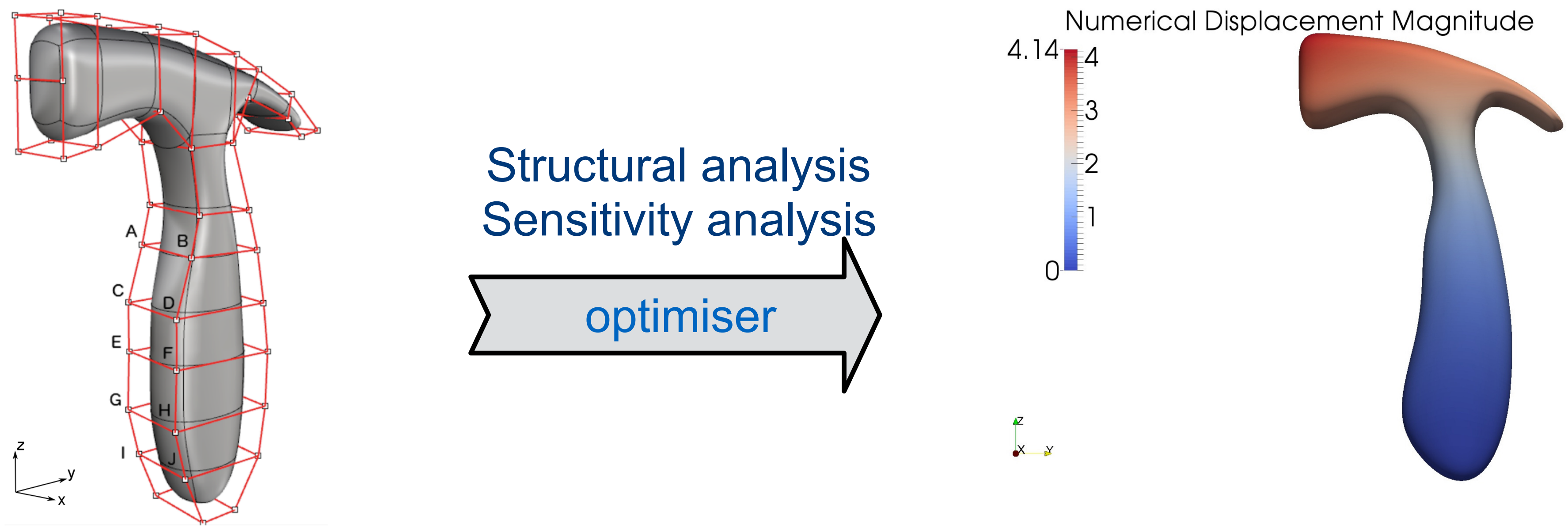

Fig. 1: T-spline model of a hammer (left: initial geometry; right: optimised geometry)

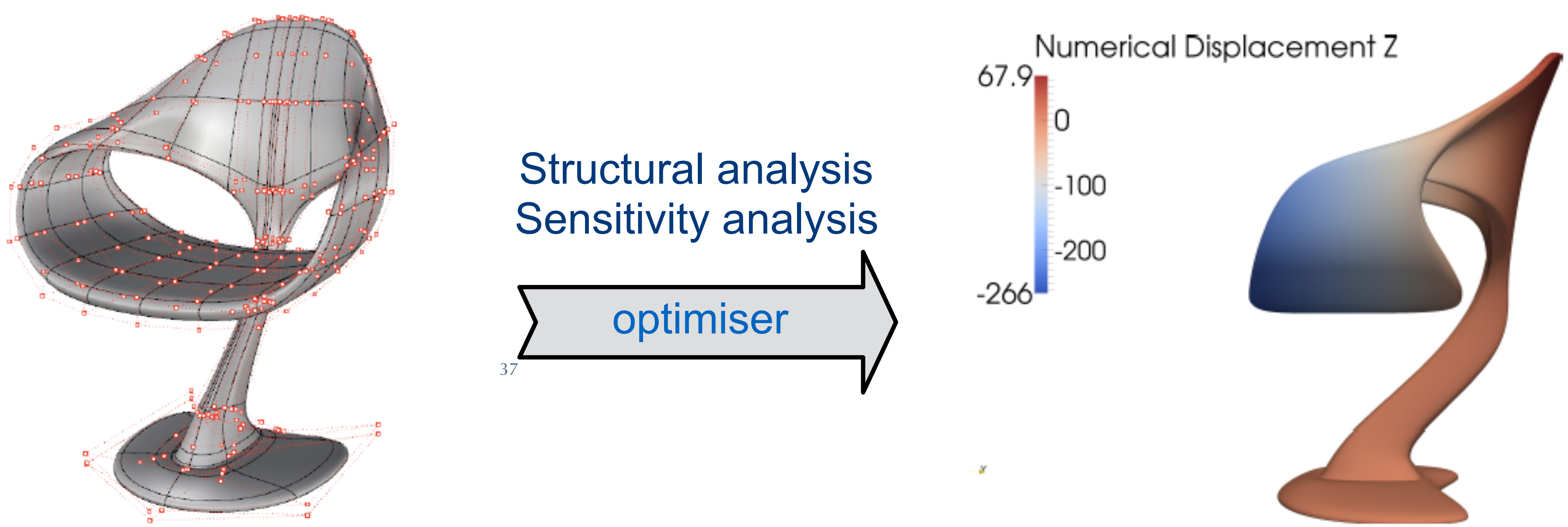

Fig. 2: T-spline model of a chair (left: initial geometry; right: optimised geometry)

H. Lian et al. (2017). CMAME: 317: 1-41. — H. Lian et al. (2015). IJNME — H. Lian et al. (2013). EACM:166(2):88-99.

Acoustic shape optimisation using IGABEM with NURBS

Exterior infinite domain problems!

$$\begin{cases} \min & \Pi_\rho = \overline{\mathbf{p}}_f \mathbf{p}_f \\ \text{s.t.} & A(\mathbf{x}) - A_0 \leqslant 0 \\ & x^{i,l} \leqslant x^i \leqslant x^{i,u}, \quad i = 1, 2, \ldots, N_x, \end{cases}$$

$$\frac{\partial \Pi_\rho}{\partial \vartheta} = \frac{\partial \left(\overline{\mathbf{p}}_f \mathbf{p}_f\right)}{\partial \vartheta} = 2\Re\left(\overline{\mathbf{p}}_f \frac{\partial \mathbf{p}_f}{\partial \vartheta}\right)$$

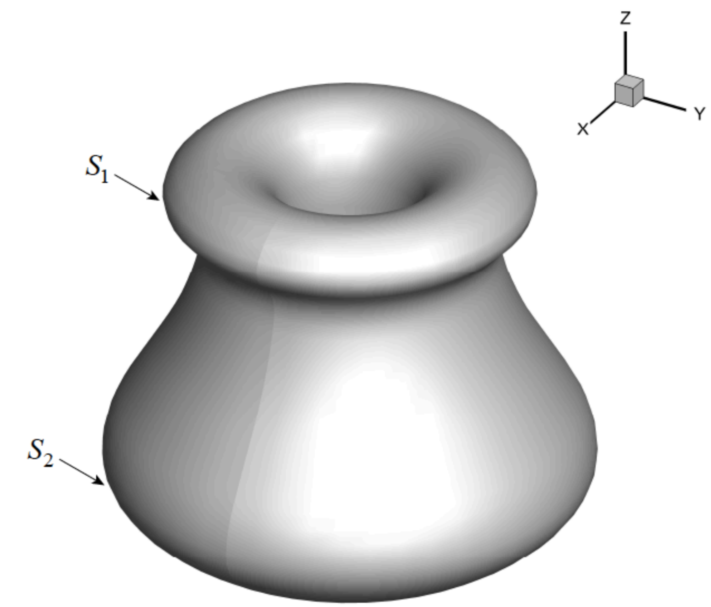

Fig. 1: Vase model with NURBS

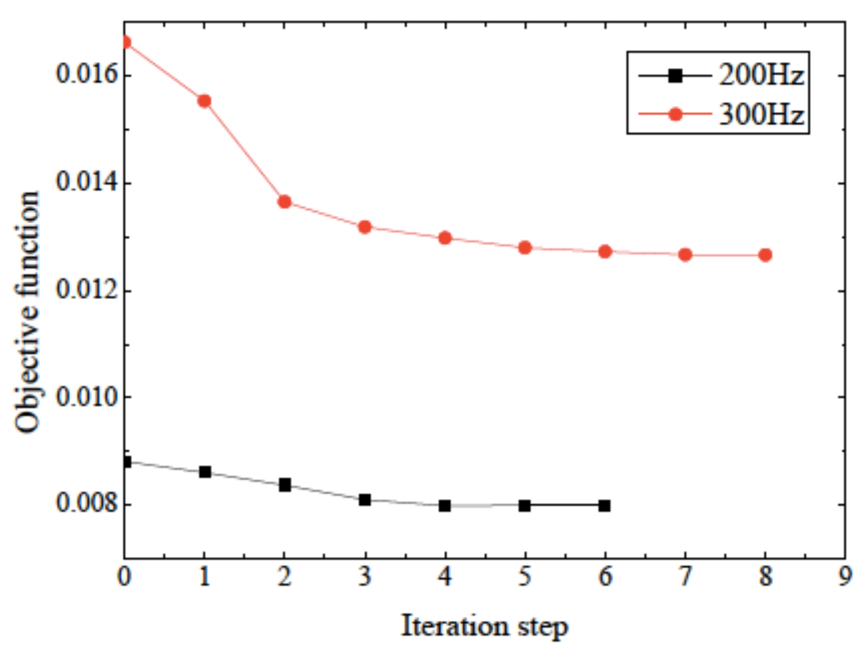

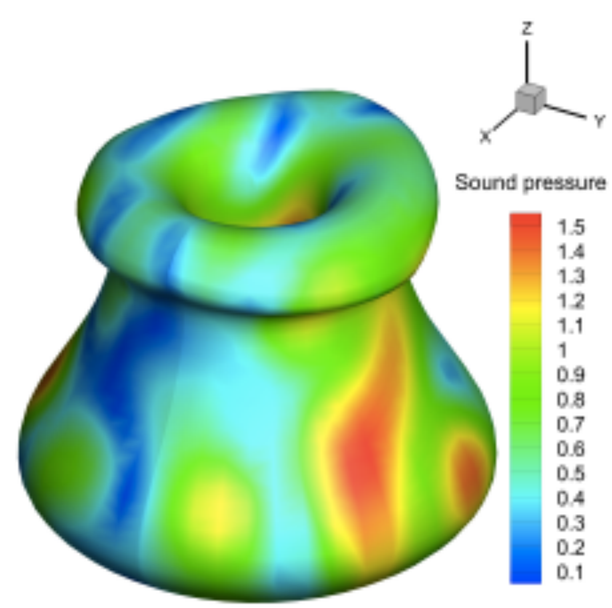

Fig. 2: Optimised model (f=100Hz)

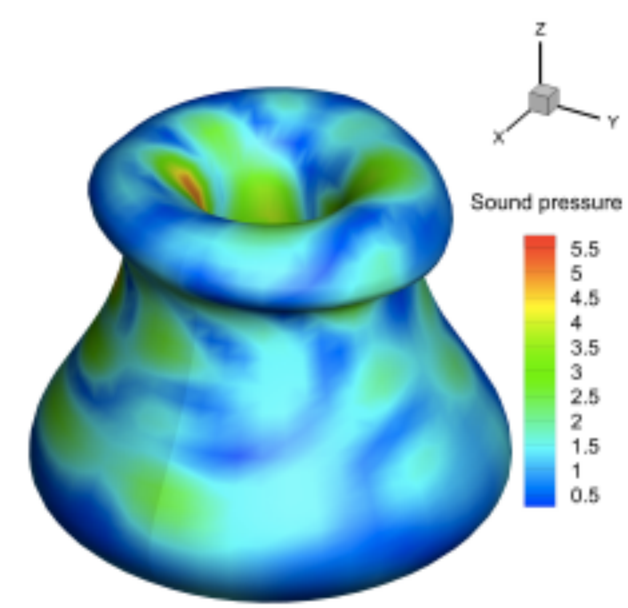

Fig. 3: Optimised model (f=300Hz)

H. Lian et al. (2017). CMAME*:* 317: 1-41. — H. Lian et al. (2015). IJNME — H. Lian et al. (2013). EACM:166(2):88-99.

Acoustic topology optimisation using IGABEM with subdivision surfaces

Exterior infinite domain problems!

$$
\begin{cases}
\min & \Pi_\rho = \overline{\mathbf{p}}_f \mathbf{p}_f \\
\text{s.t.} & \displaystyle\sum_{e=1}^{N_e} \rho_e v_e - V_0 \leqslant 0 \\
& 0 \leqslant \rho_{\min} \leqslant \rho_e \leqslant 1
\end{cases}
$$

$$
\beta_i = \beta_0 \rho_i^n + \beta_1 (1 - \rho_i^n), \quad 0 \leqslant \rho_i \leqslant 1
$$

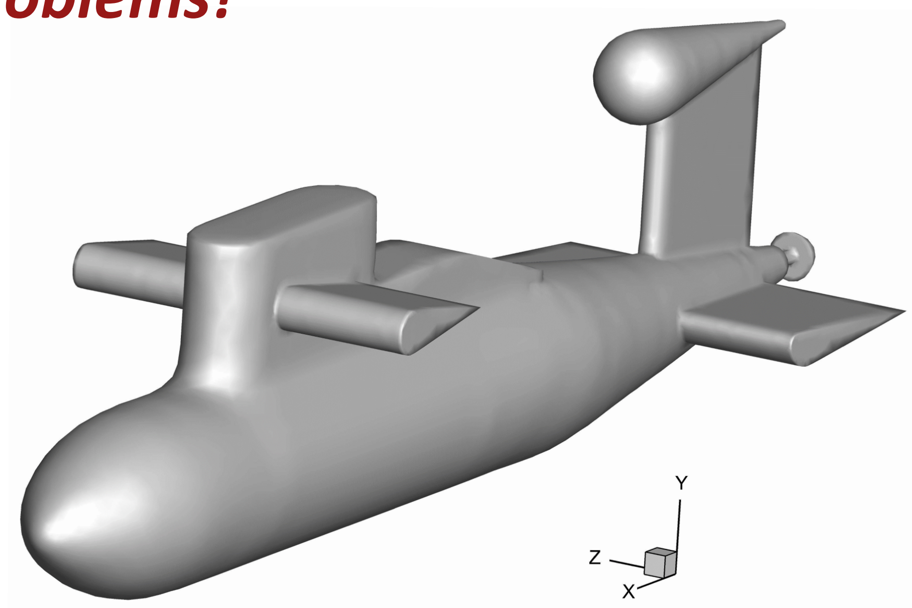

Fig. 1: Submarine model

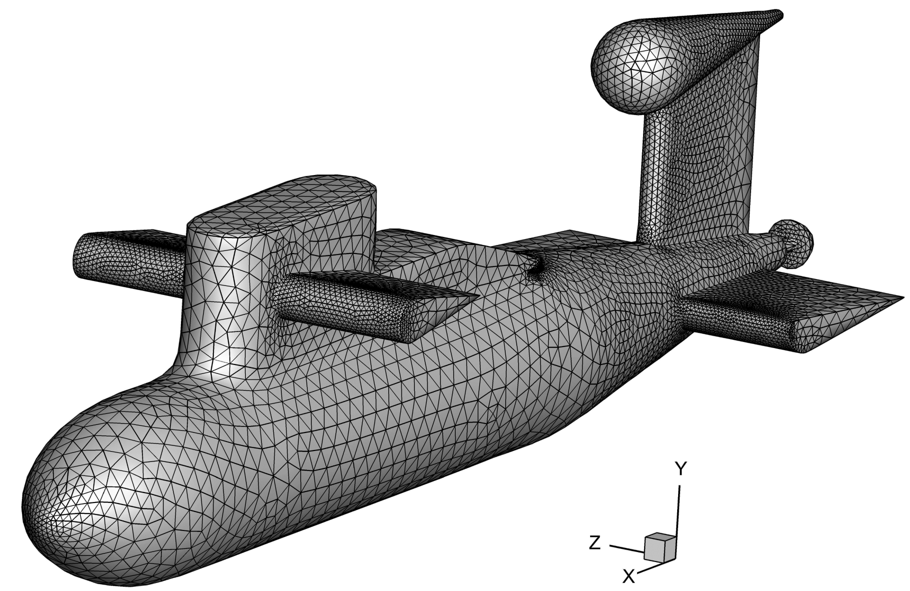

Fig. 2: Model with subdivision surfaces

problems appear naturally

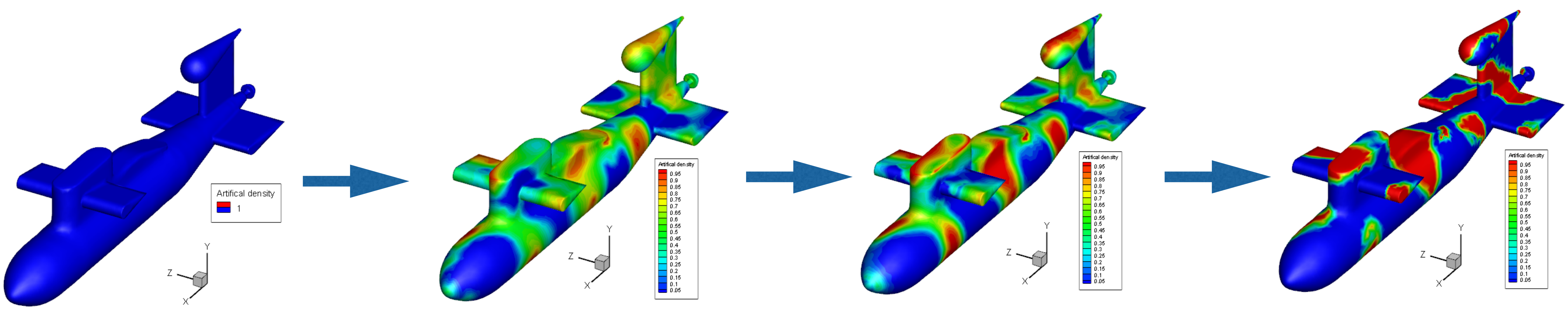

(a) Step 1 (b) Step 5 (c) Step 10 (a) Step 44

Fig. 3: Sound absorbing material distribution during Iteration

H. Lian et al. (2017). CMAME*:* 317: 1-41. — H. Lian et al. (2015). IJNME — H. Lian et al. (2013). EACM:166(2):88-99.

Acoustic topology optimisation using IGABEM with subdivision surfaces

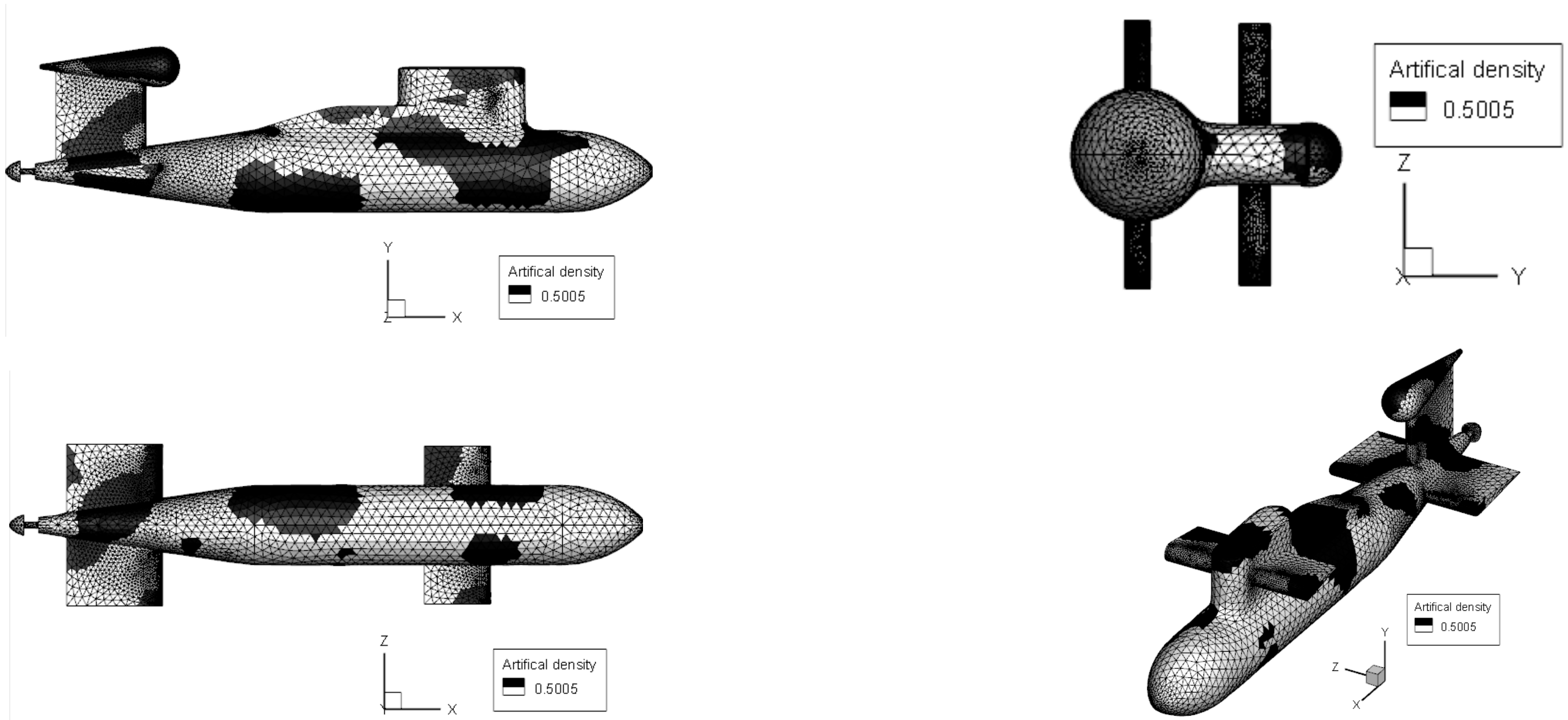

Fig. 1: The optimised sound adsorbing material distribution
(black: adhesion to sound absorbing materials; white: no adhesion)

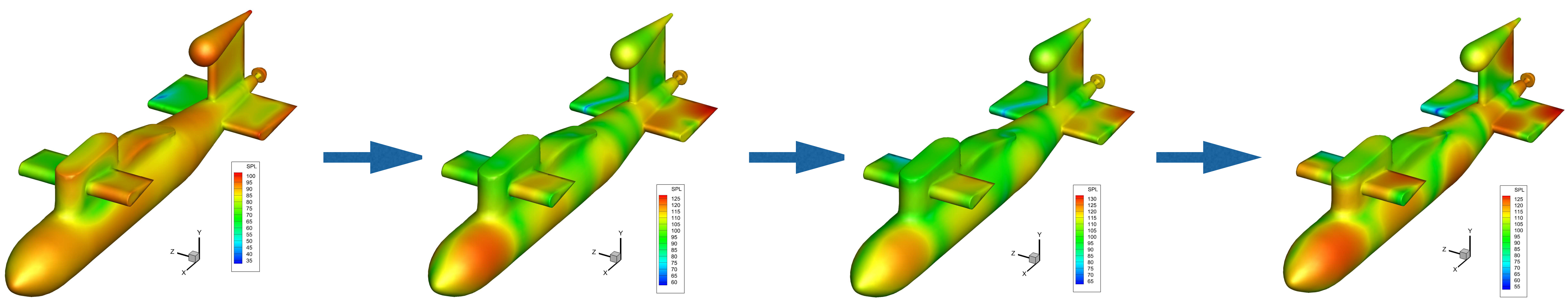

(a) Step 1 (b) Step 5 (c) Step 10 (d) Step 44

Fig. 2: The sound pressure distribution during Iteration

H. Lian et al. (2017). CMAME*:* 317: 1-41. — H. Lian et al. (2015). IJNME — H. Lian et al. (2013). EACM:166(2):88-99.

GIFT - key features

- ☑ Retain advantages of IGA, but **decouple** the geometry and field approximation
- ☑ Standard patch tests may not always pass, yet the **convergence rates are optimal** as long as the geometry is exactly represented by the geometry basis
- ☑ With geometry exactly represented by NURBS, using same degree B-splines or NURBS for the approximation of the solution field yields almost identical results
- ☑ With geometry exactly represented by NURBS, using **PHT splines** for the approximation of the solution gives additional advantage of local adaptive refinement
- ☑ Any other approximation field can be used for the field variables

Open source software

Bauhaus Universität

https://github.com/canitesc/IGAPack

University of Luxembourg

http://www.legato-team.eu

FEniCS

fenics project

```
mu = Constant(0.3)
…
S = (t**3/12)*(2.0*mu*K + \
    (2.0*mu*lmbda)/(2.0*mu + lmbda)*tr(K)*Identity(2))
```

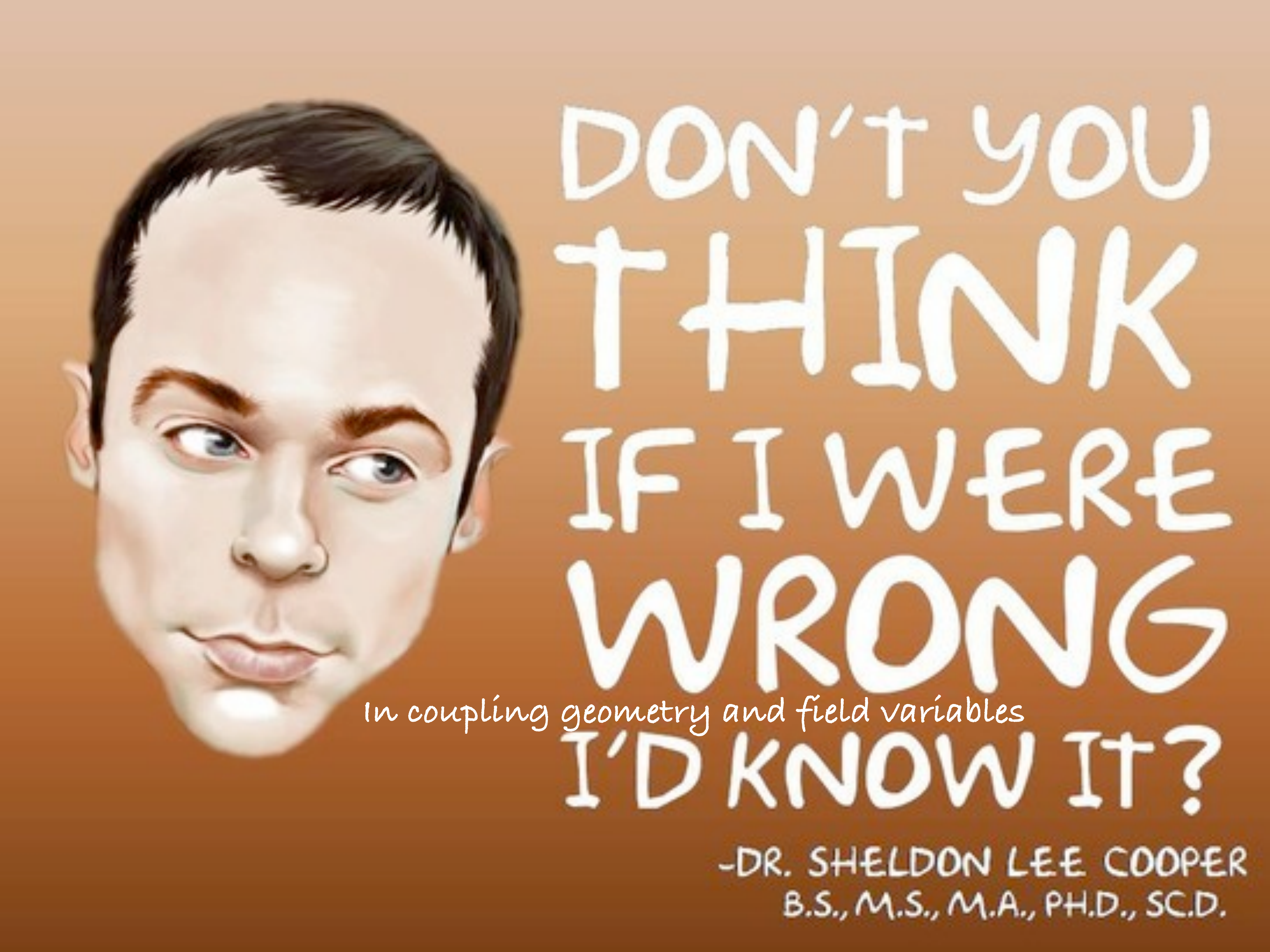
DON'T YOU
THINK
IF I WERE
WRONG
In coupling geometry and field variables
I'D KNOW IT?
-DR. SHELDON LEE COOPER
B.S., M.S., M.A., PH.D., SC.D.

Real-time simulations with XFEM

SKIP

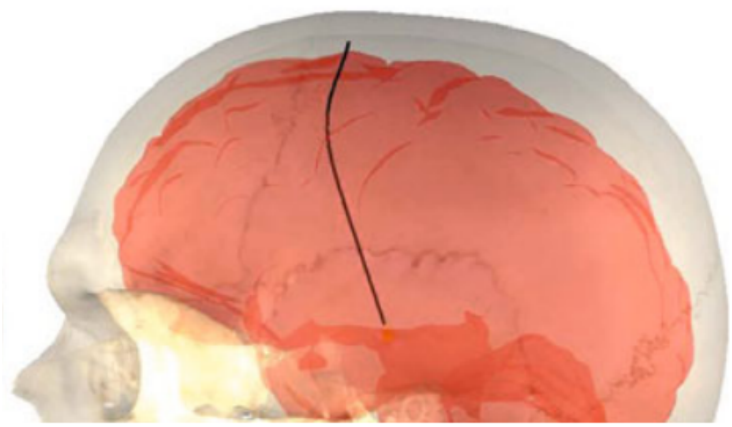

Bilger et al, MICCAI, 2011

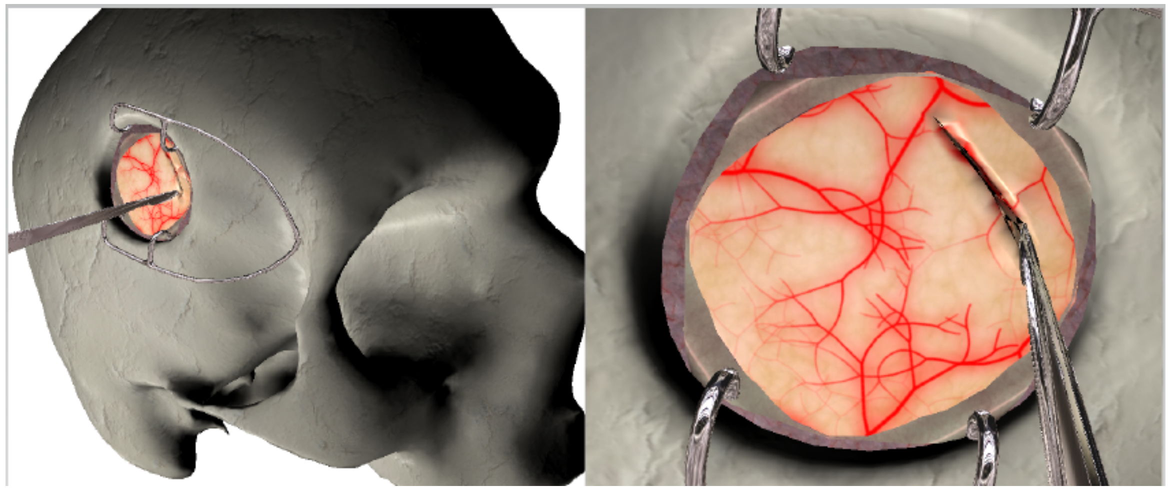

Courtecuisse et al, Med. Image Anal., 2014

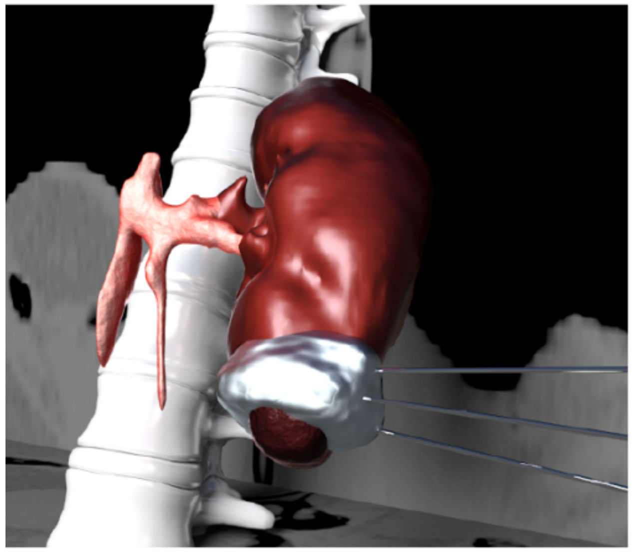

Talbot et al, SIGGRAPH, 2015

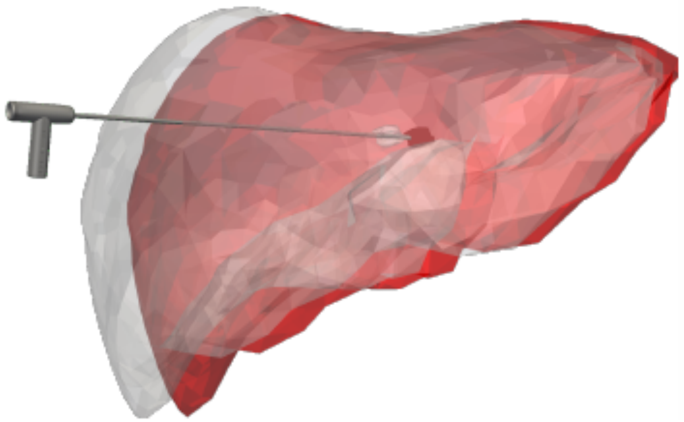

Hamzé et al, Comput. Med. Imag. Grap. 2015

H.P. Bui

erc RealTCut

Cut FE method/XFEM

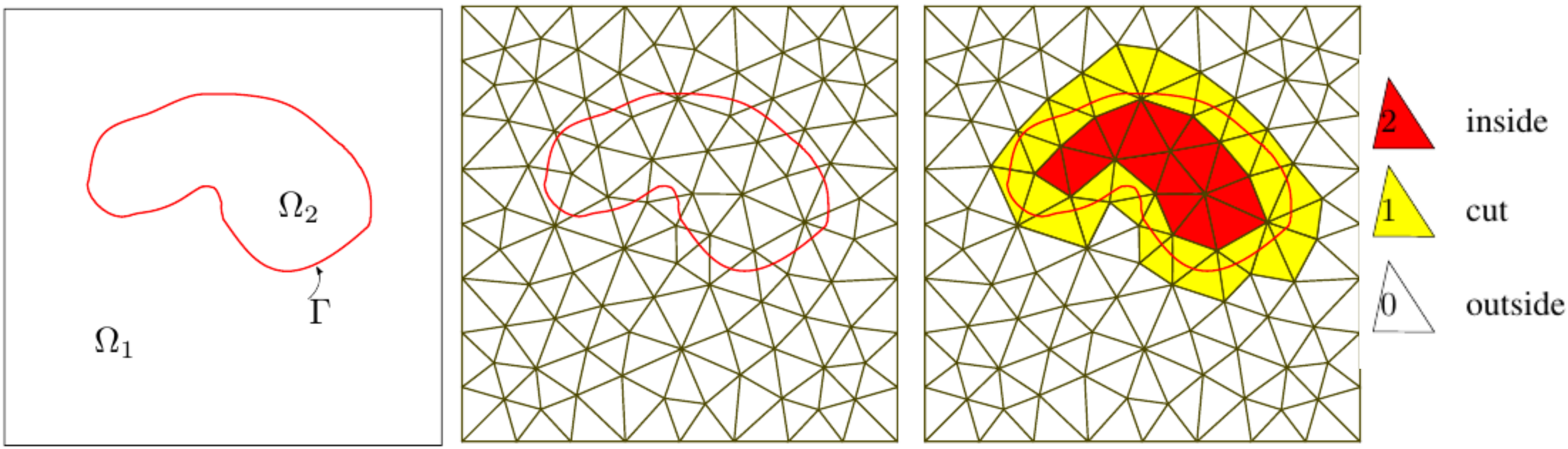

- ❑ Fictitious **Boundary** Method

- ❑ Implicit (unfitted) **Interface**: interface problems, moving boundary problems

Real-time Error Control for Surgical Simulation, HP Bui et al, IEEE Trans. Biomed. Eng., 2016.

erc RealTCut

Limit cases

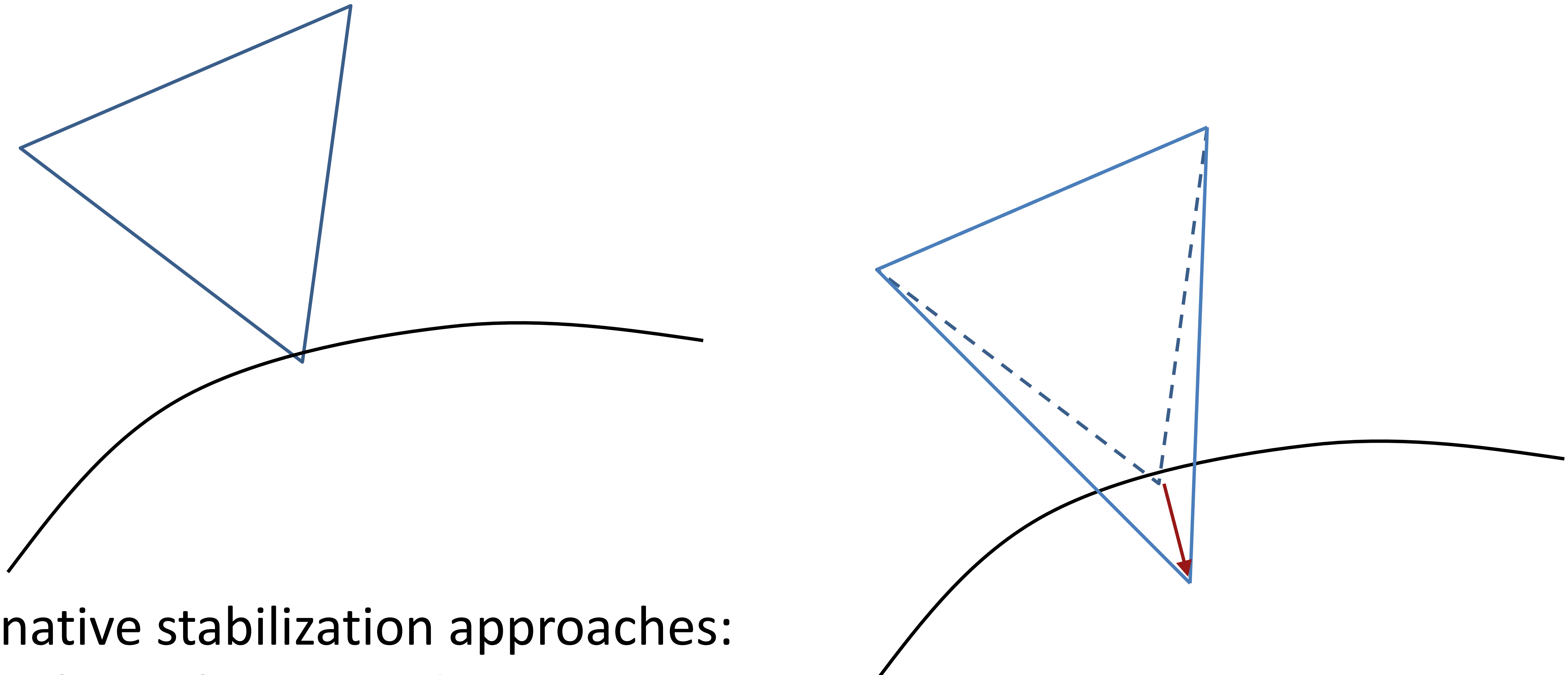

Alternative stabilization approaches:

- Agathos, Chatzi, Bordas, 2017, 2018, 2019
- Ghost penalty, Burman *et al*, 2015
- Stable XFEM, Gupta, Banerjee, Babuška, Duarte, 2013
- Neighboring gradient, Haslinger *et al*, 2009
- Menk, Bordas, 2009, Béchet, Moës, 2008

Real-time Error Control for Surgical Simulation, HP Bui et al, IEEE Trans. Biomed. Eng., 2016.

Implicit boundaries for liver

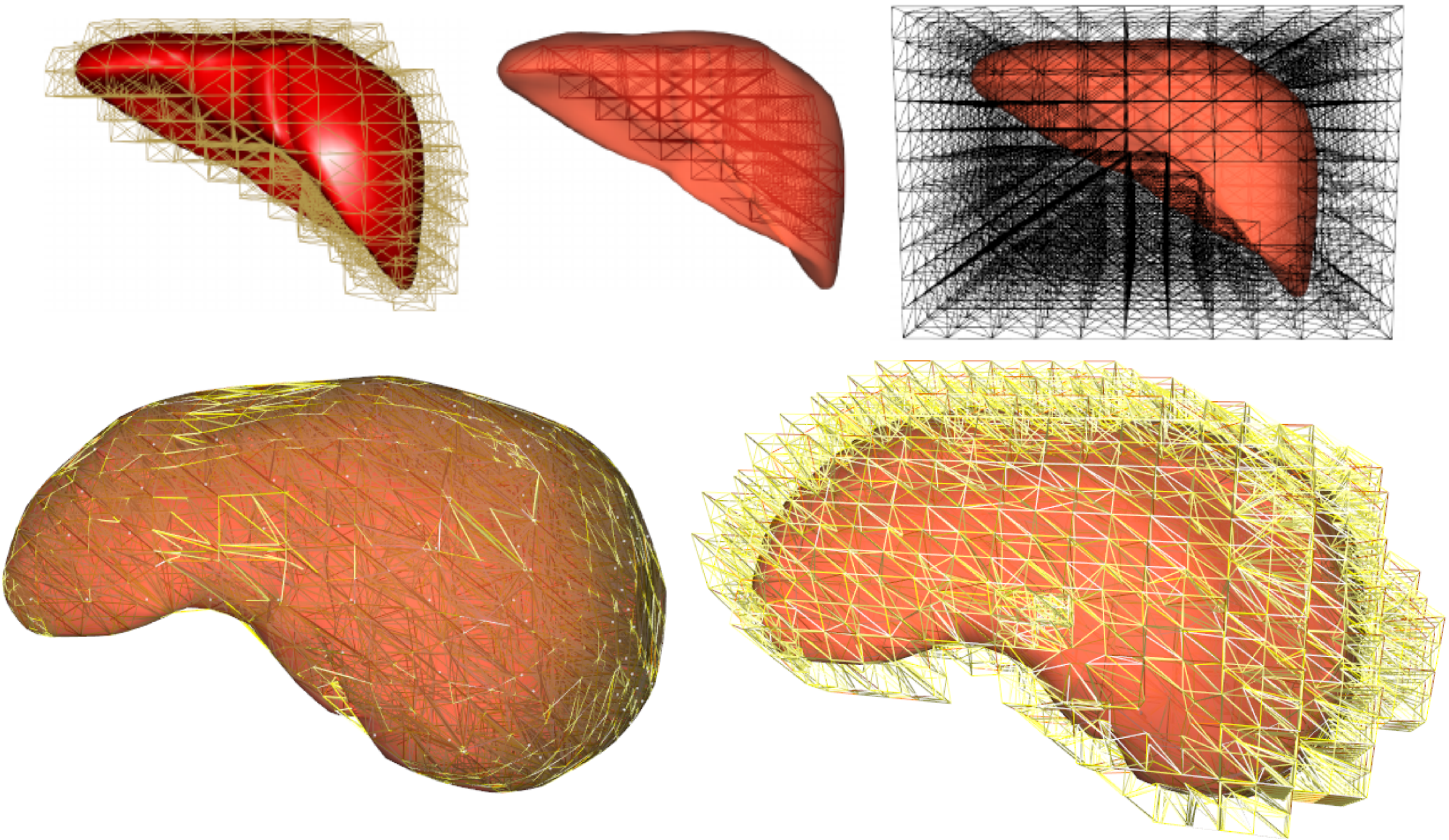

Real-time Error Control for Surgical Simulation, HP Bui et al, IEEE Trans. Biomed. Eng., 2016.

Stéphane Pierre Alain BORDAS, Department of Computational Engineering & Sciences University of Luxembourg

Models: Needle insertion simulation

Needle insertion problem

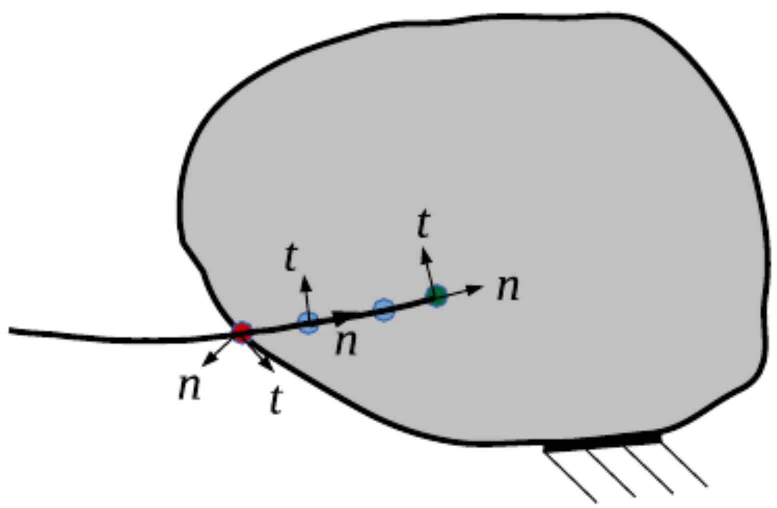

$$\operatorname{div}\boldsymbol{\sigma} + \mathbf{b} + \boldsymbol{\lambda} = \rho\ddot{\mathbf{u}} \qquad \text{in } \Omega$$

$$\boldsymbol{\epsilon} = \frac{1}{2}\left(\operatorname{grad}\mathbf{u} + (\operatorname{grad}\mathbf{u})^T\right)$$

$$\boldsymbol{\sigma} = f(\boldsymbol{\epsilon}, \boldsymbol{\nu})$$

$$\boldsymbol{\sigma}\cdot\mathbf{n} = \bar{\mathbf{t}} \text{ on } \Gamma_t;$$

$$\mathbf{u} = \bar{\mathbf{u}} \text{ on } \Gamma_u,$$

$$\lambda_n^{ts} > \lambda_{p_0}, \quad \text{(penetrate)}$$

$$\lambda_t^{ts} < \mu\lambda_n^{ts} \quad \text{(stick)}; \quad \lambda_t^{ts} = \mu\lambda_n^{ts} \quad \text{(slip)},$$

$$\mathbf{b} = \bar{\mathbf{b}} - c\dot{\mathbf{u}}$$

$$\lambda_n^{nt} < \mu\lambda_t^{nt} + \lambda_{c_0} \text{ (stick)}; \quad \lambda_n^{nt} \geq \mu\lambda_t^{nt} + \lambda_{c_0} \text{ (cut and slip)},$$

$$\lambda_n^{ns} < \mu\lambda_t^{ns} \text{ (stick)}; \quad \lambda_n^{ns} = \mu\lambda_t^{ns} \text{ (slide)}.$$

Real-time Error Control for Surgical Simulation, HP Bui et al, IEEE Trans. Biomed. Eng., 2016.

Needle Insertion with Implicit Interface

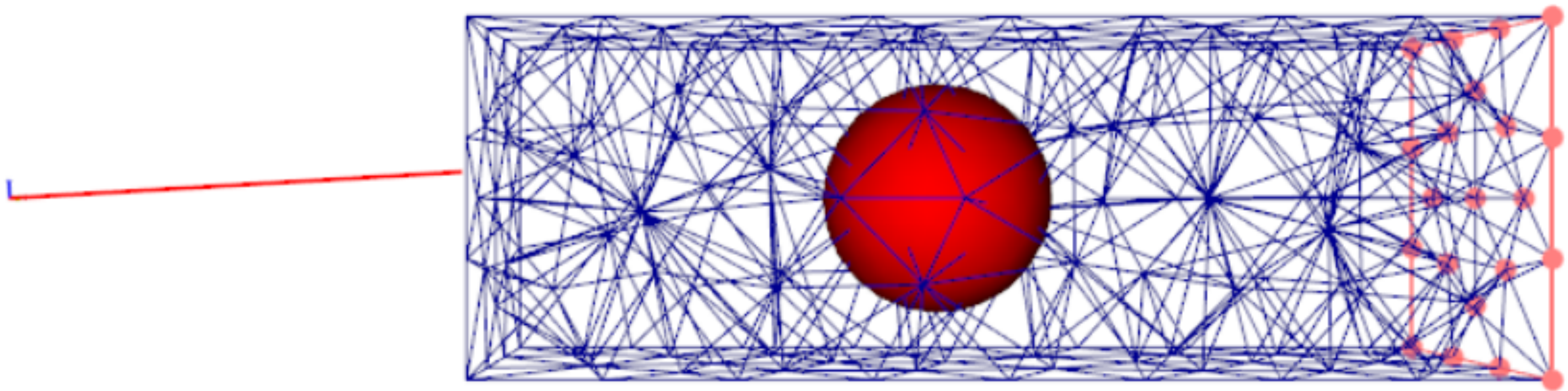

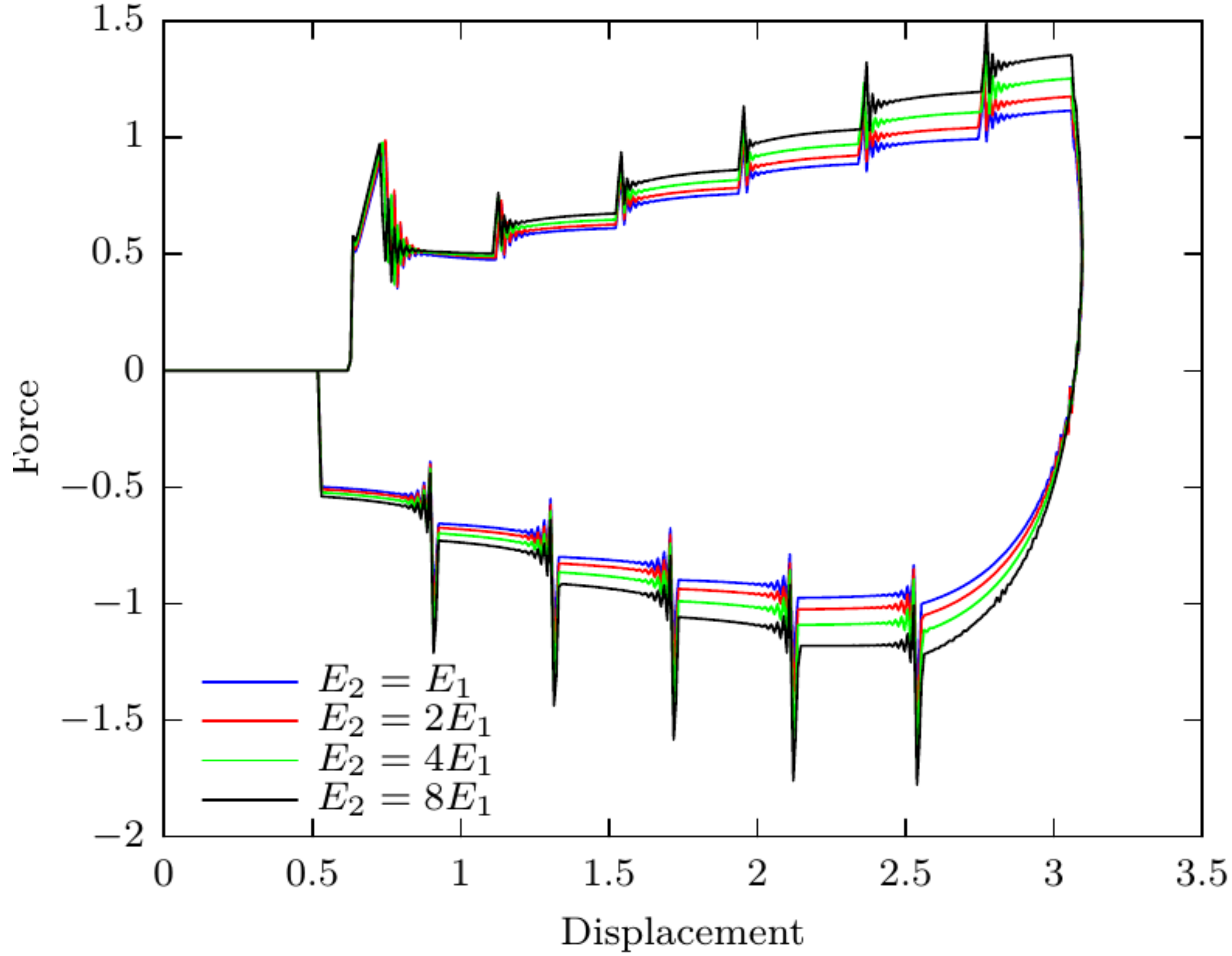

Real-time Error Control for Surgical Simulation, HP Bui et al, IEEE Trans. Biomed. Eng., 2016.

Needle Insertion with Implicit Boundary

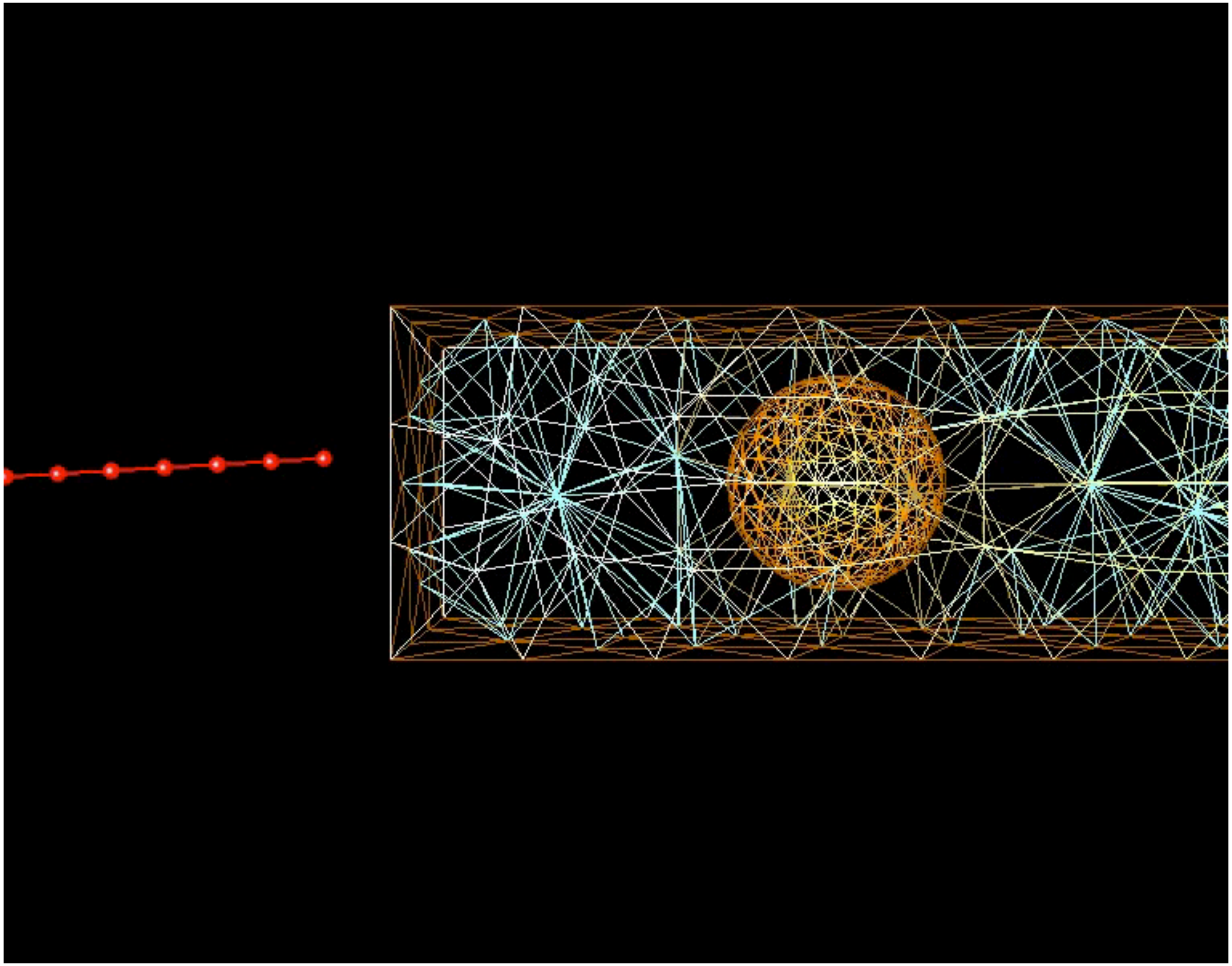

Real-time Error Control for Surgical Simulation, HP Bui et al, IEEE Trans. Biomed. Eng., 2016.

Needle insertion into liver

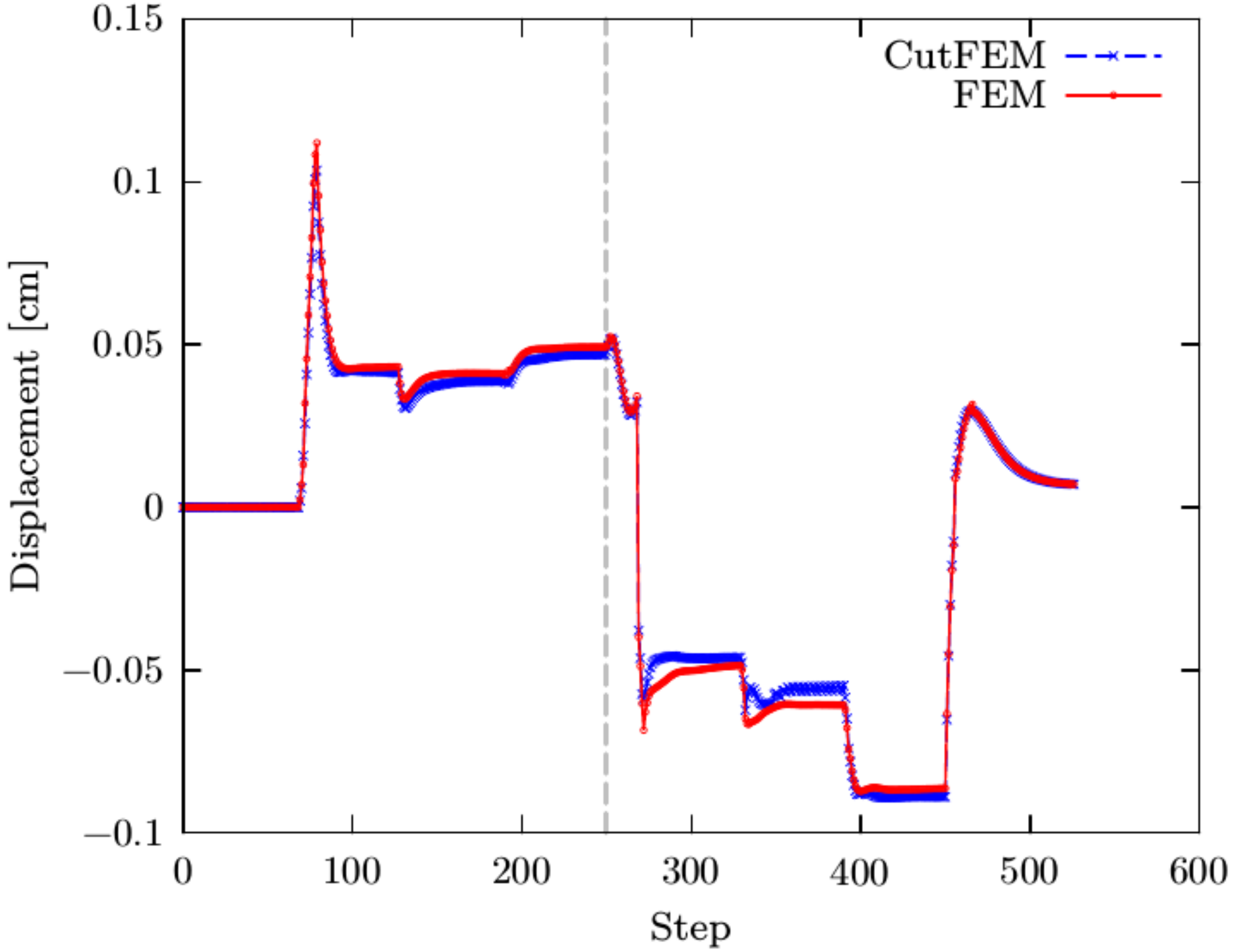

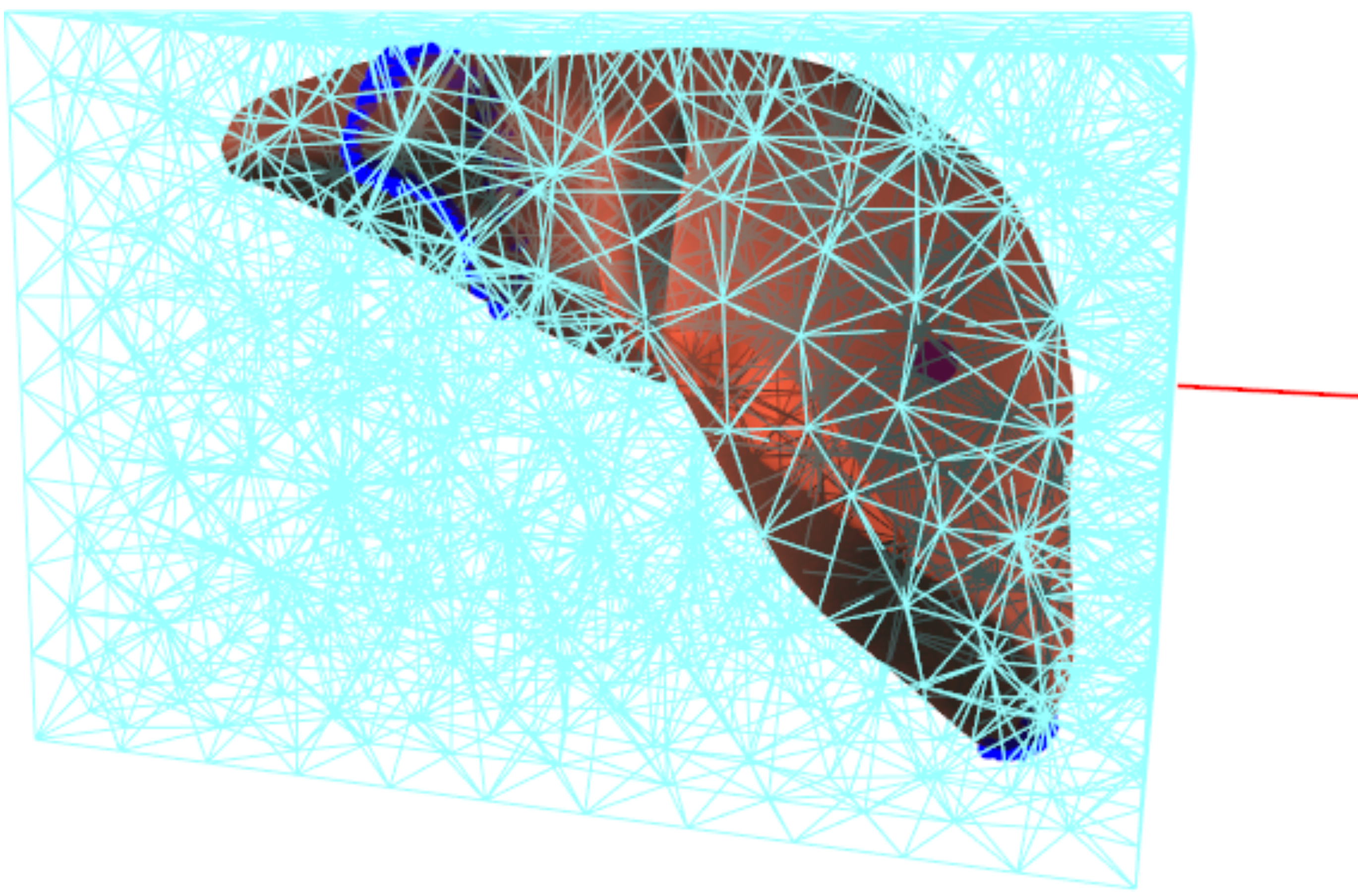

Real-time Error Control for Surgical Simulation, HP Bui et al, IEEE Trans. Biomed. Eng., 2016.

Stéphane Pierre Alain BORDAS, Department of Computational Engineering & Sciences University of Luxembourg

RealTCut

Brain shift and electrode implantation

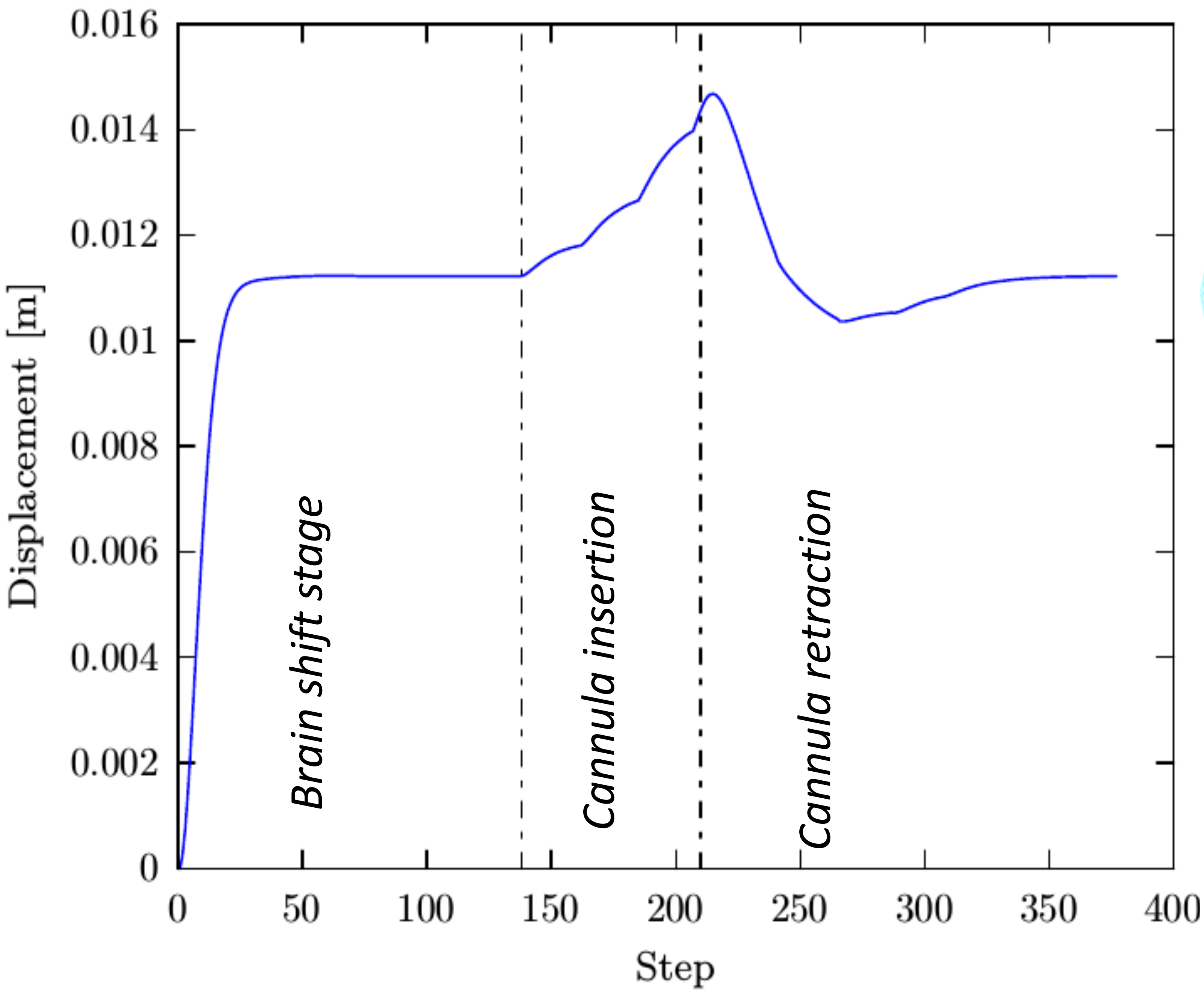

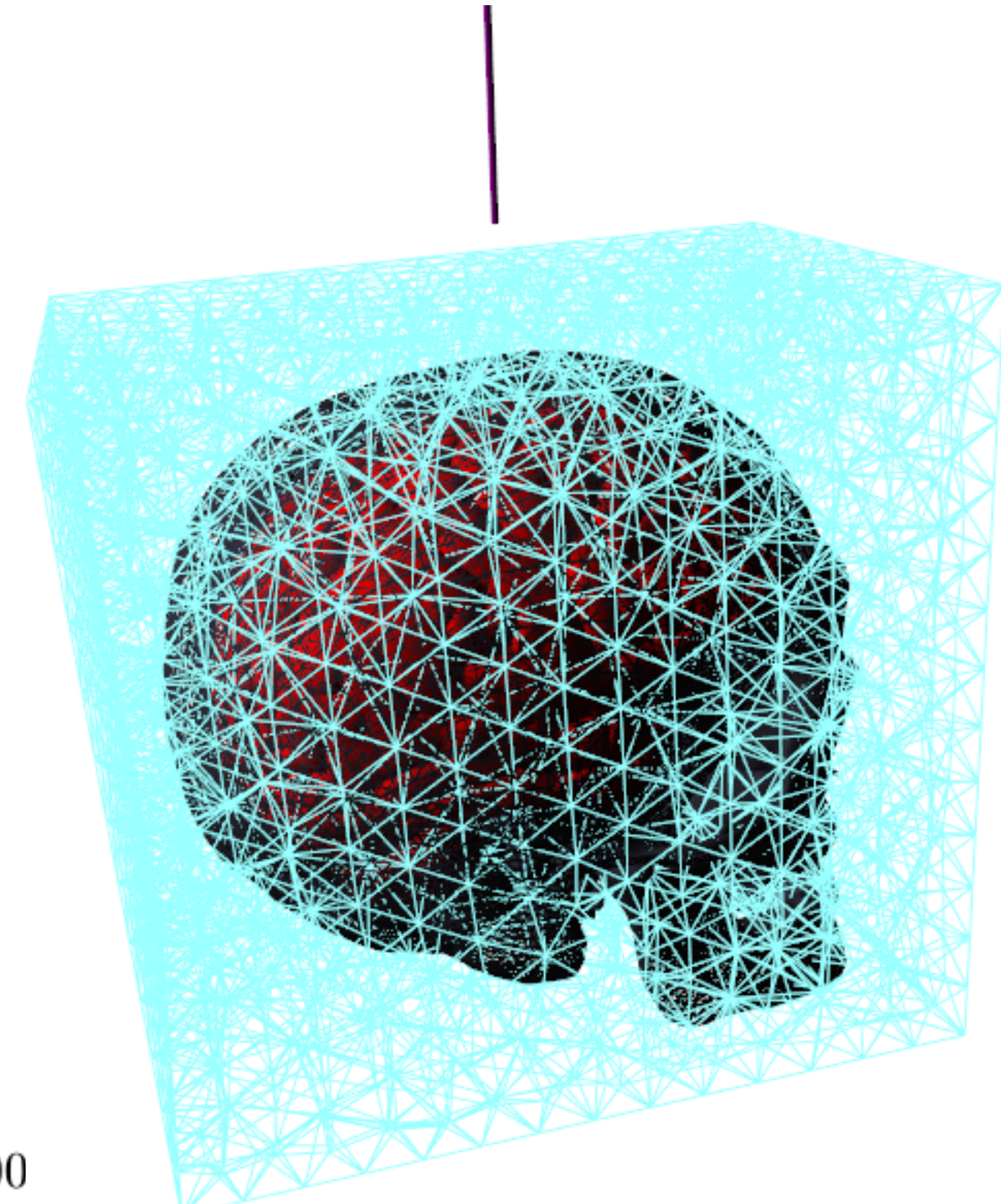

Real-time Error Control for Surgical Simulation, HP Bui et al, IEEE Trans. Biomed. Eng., 2016.

Stéphane Pierre Alain BORDAS, Department of Computational Engineering & Sciences University of Luxembourg

erc
RealTCut

Brain shift and electrode implantation

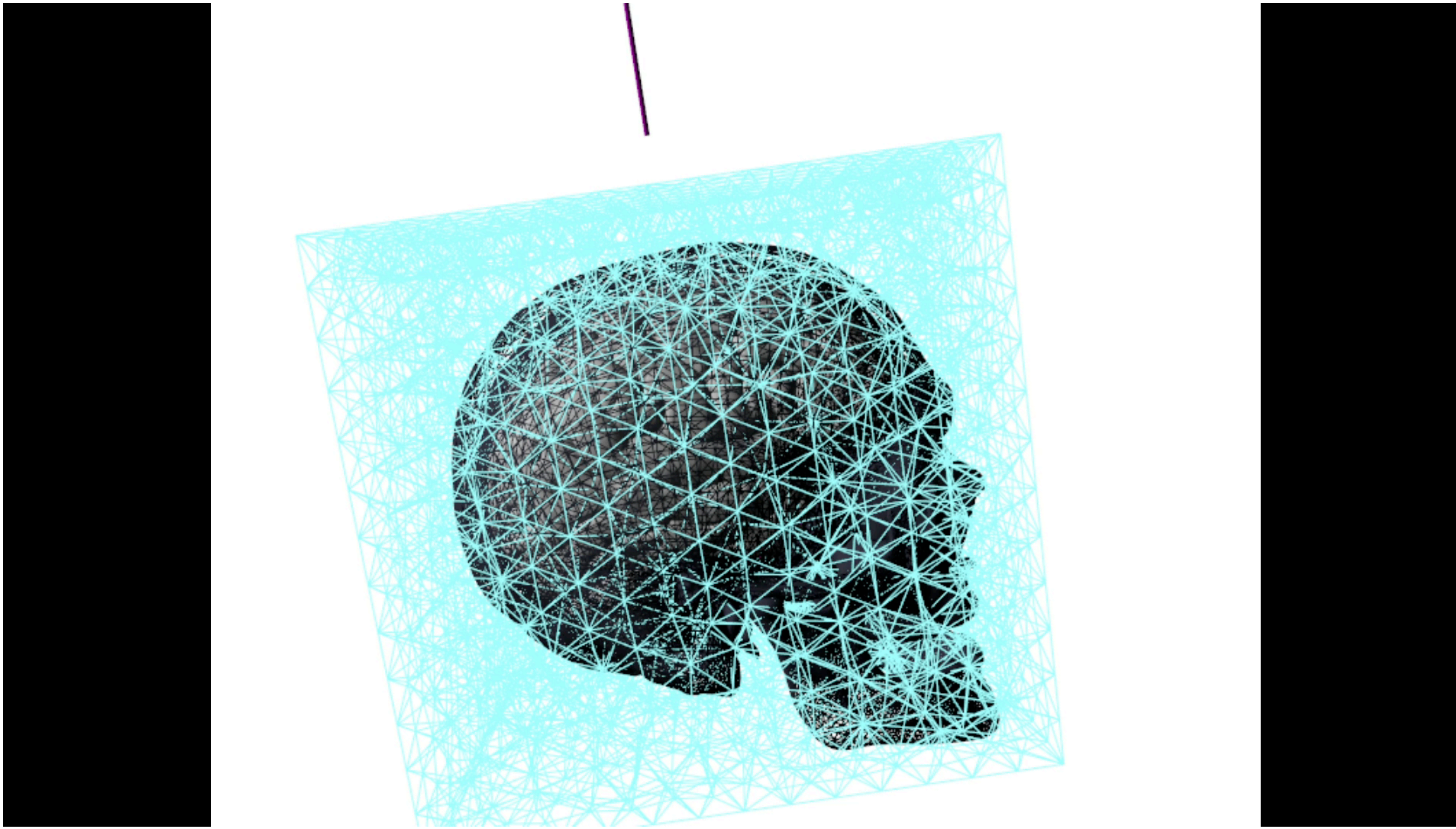

Controlling the Error on Target Motion through Real-time Mesh Adaptation: Applications to Deep Brain Stimulation, HP Bui et al, Int J Numer Meth Bio, 2017.

RealTCut

Error estimation and adaptivity

Controlling the Error on Target Motion through Real-time Mesh Adaptation: Applications to Deep Brain Stimulation, HP Bui et al, Int J Numer Meth Bio, 2017.

RealTCut

Superconvergence recovery

Controlling the Error on Target Motion through Real-time Mesh Adaptation: Application to Deep Brain Stimulation

H. P. Bui, S. Tomar, H. Courtecuisse, M. Audette, S. Cotin and S. P. A. Bordas

Controlling the Error on Target Motion through Real-time Mesh Adaptation: Applications to Deep Brain Stimulation, HP Bui et al, Int J Numer Meth Bio, 2017.

References

Real-time Error Control for Surgical Simulation, **HP Bui** *et al*, ***IEEE Trans. Biomed. Eng.*, 2016.**

Controlling the Error on Target Motion through Real-time Mesh Adaptation: Applications to Deep Brain Stimulation, **HP Bui** *et al*, ***Int J Numer Meth Bio, 2017.***

Corotational Cut Finite Element Method for real-time surgical simulation: application to needle insertion simulation, **HP Bui** *et al,* ***arXiv****:1712.03052[cs.CE]*

H.P. Bui

RealTCut

Point Collocation Methods

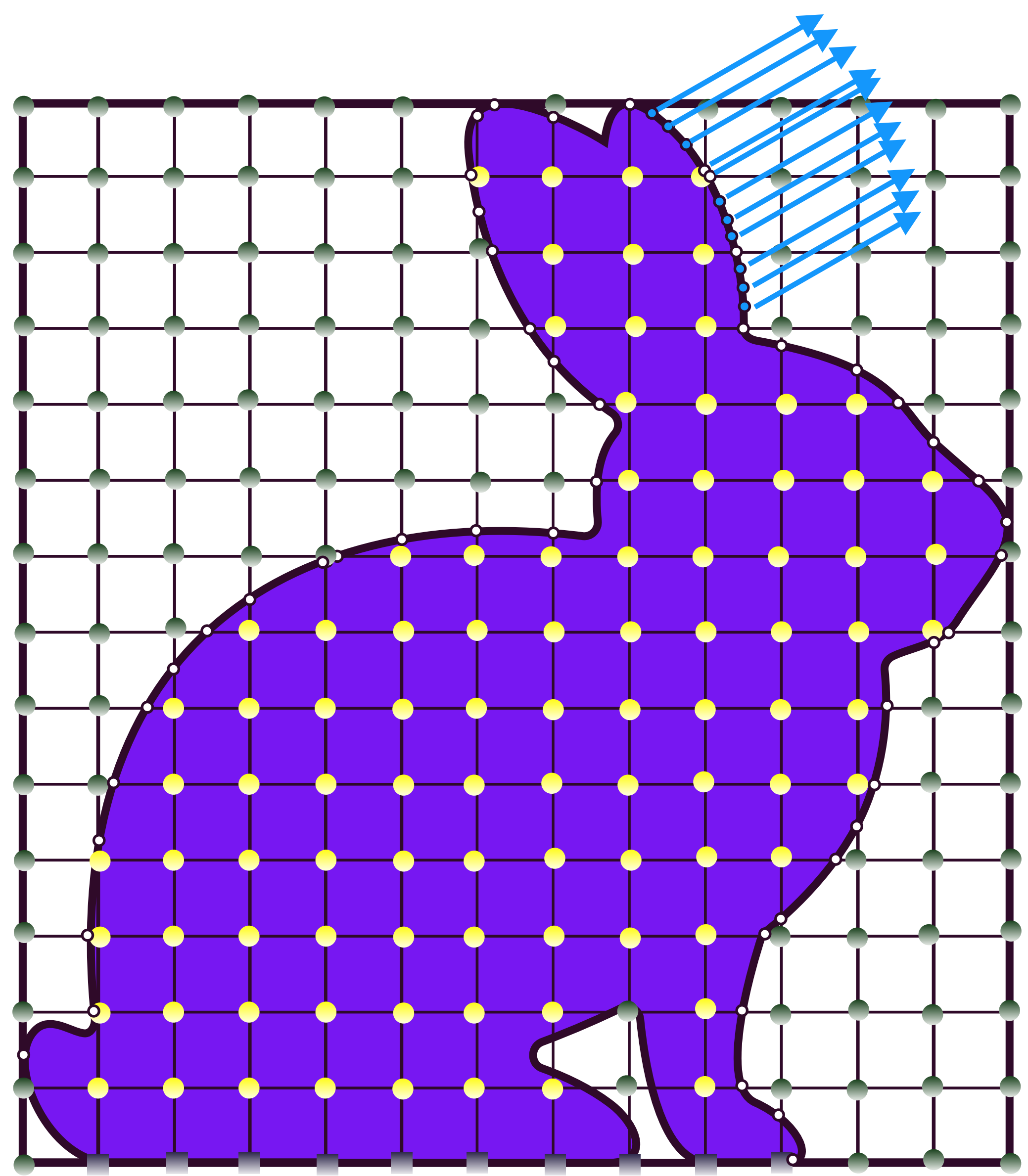

Thibault Jacquemin - Satyendra Tomar
Kostas Agathos - Shoya Mohsenimofidi

Collocation Methods

- Collocation methods belong to the family of meshless methods
- Nodes are arbitrarily distributed over the domain Ω, and the boundaries Γ_u and Γ_t

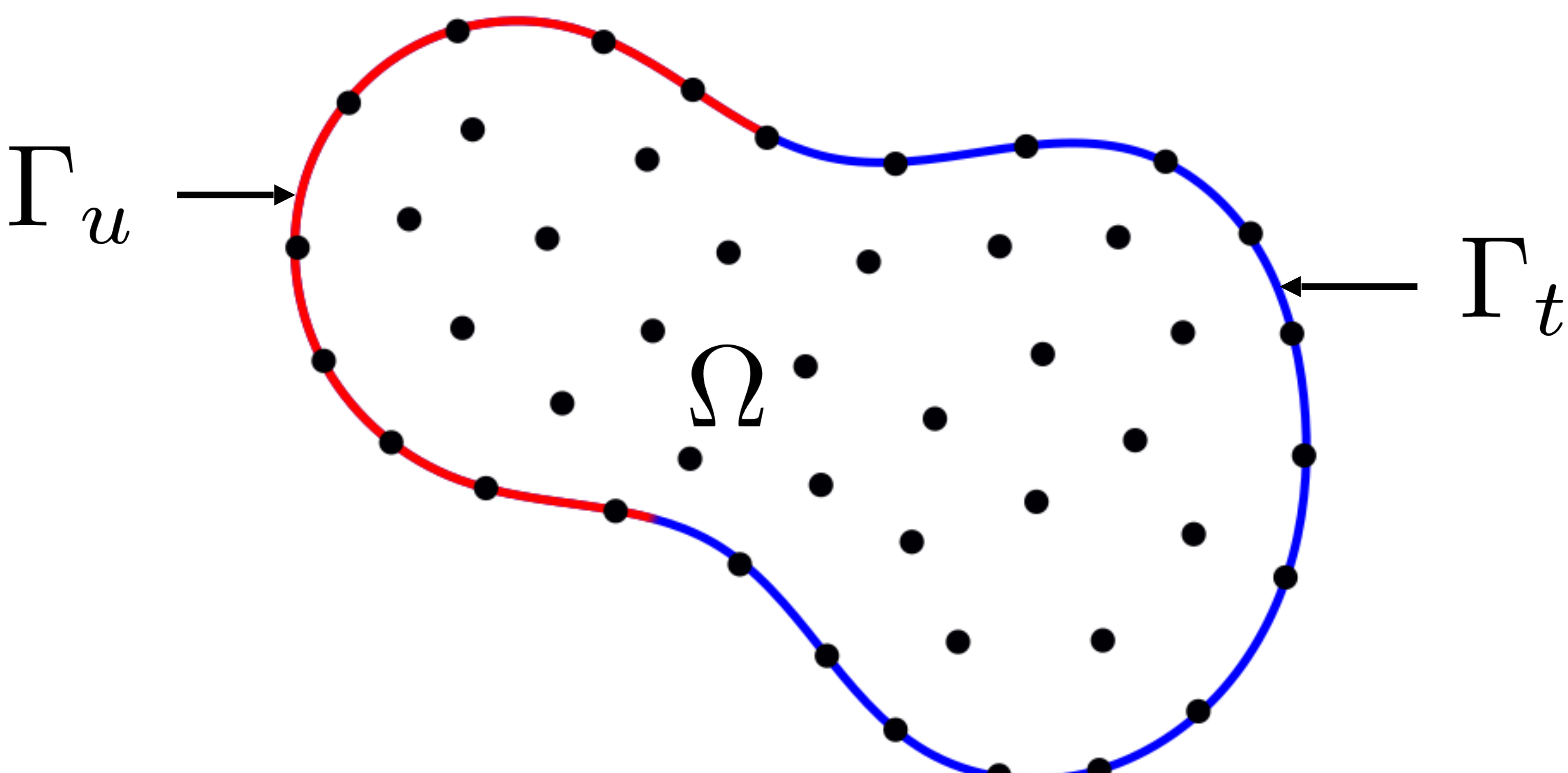

Strong form of PDE

- Typical PDE for a field f:

$$\mathcal{A}(f) = 0 \quad \text{in} \quad \Omega$$
$$f - \overline{f} = 0 \quad \text{on} \quad \Gamma_u$$
$$\mathcal{B}(f) = 0 \quad \text{on} \quad \Gamma_t$$

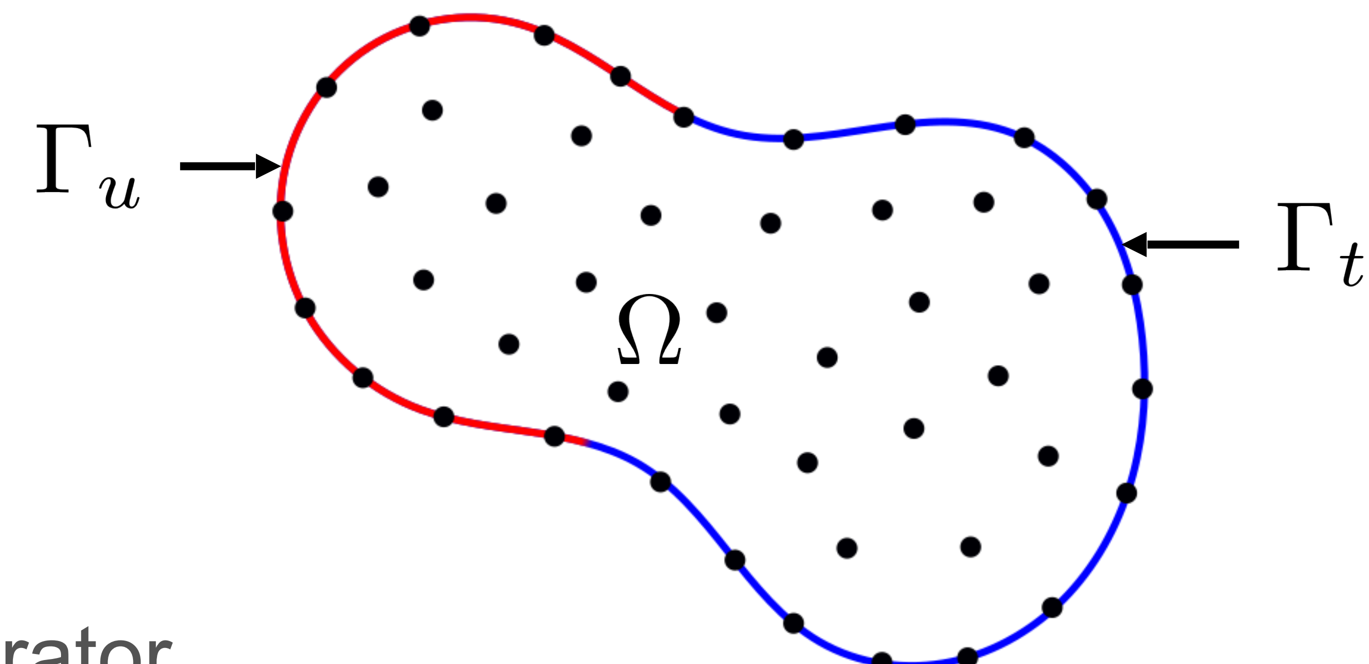

- A is the PDE differential operator
  The known field values f are applied to Γ_u
  B is a differential operator applied to Γ_t
- The PDE is solved only at collocation points
- The collocation points are typically the nodes of the domain

Advantages and Drawbacks of Collocation Methods

- Advantages:
  - ✓ Fewer constrains than element based methods with regards to point placement
  - ✓ Easy adaptation of the approximation to reduce the error
  - ✓ Low observed error for many problems

- Drawbacks:
  - ✗ Slower to solve than the Finite Element Method as the system matrix is non-symmetric, and denser due to larger support

Various Types of Collocation Methods

- Based on an approximation of the unknown field
  - ➢ Moving Least Square Approximation (MLS)
  - ➢ Isogeometric Analysis (IGA)
  - ➢ Radial Basis Functions (RBF)
  - ➢ …
- Based on an approximation of the differential operator
  - ➢ Finite Difference (FD)
  - ➢ Generalized Finite Difference (GFD)
  - ➢ Radial Basis Function Finite Difference (RBF-FD)
  - ➢ Discretization-Corrected Particle Strength Exchange (DCPSE)

Methods of Particular Interest

- Two methods:
  - ➢ The Generalized Finite Difference
  - ➢ The Discretization-Corrected Particle Strength Exchange

- These methods are based on a Taylor's series expansion to approximate the differential operator
- As compared to other collocation methods:
  - ➢ They lead to relatively low error
  - ➢ Fast to compute the solution

The GFD Method: Step by Step

- Step 1: Discretization & Support Node Selection
- Step 2: Taylor's Series Approximation
- Step 3: Derivatives' Approximation
- Step 4: Assembly of the Linear System
- Step 5: Solution of the Linear System

The GFD Method: Step by Step

- Consider the domain $\boldsymbol{\Omega}$ in 1D:

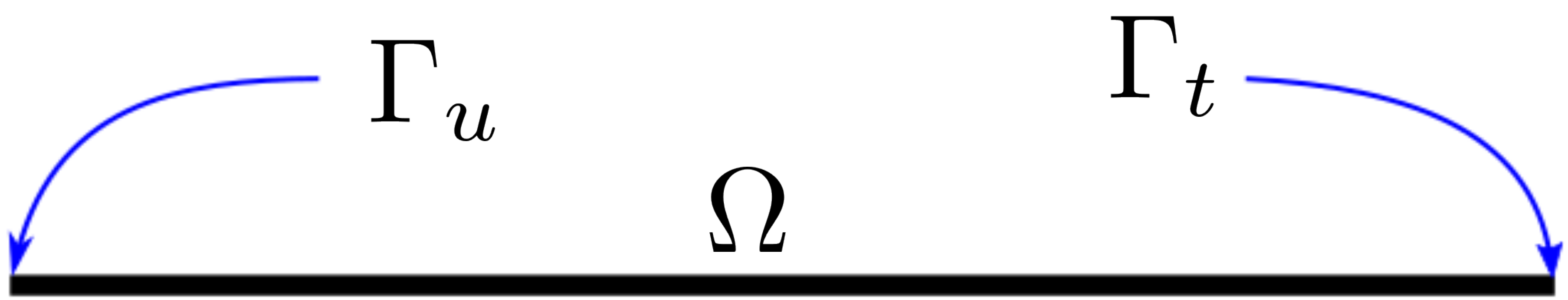

- The PDE to be solved:

$$
\begin{aligned}
\mathcal{A}(f) &= 0 \quad \text{in} \quad \Omega \\
f - \overline{f} &= 0 \quad \text{on} \quad \Gamma_u \\
\mathcal{B}(f) &= 0 \quad \text{on} \quad \Gamma_t
\end{aligned}
$$

Discretization/Support Node Selection

- Nodes are distributed over the domain Ω
- To each collocation node X_c , a radius R_c is associated which defines a sub-domain Ω_c as the support of X_c
- The nodes X_{pi} in Ω_c are called the support nodes of X_c
- The size of Ω_c depends on the order of the differential operator

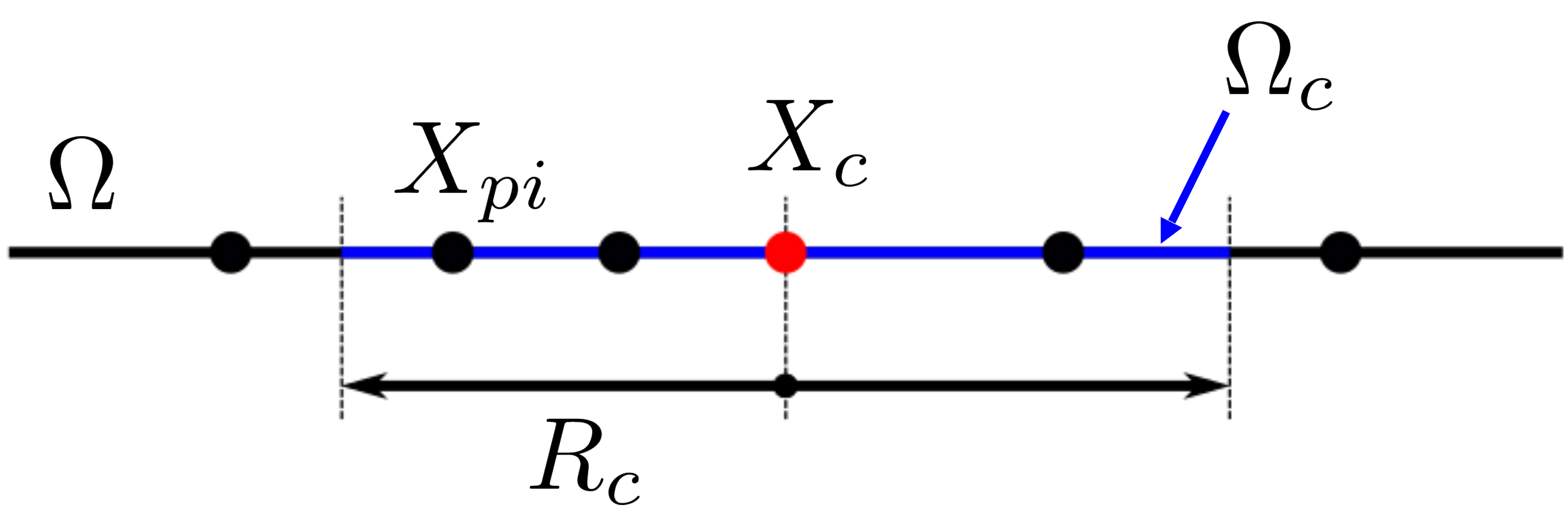

Taylor's Series Approximation

- Based on a Taylor's Series Expansion, the nodes X_{pi} are used to approximate the derivatives in X_c

- Since X_{pi} is located in the vicinity of X_c we can write:

$$f(X_{pi}) = f(X_c) + \sum_{i=1}^{\infty} \frac{(X_{pi} - X_c)^i}{i!} \frac{\partial^i f(X_c)}{\partial x^i}$$

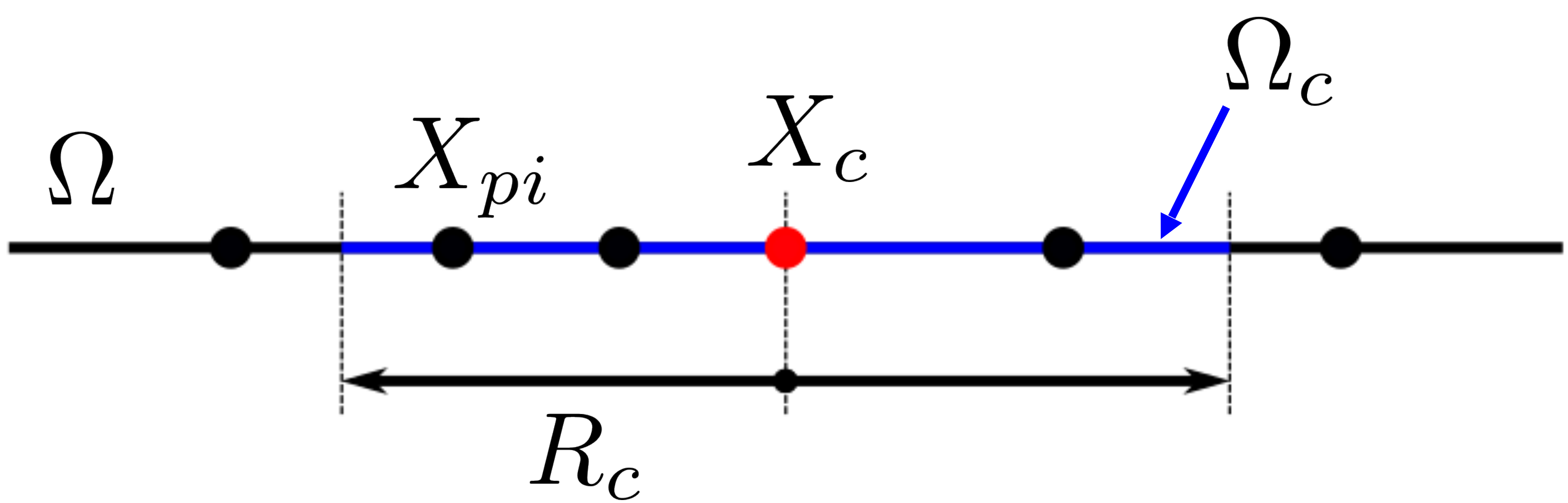

Taylor’s Series Approximation

- Considering a second order PDE, the second order approximation of the Taylor’s series expansion is:

$$f_h(X_{pi}) = f(X_c) + (x_{pi} - x_c)\frac{\partial f(X_c)}{\partial x} + \frac{(x_{pi}-x_c)^2}{2!}\frac{\partial^2 f(X_c)}{\partial x^2}$$

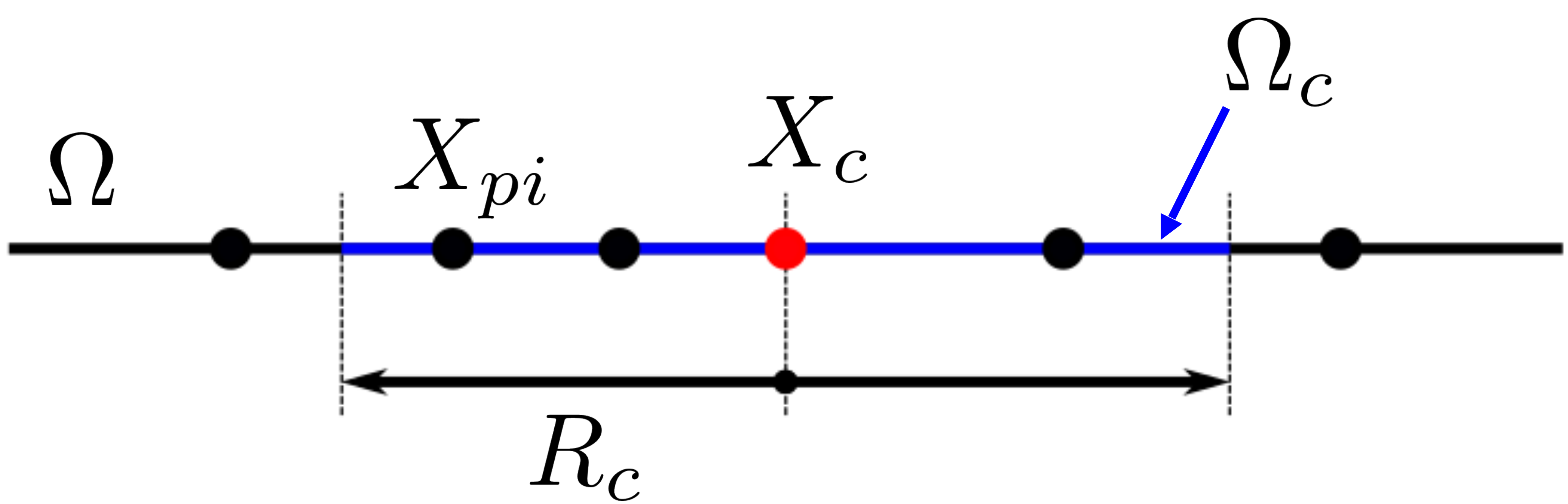

Derivatives' Approximation

- Taylor's series expansion can be written for all nodes X_{pi} (3 for the considered example) in Ω_c

$$\begin{cases} f_h(X_{p1}) = f(X_c) + (x_{p1} - x_c)\frac{\partial f(X_c)}{\partial x} + \frac{(x_{p1}-x_c)^2}{2!}\frac{\partial^2 f(X_c)}{\partial x^2} \\ f_h(X_{p2}) = f(X_c) + (x_{p2} - x_c)\frac{\partial f(X_c)}{\partial x} + \frac{(x_{p2}-x_c)^2}{2!}\frac{\partial^2 f(X_c)}{\partial x^2} \\ f_h(X_{p3}) = f(X_c) + (x_{p3} - x_c)\frac{\partial f(X_c)}{\partial x} + \frac{(x_{p3}-x_c)^2}{2!}\frac{\partial^2 f(X_c)}{\partial x^2} \end{cases}$$

- 2 unknowns $\frac{\partial f}{\partial x}(X_c)$ and $\frac{\partial^2 f}{\partial x^2}(X_c)$, 3 equations in this example

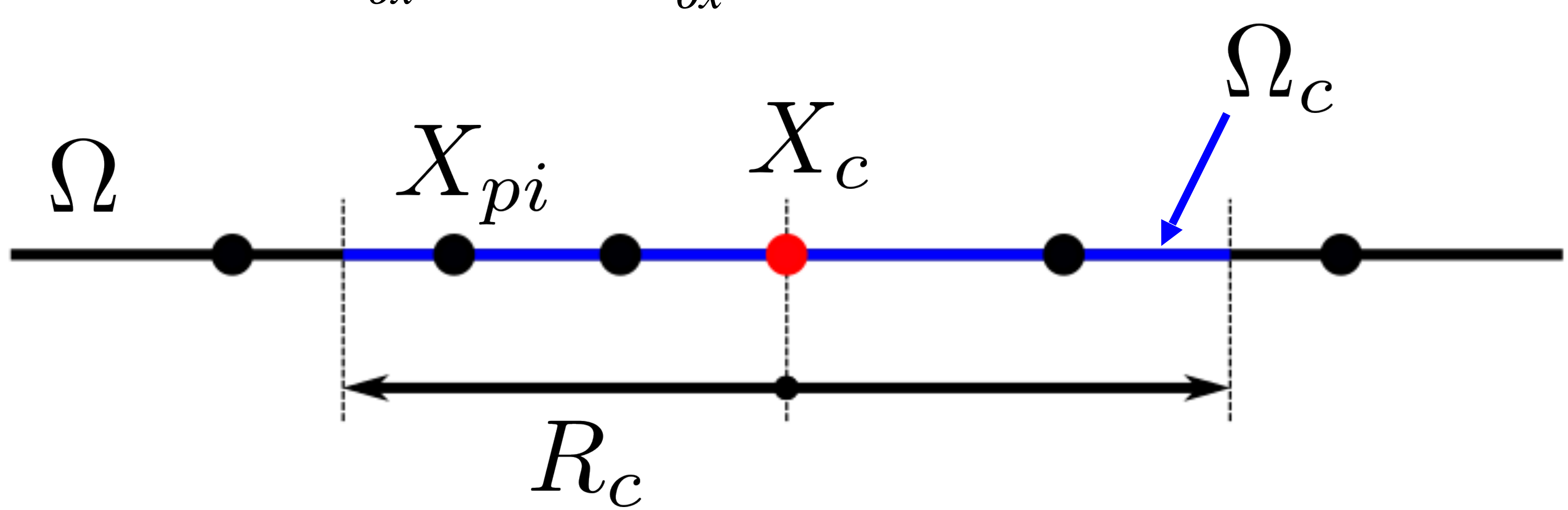

Derivatives' Approximation

- What are the values of derivatives $\frac{\partial f}{\partial x}$ and $\frac{\partial^2 f}{\partial x^2}$ that allow to best reproduce the field values $f(X_{pi}), i = 1,2,3$?

- Minimization problem described by the functional B:

$$B(X_c) = \sum_{i=1}^{3} w(X_{pi} - X_c)\left[f(X_c) - f(X_{pi}) + (x_{pi} - x_c)\frac{\partial f(X_c)}{\partial x} + \frac{(x_{pi} - x_c)^2}{2!}\frac{\partial^2 f(X_c)}{\partial x^2}\right]^2$$

- w is a weight function centred in X_c
- w balances the contribution of each support node as a function of its distance to X_c

Derivatives' Approximation

- What are the derivatives $\frac{\partial f}{\partial x}$ and $\frac{\partial^2 f}{\partial x^2}$ that allow to best reproduce the field values $f(X_{pi}), i = 1,2,3$?

$$\left.\frac{\partial B(X)}{\partial Df(X)}\right|_{X=X_c} = 0$$

where

$$Df(X) = \left[\frac{\partial f(X)}{\partial x}, \frac{\partial^2 f(X)}{\partial x^2}\right]^T$$

Derivatives' Approximation

- Derivatives of $B(X)$ w.r.t. $\frac{\partial f}{\partial x}$ and $\frac{\partial^2 f}{\partial x^2}$ at X_c are

$$\sum_{i=1}^{3} w(X_{pi} - X_c)(x_{pi} - x_c)\left[f(X_c) - f(X_{pi}) + (x_{pi} - x_c)\frac{\partial f(X_c)}{\partial x} + \frac{(x_{pi} - x_c)^2}{2!}\frac{\partial^2 f(X_c)}{\partial x^2}\right]$$

$$\sum_{i=1}^{3} w(X_{pi} - X_c)\frac{(x_{pi} - x_c)^2}{2!}\left[f(X_c) - f(X_{pi}) + (x_{pi} - x_c)\frac{\partial f(X_c)}{\partial x} + \frac{(x_{pi} - x_c)^2}{2!}\frac{\partial^2 f(X_c)}{\partial x^2}\right]$$

- Equating these terms to zero, this can be written in a matrix form as:

$$\begin{bmatrix} m_{11} & m_{12} \\ m_{21} & m_{22} \end{bmatrix} \begin{bmatrix} \frac{\partial f(X_c)}{\partial x} \\ \frac{\partial^2 f(X_c)}{\partial x^2} \end{bmatrix} = \begin{bmatrix} -m_{01} & m_{01,1} & m_{01,2} & m_{01,3} \\ -m_{02} & m_{01,1} & m_{02,2} & m_{02,3} \end{bmatrix} \begin{bmatrix} f(X_c) \\ f(X_{p1}) \\ f(X_{p2}) \\ f(X_{p3}) \end{bmatrix}$$

Derivatives' Approximation

$$\begin{bmatrix} m_{11} & m_{12} \\ m_{21} & m_{22} \end{bmatrix} \begin{bmatrix} \frac{\partial f(X_c)}{\partial x} \\ \frac{\partial^2 f(X_c)}{\partial x^2} \end{bmatrix} = \begin{bmatrix} -m_{01} & m_{01,1} & m_{01,2} & m_{01,3} \\ -m_{02} & m_{01,1} & m_{02,2} & m_{02,3} \end{bmatrix} \begin{bmatrix} f(X_c) \\ f(X_{p1}) \\ f(X_{p2}) \\ f(X_{p3}) \end{bmatrix}$$

- The coefficients of this system are:

$$m_{ij,k} = w(X_{pk} - X_c) P_{(i+1)k}(X_c) P_{(j+1)k}(X_c)$$

$$m_{ij} = \sum_{k=1}^{3} m_{ij,k}$$

$$P(X_c) = \begin{bmatrix} 1 & 1 & 1 \\ (x_{p1} - x_c) & (x_{p2} - x_c) & (x_{p3} - x_c) \\ \frac{(x_{p1}-x_c)^2}{2!} & \frac{(x_{p2}-x_c)^2}{2!} & \frac{(x_{p3}-x_c)^2}{2!} \end{bmatrix}$$

Derivatives' Approximation

- The derivatives $\frac{\partial f}{\partial x}$ and $\frac{\partial^2 f}{\partial x^2}$ can then be approximated as a function of the field values $F(X_c)$

$$\underbrace{\begin{bmatrix} m_{11} & m_{12} \\ m_{21} & m_{22} \end{bmatrix}}_{A(X_c)} \underbrace{\begin{bmatrix} \frac{\partial f(X_c)}{\partial x} \\ \frac{\partial^2 f(X_c)}{\partial x^2} \end{bmatrix}}_{Df(X_c)} = \underbrace{\begin{bmatrix} -m_{01} & m_{01,1} & m_{01,2} & m_{01,3} \\ -m_{02} & m_{01,1} & m_{02,2} & m_{02,3} \end{bmatrix}}_{E(X_c)} \underbrace{\begin{bmatrix} f(X_c) \\ f(X_{p1}) \\ f(X_{p2}) \\ f(X_{p3}) \end{bmatrix}}_{F(X_c)}$$

- $Df(X_c) = A^{-1}(X_c)E(X_c)F(X_c)$

Derivatives' Approximation

- Different types of weight functions:
  - ➢ 3rd Order Splines

$$w(s) = \begin{cases} \frac{2}{3} - 4s^2 + 4s^3 & \text{if } s \le 0.5 \\ \frac{4}{3} - 4s + 4s^2 - \frac{4}{3}s^3 & \text{if } 0.5 < s \le 1 \\ 0 & \text{if } s > 1 \end{cases}$$

  - ➢ 4th Order Splines

$$w(s) = \begin{cases} 1 - 6s^2 + 8s^3 - 3s^4 & \text{if } s \le 1 \\ 0 & \text{if } s > 1 \end{cases}$$

Assembly of Linear System

$$\begin{array}{c} 1 \\ i \\ \\ n \end{array} \begin{bmatrix} \\ \text{Equation for Collocation Node “i”} \\ A \\ \\ \end{bmatrix} \begin{bmatrix} \\ \\ F \\ \\ \end{bmatrix} = \begin{bmatrix} \\ \\ B \\ \\ \end{bmatrix}$$

The DCPSE Method: Step by Step

- Step 1: Discretization & Support Node Selection
- Step 2: Taylor’s Series Approximation
- Step 3: Derivatives Approximation
- Step 4: Assembly of the Linear System
- Step 5: Resolution of the Linear System

➔ The operations performed during the steps 1, 2, 4 and 5 are the same as for the GFD method

DCPSE: Derivatives' Approximation

- The Taylor's series expansion is convoluted by a function η over the domain Ω_c

$$
\begin{aligned}
\int_{\Omega_c} f_h(X_p)\, \eta(X_p - X_c)\, dX_p = & \int_{\Omega_c} f(X_c)\, \eta(X_p - X_c)\, dX_p \\
& + \int_{\Omega_c} \frac{\partial f(X_c)}{\partial x}(x_p - x_c)\, \eta(X_p - X_c)\, dX_p \\
& + \int_{\Omega_c} \frac{\partial^2 f(X_c)}{\partial x^2} \frac{(x_p - x_c)^2}{2!}\, \eta(X_p - X_c)\, dX_p
\end{aligned}
$$

- Compare with the GFD terms

$$
\begin{cases}
f_h(X_{p1}) = f(X_c) + (x_{p1} - x_c)\frac{\partial f(X_c)}{\partial x} + \frac{(x_{p1}-x_c)^2}{2!}\frac{\partial^2 f(X_c)}{\partial x^2} \\
f_h(X_{p2}) = f(X_c) + (x_{p2} - x_c)\frac{\partial f(X_c)}{\partial x} + \frac{(x_{p2}-x_c)^2}{2!}\frac{\partial^2 f(X_c)}{\partial x^2} \\
f_h(X_{p3}) = f(X_c) + (x_{p3} - x_c)\frac{\partial f(X_c)}{\partial x} + \frac{(x_{p3}-x_c)^2}{2!}\frac{\partial^2 f(X_c)}{\partial x^2}
\end{cases}
$$

DCPSE: Derivatives' Approximation

- The coefficient vector a of the correction function is selected in order to satisfy the moment condition
- For instance, for a second order derivative approximation :

$$
\begin{cases}
M_0(X_c) = 0 \quad \Leftrightarrow \quad \sum_{i=1}^{3} P(X_{pi} - X_c)^T a w(X_{pi} - X_c) = 0 \\
M_1(X_c) = 0 \quad \Leftrightarrow \quad \sum_{i=1}^{3} (x_{pi} - x_c) P(X_{pi} - X_c)^T a w(X_{pi} - X_c) = 0 \\
M_2(X_c) = 1 \quad \Leftrightarrow \quad \sum_{i=1}^{3} \frac{(x_{pi} - x_c)^2}{2!} P(X_{pi} - X_c)^T a w(X_{pi} - X_c) = 1
\end{cases}
$$

DCPSE: Derivatives' Approximation

- This problem can be put in a matrix form:

$$\begin{bmatrix} A_{11} & A_{12} & A_{13} \\ A_{21} & A_{22} & A_{23} \\ A_{31} & A_{32} & A_{33} \end{bmatrix} \begin{bmatrix} a_1 \\ a_2 \\ a_3 \end{bmatrix} = \begin{bmatrix} 0 \\ 0 \\ 1 \end{bmatrix}$$

- The coefficients are

$$A_{i,j}(X_c) = \sum_{i=1}^{3} Q_i(X_c, X_{pi})\ P_j(X_{pi} - X_c)\ w(X_{pi} - X_c)$$

$$Q(X_c, X_p) = \left[1, (x_p - x_c), \frac{(x_p - x_c)^2}{2!}\right]^T$$

DCPSE: Derivatives' Approximation

- The vector a can be calculated for the derivative $D^{n_x}(f(X_c))$
- The derivative can then be approximated as:

$$D^{n_x} f(X_c) = \sum_{i=1}^{3} f_h(X_{pi}) P(X_p - X_c)^T a \; w(X_p - X_c)$$

DCPSE vs. GFD

- Means of approximating the derivatives
- Derivatives approximated by GFD reproduce the field values at the support nodes using Taylor's series expansion
- DCPSE also uses Taylor's series expansion to approximate the derivatives but it uses a convolution function to cancel selected terms

Sensitivity to various parameters

- Based on a sensitivity study, the following parameters are chosen for the case of 2D and 3D linear elastic problems

Parameter	GFD	DC PSE
Weight Function Type	4th Order Spline	Exponential
Correction Function	N/A	Polynomial
Size of Inner Nodes Support (2D/3D)	11/37	13/37
Size of Boundary Nodes Support (2D/3D)	19/75	17/75

Model problem

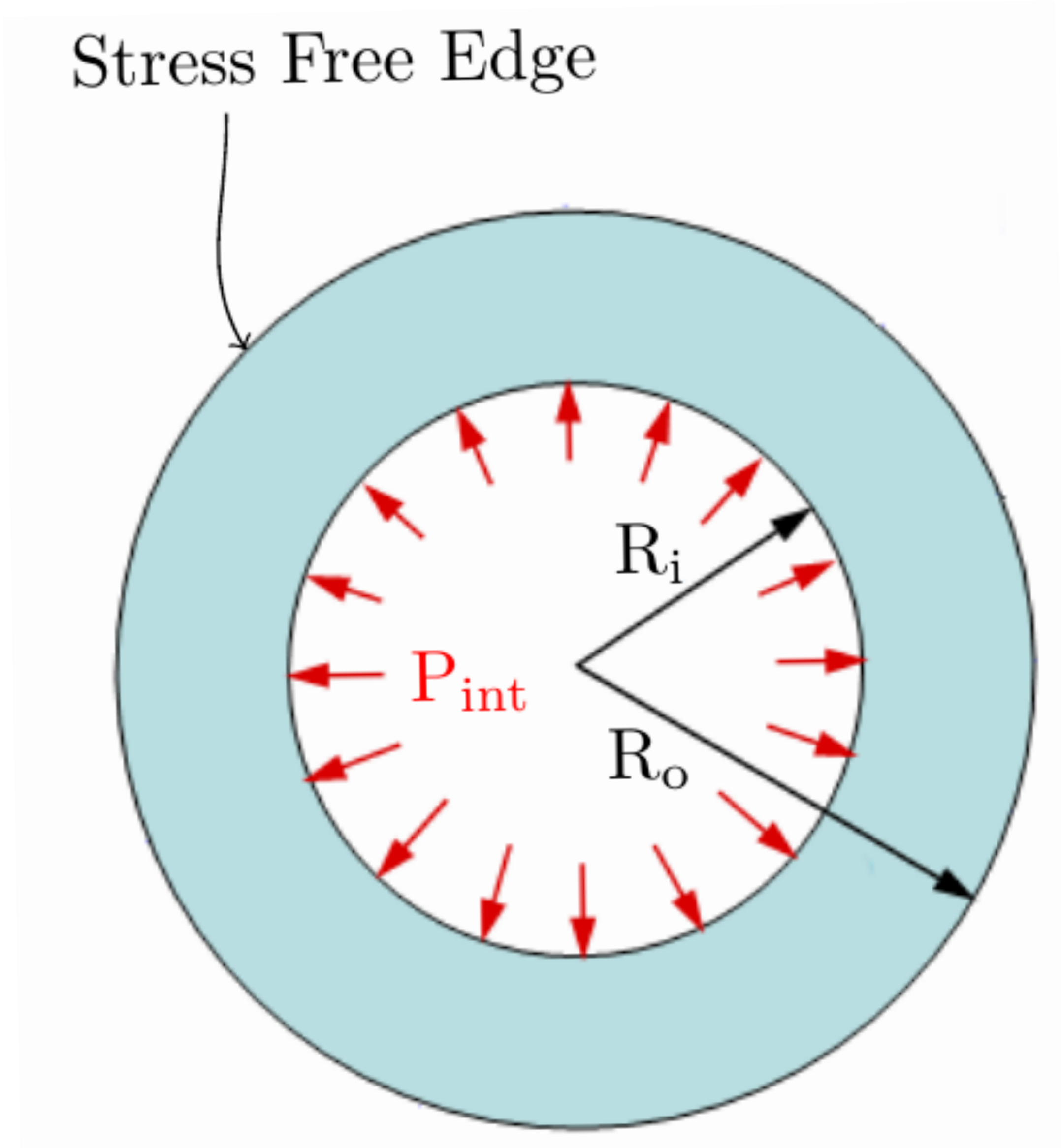

Plane Stress Cylinder
under Internal Pressure

- Only a quarter of the cylinder modelled due to the symmetries in the cartesian coordinate system

Nodes arrangements, structured vs. Delaunay triangulation

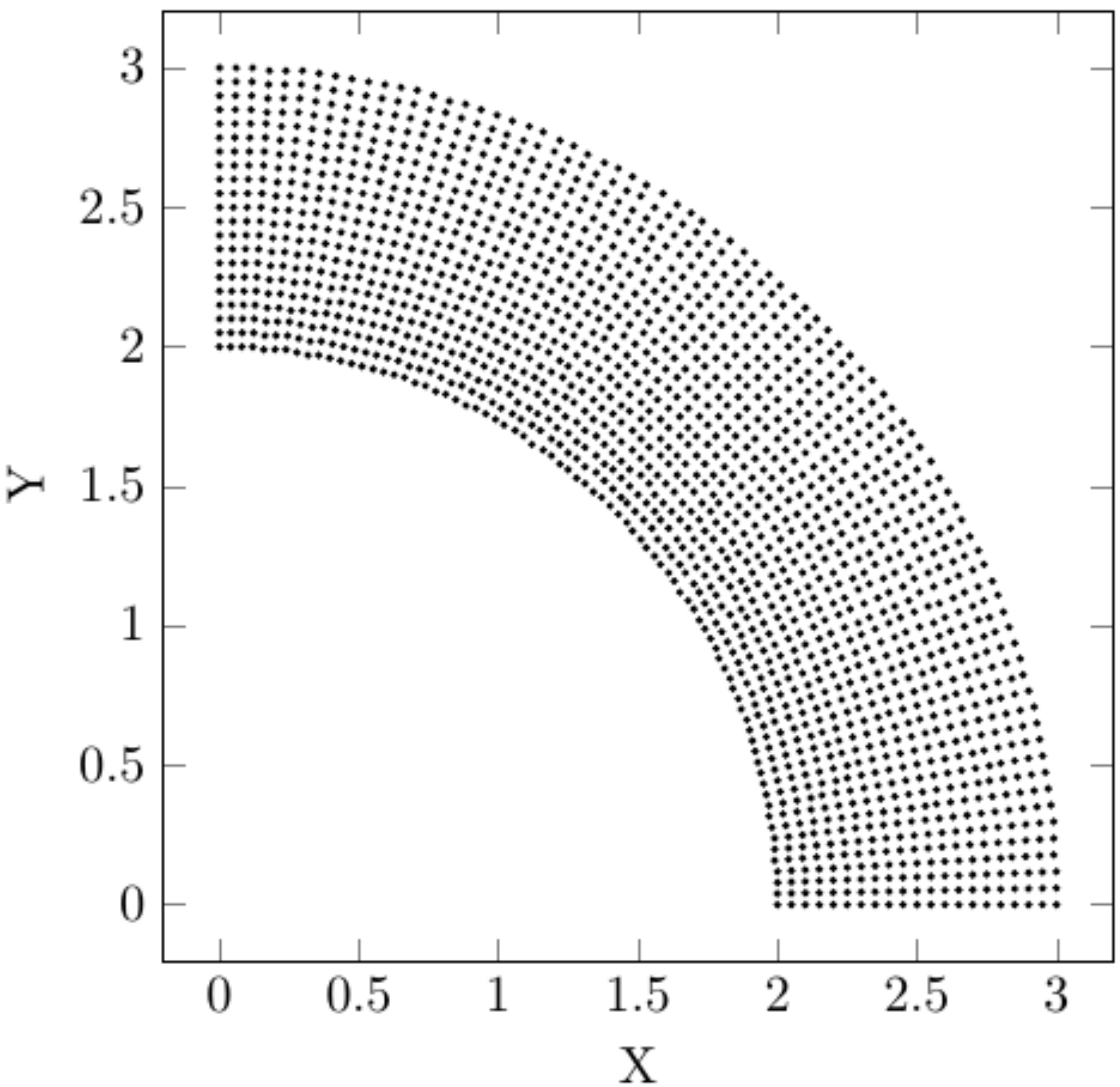

Structured Node Arrangement

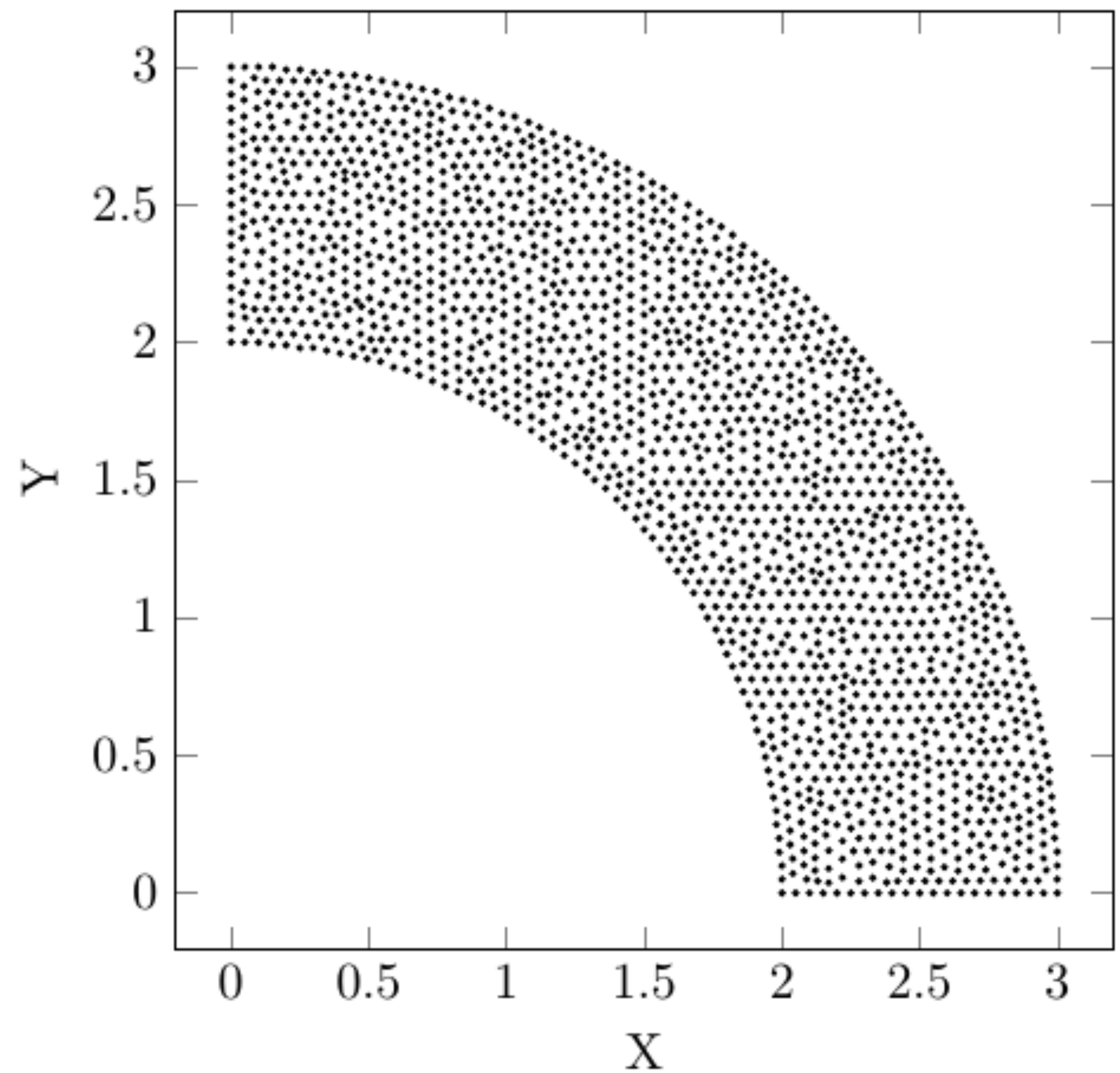

Delaunay Triangulation Node Arrangement (Free)

No significant impact on accuracy/convergence

Voronoi Based Weights: GFD

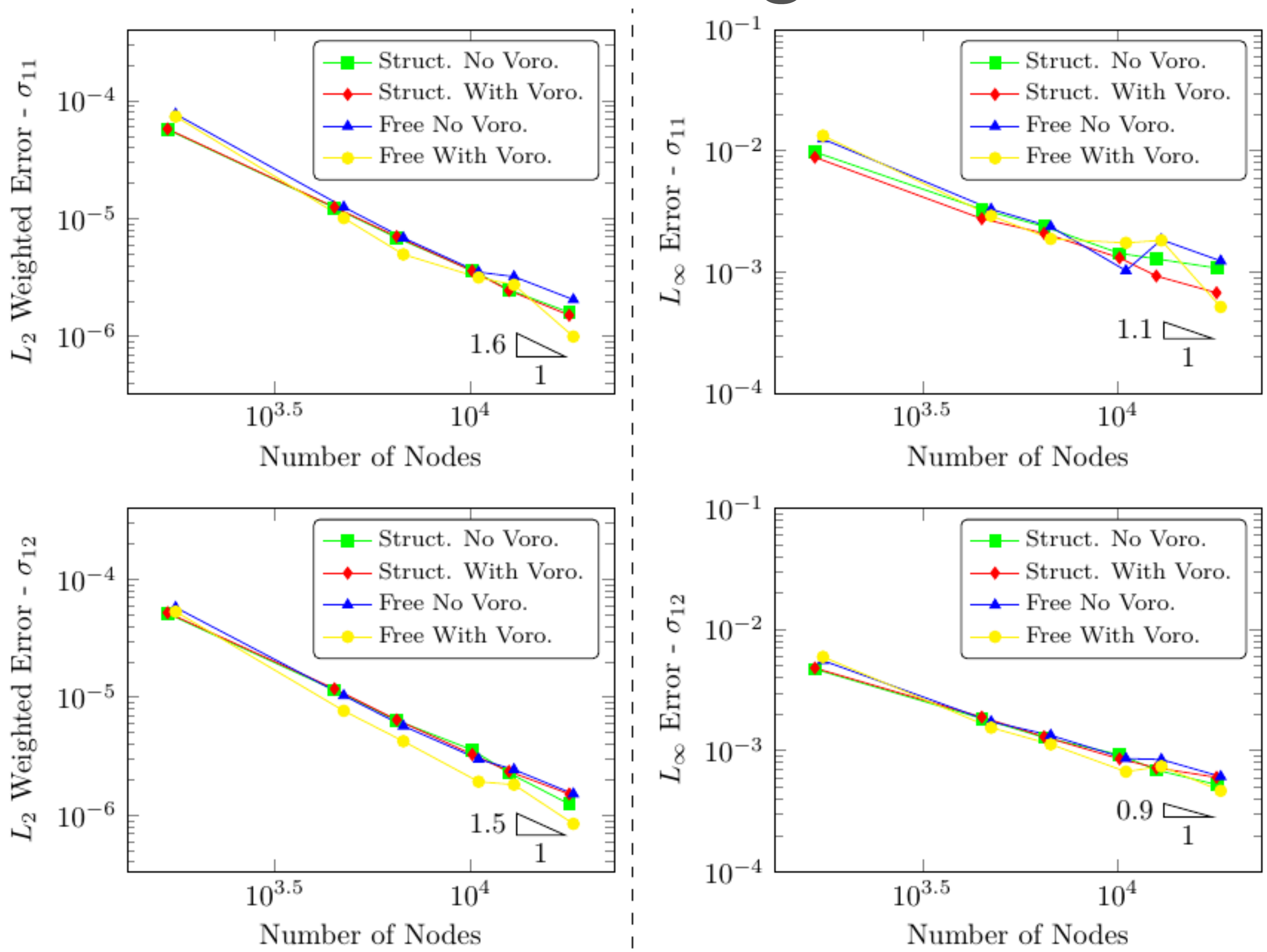

- No improvement or worse results for the structured node arrangement
- Small improvement for the node arrangement based on a Delaunay Triangulation

Node Selection Around Singularities

- <u>The visibility criterion:</u>
  Only the nodes visible from the collocation nodes are selected in the support of the collocation node

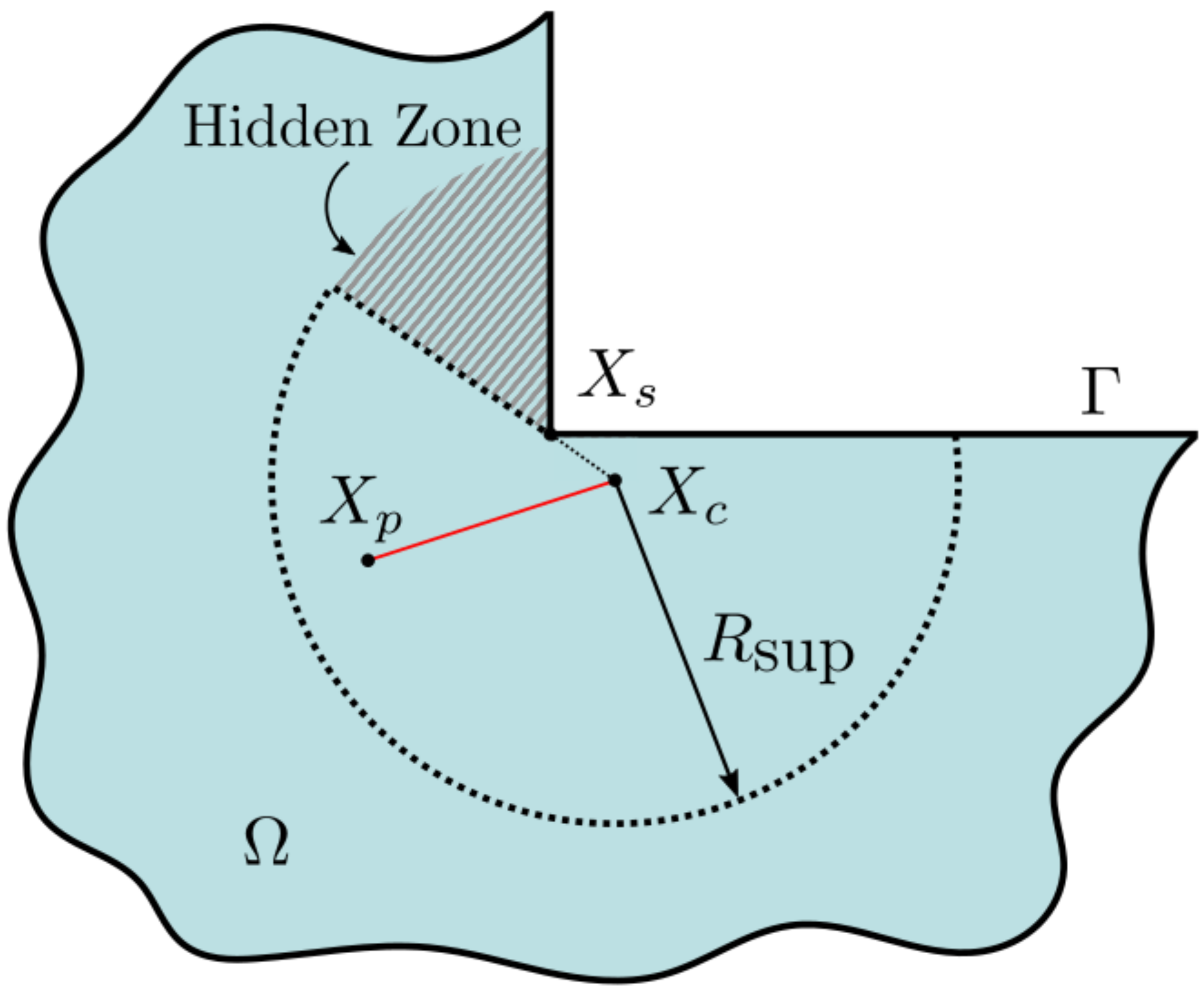

Node Selection Around Singularities

- <u>The diffraction criterion:</u>
  The “hidden” nodes are included in the support of the collocation node only if the “diffracted” length is smaller than the support radius

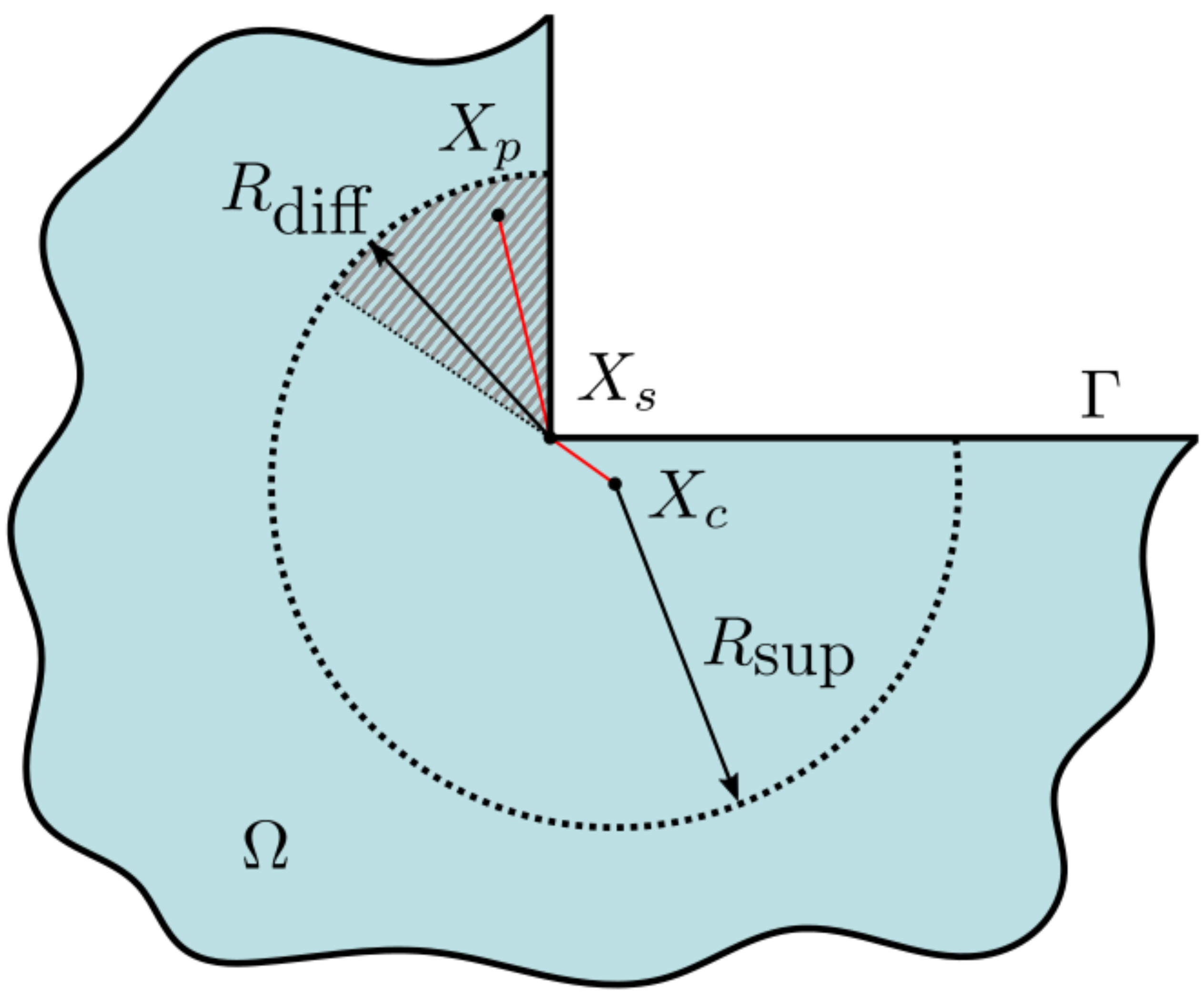

Node Selection Around Singularities: Model Problem

L-Shape in Mode I Loading

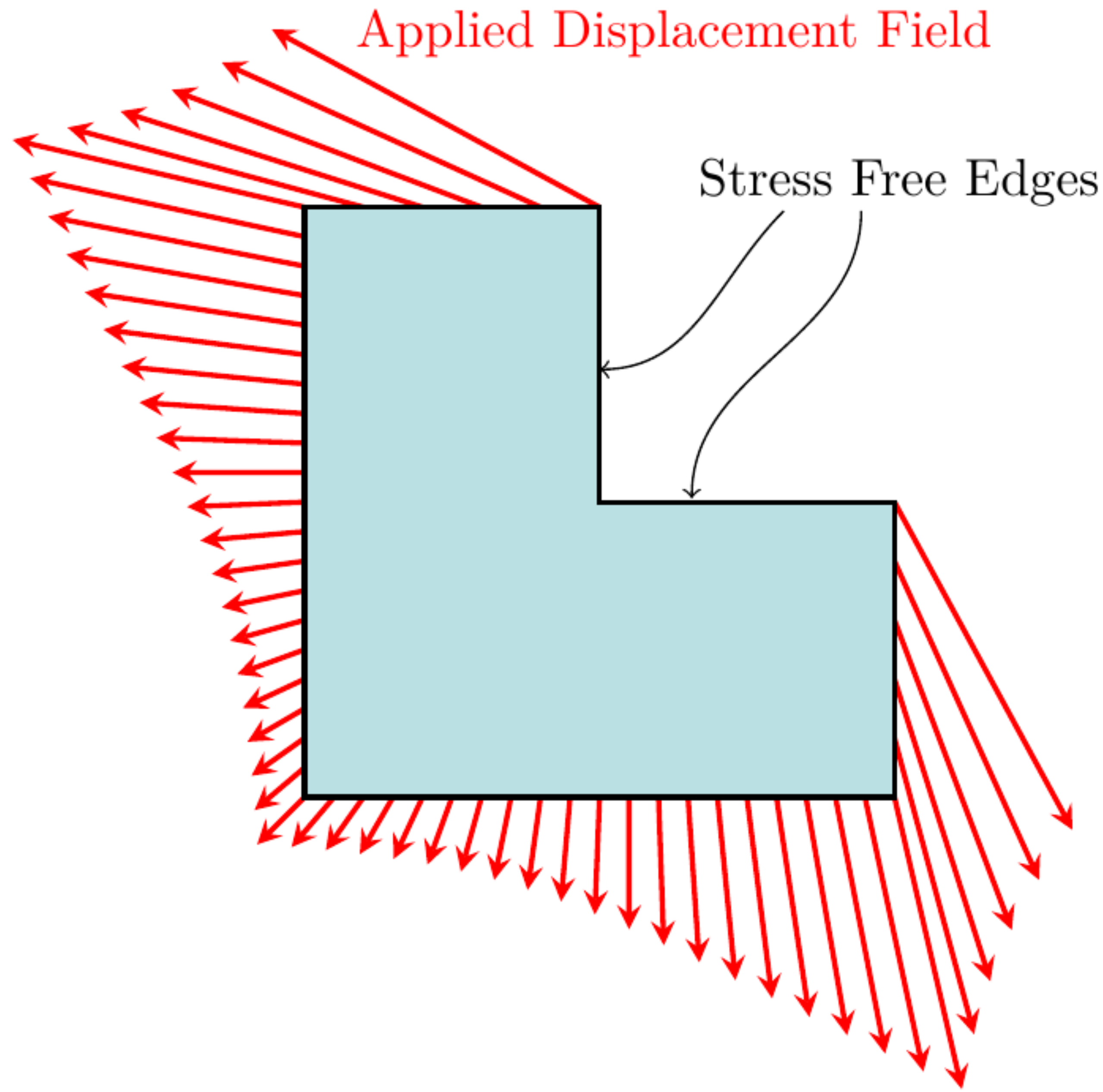

Visibility superior to diffraction

DCPSE

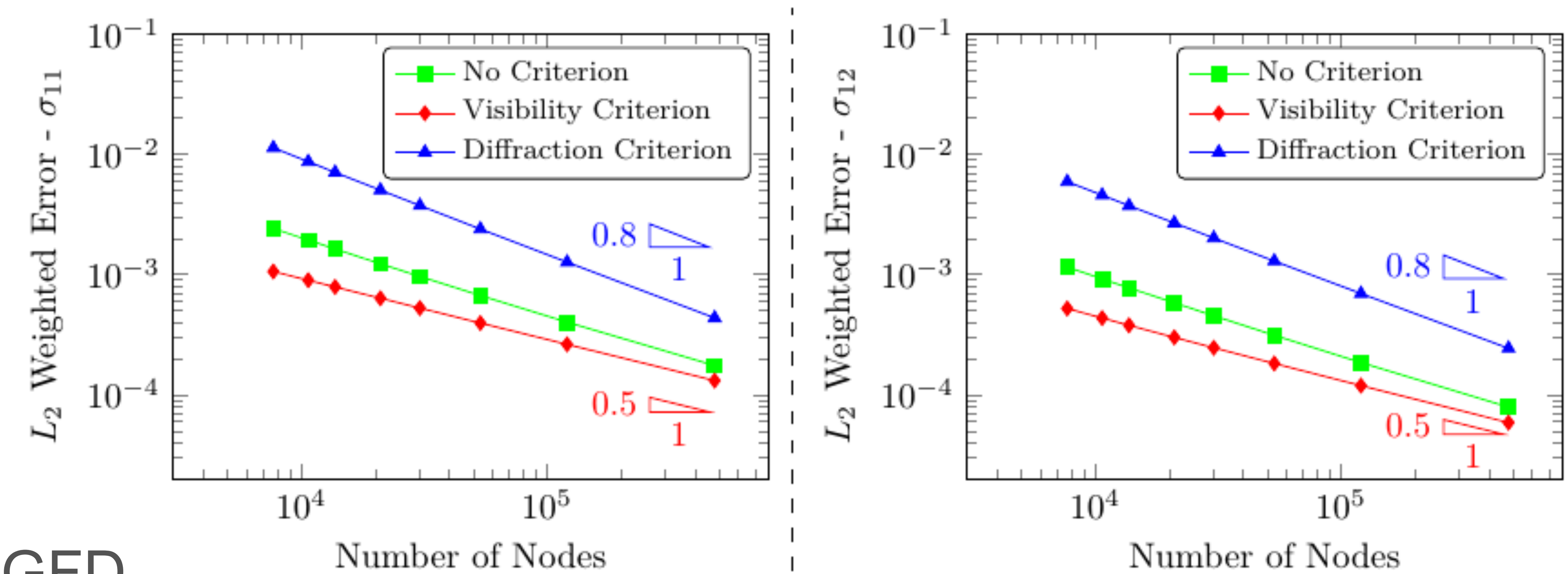

GFD

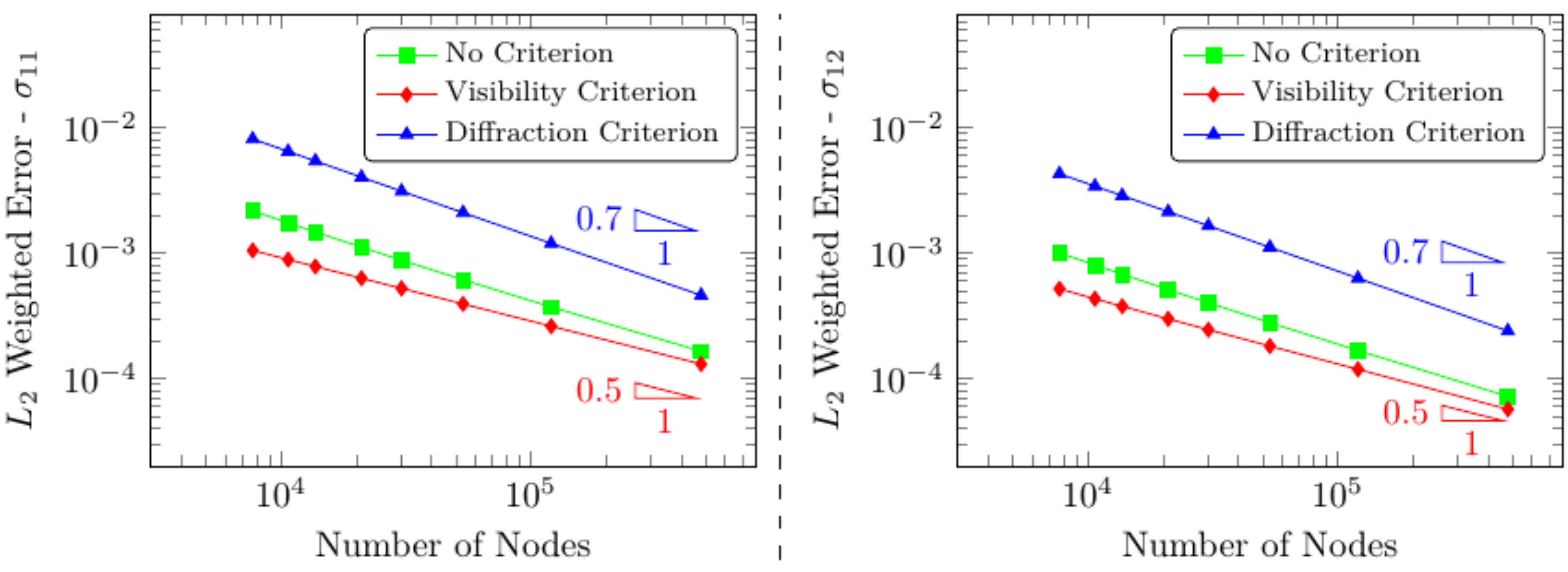

Timings Analysis – L-Shaped Problem

- Similar analysis durations and time split are observed for the GFD and the DCPSE methods (right axes for total time)
- For problems of large dimension, the largest fraction of the analysis is spent in the solution step

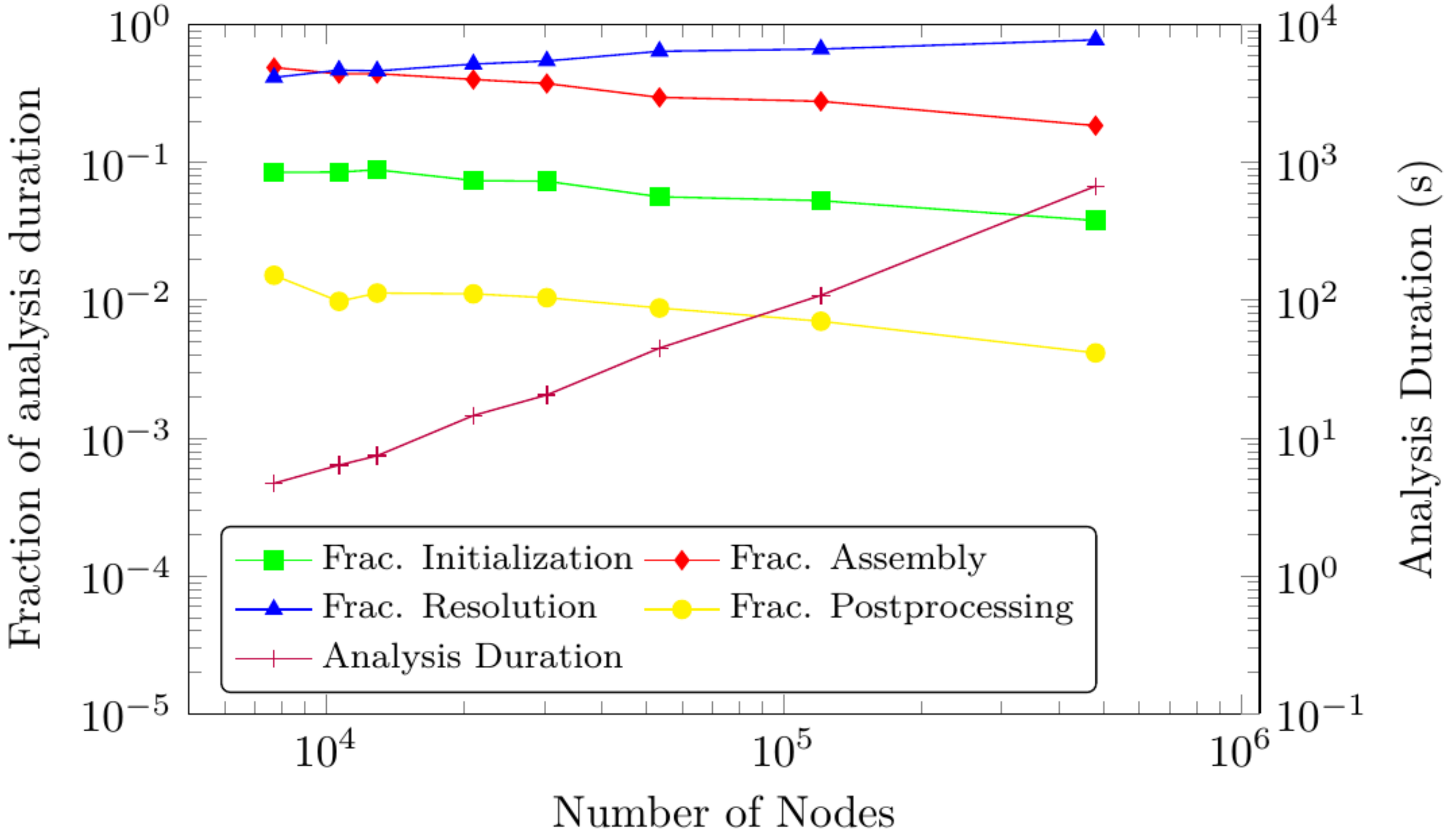

3D Results – ISO Flange: Model and Boundary Conditions

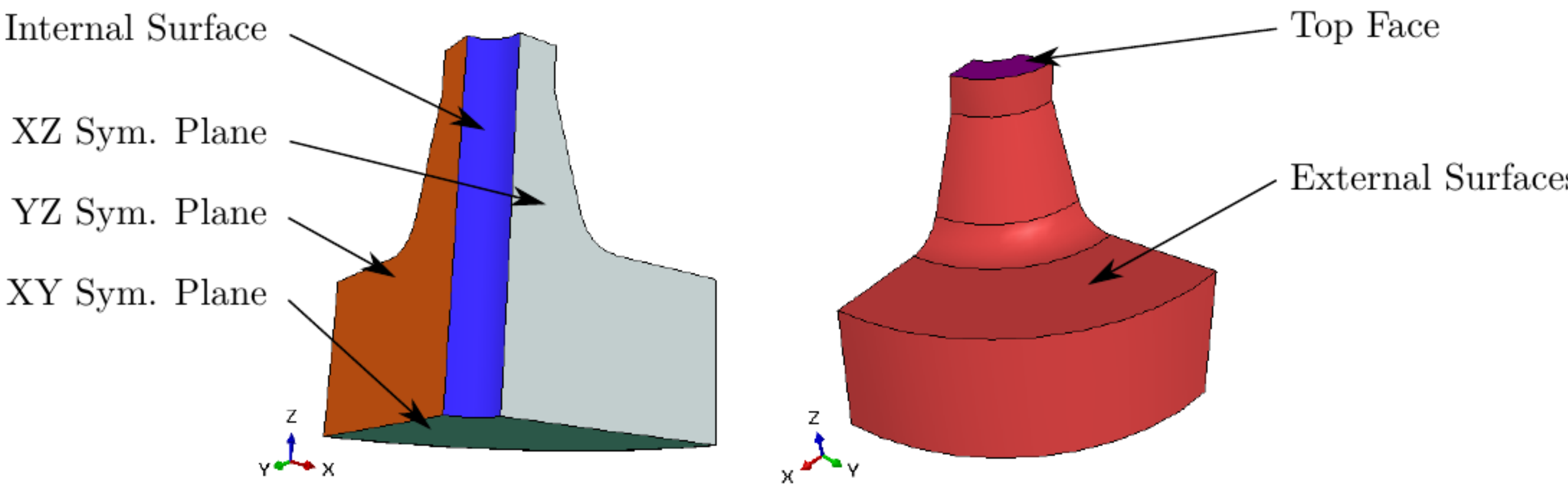

Surface(s)	Pressure Loading	Displacement Loading
XZ, YZ and XY Sym. Planes	Resp. constrained in the Y, X and Z directions	
External Surface	Stress free	
Top Face	Constrained in Z	Applied displacement in Z
Internal Surface	Constant pressure	Stress free

3D Results – ISO Flange: Difference (GFD - FEA)

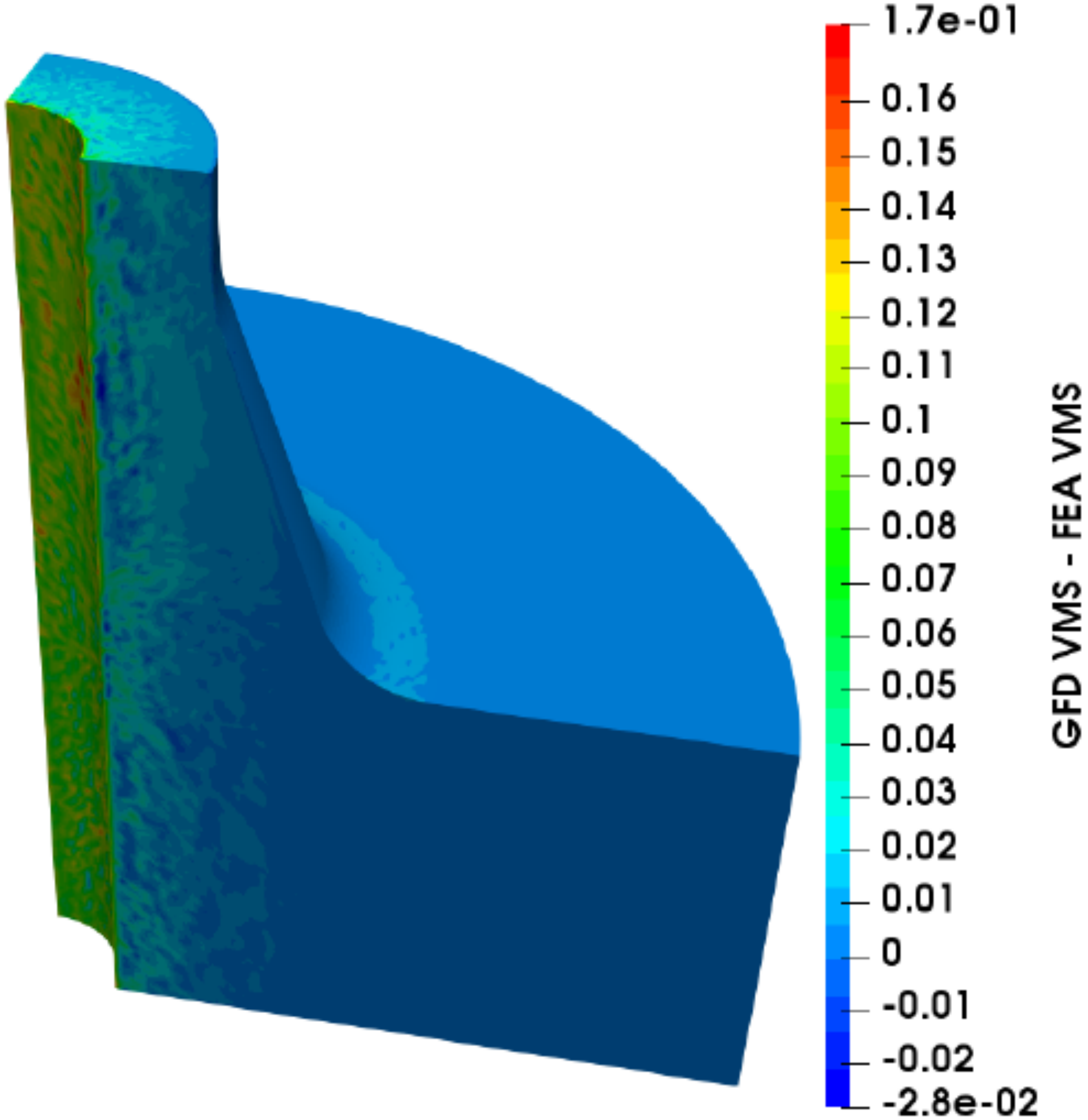

Pressure Loading

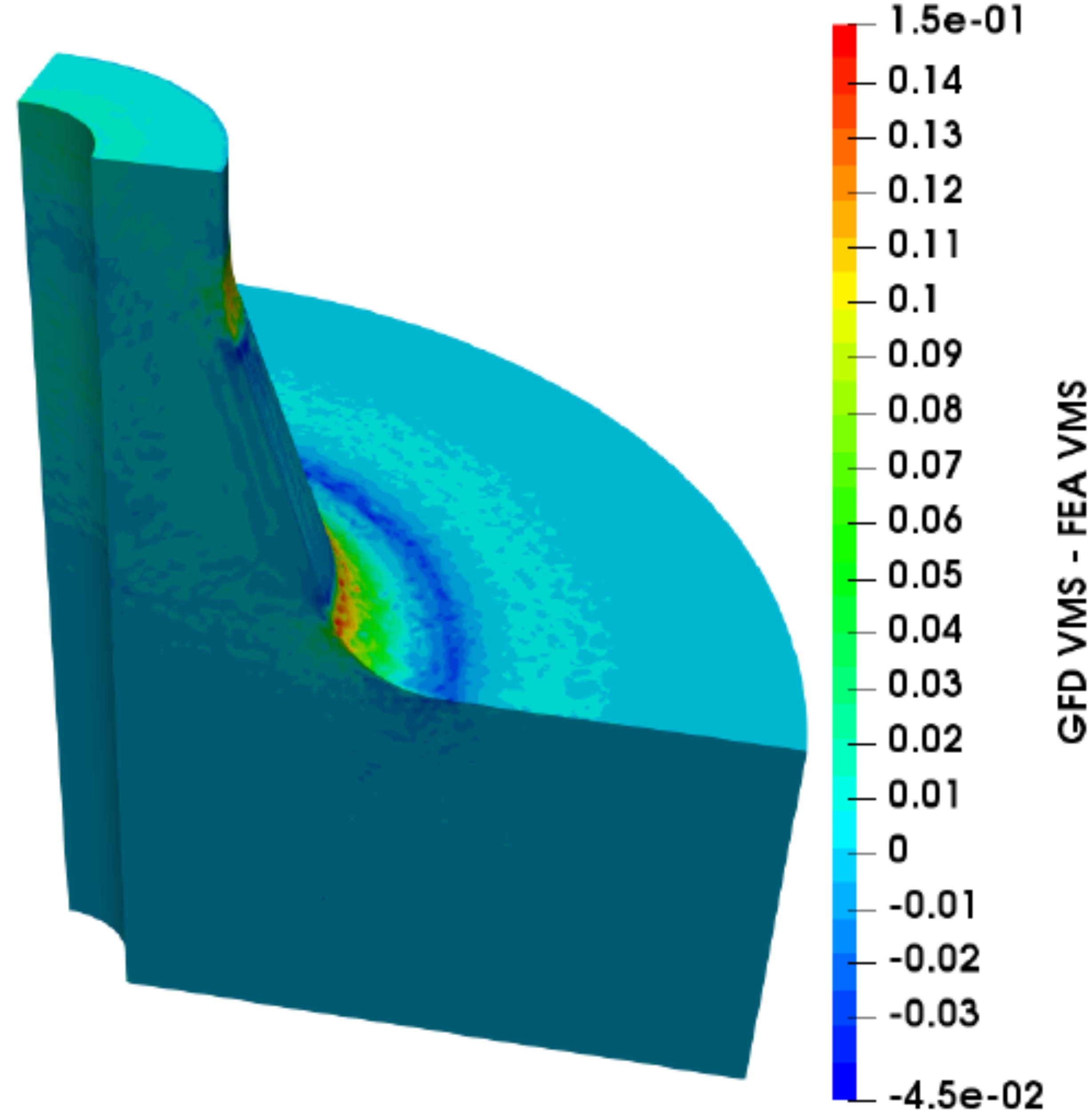

Displacement Loading

3D Results – Simplified Blade: Model and Boundary Conditions

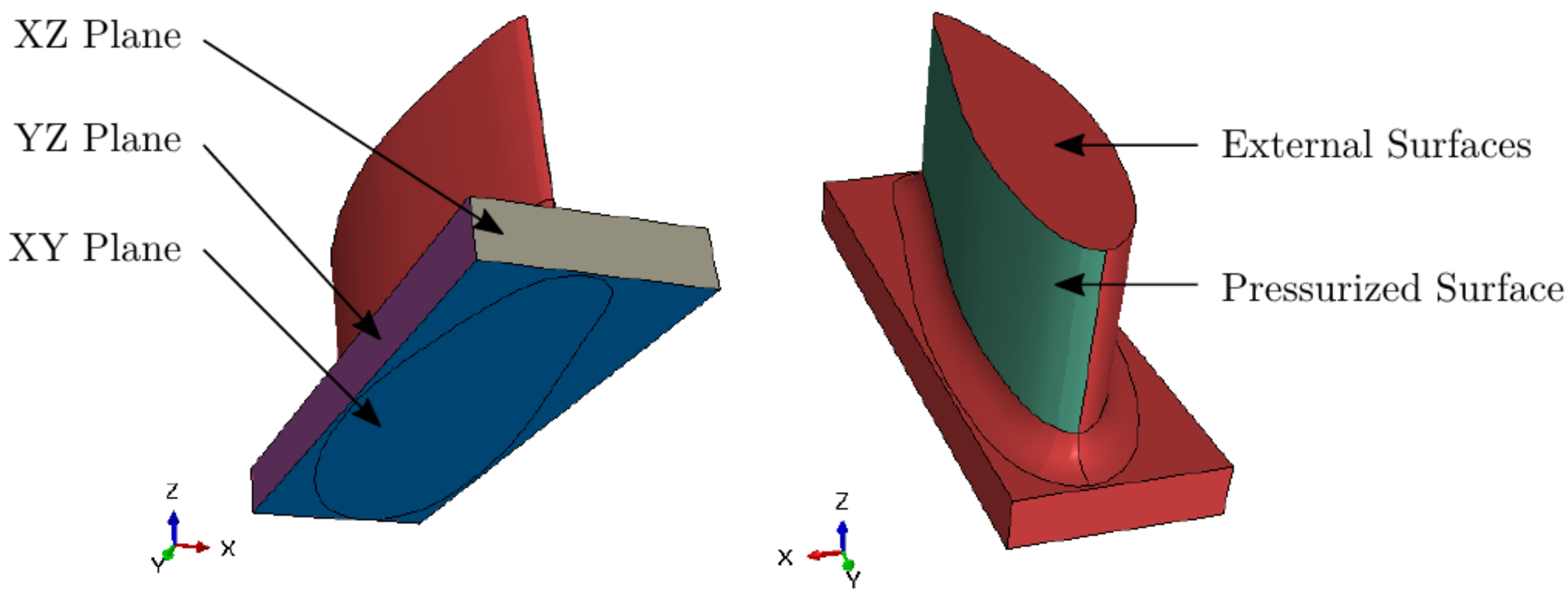

Surface(s)	Pressure Loading
XZ, YZ and XY Sym. Planes	Resp. constrained in the Y, X and Z directions
External Surface	Stress free
Pressurized Surface	Constant pressure

3D Results – Simplified Blade: Difference (GFD - FEA)

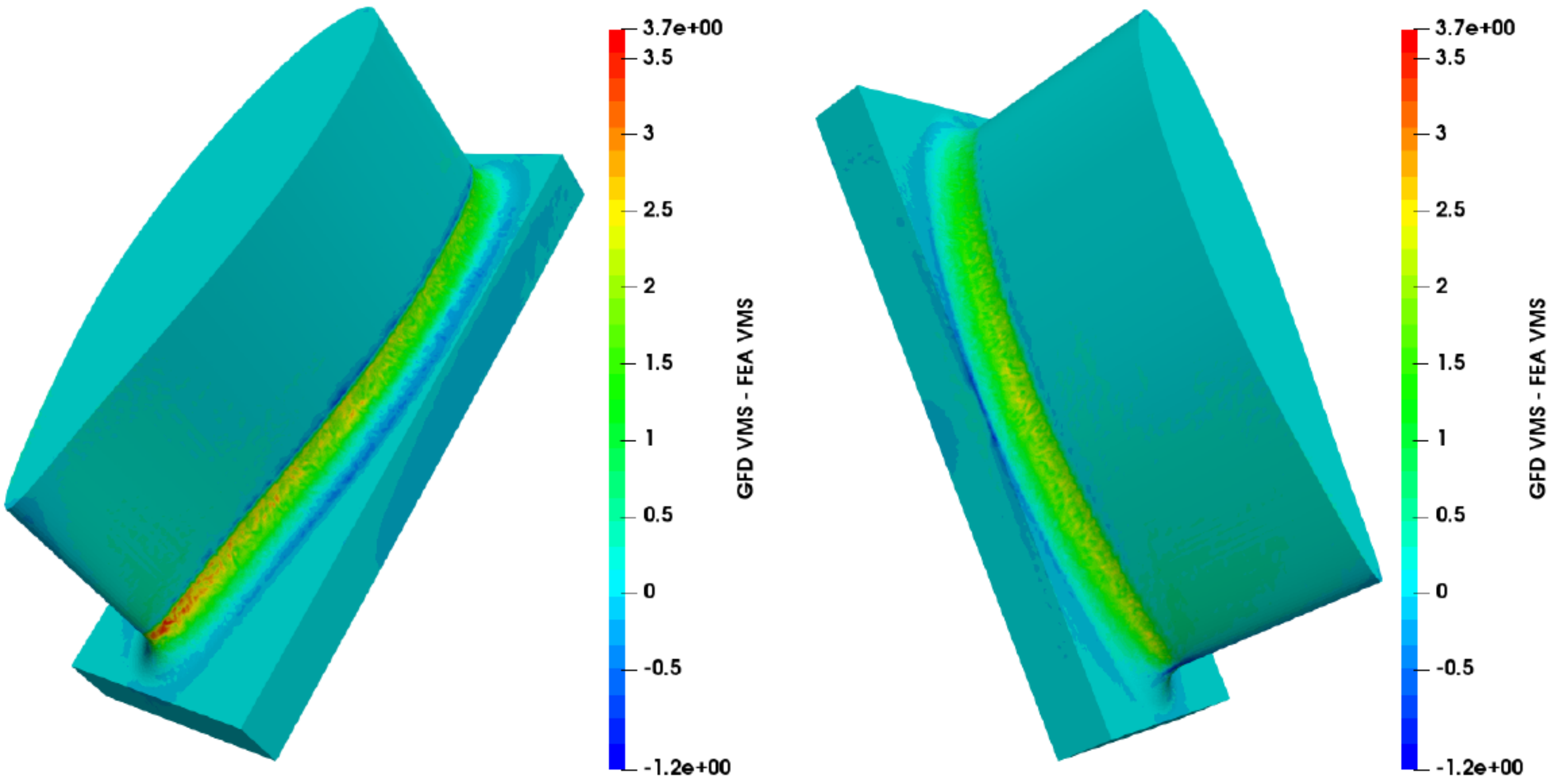

(a) (b)

Analysis of 3D Results

- Large number of nodes
  - ➢ 548,648 nodes for the ISO flange
  - ➢ 484,238 nodes for the blade
- The results obtained with GFD and FEA are very close
- The observed stress concentrations are larger with the collocation method

Sensitivity to various parameters

- Both the GFD and the DCPSE methods are sensitive to the parameters on which they depend
- Some of the parameters are:
  - ➢ The weight function considered (e.g. spline, exponential…)
  - ➢ The correction function for DCPSE (e.g. polynomial, exponential)
  - ➢ The number of nodes considered in the inner nodes support
  - ➢ The number of nodes considered in the boundary nodes support

Programs used

- CGAL: Node neighbour search and geometry of the boundary
- Voro++: Voronoi diagram for 2D and 3D problems
- Eigen: Matrix and vector classes for the assembly step
- OpenMP: Multithreading
- MPICH: Parallel multi-node computing
- PETSc: Matrix preconditioners (algebraic multigrid), parallel iterative solver (GMRES),
- MUMPS: MUltifrontal Massively Parallel Sparse direct solver

Legato-team

University of Luxembourg